INTERNATIONAL JOURNAL

of

COMPUTERS, COMMUNICATIONS & CONTROL

ISSN 1841-9836

ISSN-L 1841-9836

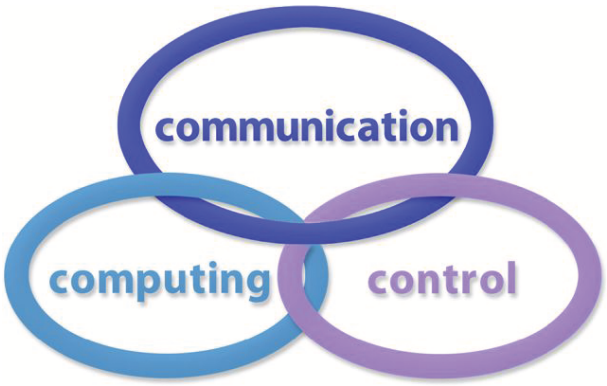

A Bimonthly Journal
With Emphasis on the Integration of Three Technologies

Year: 2013 Volume: 8 Issue: 3 (June)

This journal is a member of, and subscribes to the principles of,
the Committee on Publication Ethics (COPE).

Agora University Editing House

CCC Publications

http://univagora.ro/jour/index.php/ijccc/

International Journal of Computers, Communications & Control

EDITORIAL ADDRESS:
R&D Agora Ltd. / S.C. Cercetare Dezvoltare Agora S.R.L.
Piaţa Tineretului 8, Oradea, jud. Bihor, Romania, Zip Code 410526
Tel./ Fax: +40 359101032
E-mail: ijccc@univagora.ro, rd.agora@univagora.ro, ccc.journal@gmail.com
Journal website: http://univagora.ro/jour/index.php/ijccc/

International Journal of Computers, Communications & Control

EDITORIAL BOARD

Mario de J. Pérez Jiménez
Dept. of CS and Artificial Intelligence
University of Seville, Sevilla,
Avda. Reina Mercedes s/n, 41012, Spain
marper@us.es

Dana Petcu
Computer Science Department
Western University of Timisoara
V.Parvan 4, 300223 Timisoara, Romania
petcu@info.uvt.ro

Radu Popescu-Zeletin
Fraunhofer Institute for Open
Communication Systems
Technical University Berlin, Germany
rpz@cs.tu-berlin.de

Imre J. Rudas
Institute of Intelligent Engineering Systems
Budapest Tech
Budapest, Bécsi út 96/B, H-1034, Hungary
rudas@bmf.hu

Yong Shi
Research Center on Fictitious Economy
& Data Science
Chinese Academy of Sciences
Beijing 100190, China
yshi@gucas.ac.cn
and
College of Information Science & Technology
University of Nebraska at Omaha
Omaha, NE 68182, USA
yshi@unomaha.edu

Athanasios D. Styliadis
Alexander Institute of Technology
Agiou Panteleimona 24, 551 33
Thessaloniki, Greece
styl@it.teithe.gr

Gheorghe Tecuci
Learning Agents Center
George Mason University, USA
University Drive 4440, Fairfax VA 22030-4444
tecuci@gmu.edu

Horia-Nicolai Teodorescu
Faculty of Electronics and Telecommunications
Technical University "Gh. Asachi" Iasi
Iasi, Bd. Carol I 11, 700506, Romania
hteodor@etc.tuiasi.ro

Dan Tufiş
Research Institute for Artificial Intelligence
of the Romanian Academy
Bucharest, "13 Septembrie" 13, 050711, Romania
tufis@racai.ro

Lotfi A. Zadeh
Professor,
Graduate School,
Director,
Berkeley Initiative in Soft Computing (BISC)
Computer Science Division
Department of Electrical Engineering
& Computer Sciences
University of California Berkeley,
Berkeley, CA 94720-1776, USA
zadeh@eecs.berkeley.edu

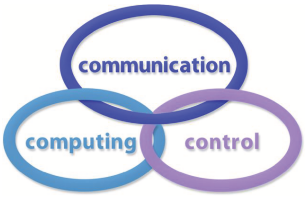

DATA FOR SUBSCRIBERS
Supplier: Cercetare Dezvoltare Agora Srl (Research & Development Agora Ltd.)
Fiscal code: 24747462
Headquarter: Oradea, Piata Tineretului Nr.8, Bihor, Romania, Zip code 410526
Bank: MILLENNIUM BANK, Bank address: Piata Unirii, str. Primariei, 2, Oradea, Romania
IBAN Account for EURO: RO73MILB0000000000932235
SWIFT CODE (eq.BIC): MILBROBU

International Journal of Computers, Communications & Control

Short Description of IJCCC

Title of journal: International Journal of Computers, Communications & Control
Acronym: IJCCC
Abbreviated Journal Title: INT J COMPUT COMMUN
International Standard Serial Number: ISSN 1841-9836, ISSN-L 1841-9836
Publisher: CCC Publications - Agora University
Starting year of IJCCC: 2006
Founders of IJCCC: Ioan Dzitac, Florin Gheorghe Filip and Mişu-Jan Manolescu
Logo:

Publication frequency: Bimonthly: Issue 1 (February); Issue 2 (April); Issue 3 (June); Issue 4 (August); Issue 5 (October); Issue 6 (December).

Coverage:

- Beginning with Vol. 1 (2006), Supplementary issue: S, IJCCC is covered by Thomson Reuters - SCI Expanded and is indexed in ISI Web of Science.
- Journal Citation Reports(JCR)/Science Edition:
  - Impact factor (IF): JCR2009, IF = 0.373; JCR2010, IF = 0.650; JCR2011, IF = 0.438.
- Beginning with Vol. 2 (2007), No.1, IJCCC is covered in EBSCO.
- Beginning with Vol. 3 (2008), No.1, IJCCC, is covered in Scopus.

Scope: International Journal of Computers Communications & Control is directed to the international communities of scientific researchers in computer and control from the universities, research units and industry.

To differentiate from other similar journals, the editorial policy of IJCCC encourages the submission of scientific papers that focus on the integration of the 3 "C" (Computing, Communication, Control).

In particular the following topics are expected to be addressed by authors:

- Integrated solutions in computer-based control and communications;
- Computational intelligence methods (with particular emphasis on fuzzy logic-based methods, ANN, evolutionary computing, collective/swarm intelligence);
- Advanced decision support systems (with particular emphasis on the usage of combined solvers and/or web technologies).

International Journal of Computers, Communications & Control/
INT J COMPUT COMMUN, ISSN 1841-9836, ISSN-L 1841-9836, Volume 8, Issue 3, June, 2013.

Contents

INT J COMPUT COMMUN, ISSN 1841-9836
8(3):354-365, June, 2013.

Breast Cancer Diagnosis based on Spiculation Feature and Neural Network Techniques

V. Bălănică, I. Dumitrache, L. Preziosi

Victor Bălănică, Ioan Dumitrache
University Politechnica of Bucharest
Romania, 060042 Bucharest, Splaiul Independentei, 313
vicord20011@gmail.com, idumitrache@ics.pub.ro

Luigi Preziosi
University of Politechnics Torino
Italy, 10129 Torino, Corso Duca degli Abruzzi, 24
luigi.preziosi@polito.it

Abstract: The degree of spiculation of the tumor edge is a particularly relevant indicator of malignancy in the analysis of breast tumoral masses. This paper introduces four new methods for extracting the spiculation feature of a detected breast lesion on mammography by segmenting the contour of the lesion in a number of regions which are separately analysed, determining a characterizing spiculation feature set. In order to differentiate between benign and malignant tumors based on the extracted spiculation sets, an intelligent neural network is first trained on a number of 96 cases of known breast cancer malignancy and then tested for diagnosing and classifying breast cancer tumors. The input of the neural network is thus the extracted spiculation feature set and the output is represented by the histopatological diagnostic given by doctors. Finally, the performance of the introduced methods is analysed depending on the number of regions in which the contour is segmented and the performance-related conclusions are stated for each of the methods.
The highlight of this paper is the division of the tumour contour in regions and the assessment of a spiculation indicator for each region, resulting a set of spiculation indicators that characterise the tumour and - by training a neural network - can be used in classifying breast tumours with high performance.
Keywords: breast cancer, spiculation feature extraction, neural network, diagnosis.

1 Introduction

In the detection process of suspicious breast cancer lesions, mammography screening is usually followed by an analysis of diagnostic mammography, i.e. a more detailed analysis of the artifacts visible on the mammographic imaging results, such as: breast tissue density, tumoral masses, (macro- and micro-) calcifications, architectural distortion, etc, [1]. Among them, the detected microcalcifications and the identified masses (also known as tumours) are considered the most relevant signs of malignancy that need to be investigated in detail. On one hand, the microcalcifications are tiny mineral deposits within the breast, representing an early indicator of the presence of a tumor. On the other hand, the tumoral mass is a tissue composed of an abnormal growth of cells (normal or neoplastic, cancerous, cells) with or without integrated calcifications that are also being detected on the mammographic results. When analyzing any pathology of breast cancer, the location, the size, the shape of the mass are usually assessed and the mass density and the tumoral margins are moreover evaluated. While the benign masses have usually smooth edges, are well circumscribed, compact and approximately circular or elliptical (see Figure 1), malignant lesions usually have vague edges and irregular form, presenting spiculations (i.e. a radial pattern of spiculs), [2]. Thus, in analyzing the tumoral mass, in addition to the lesion size, the degree of spiculation of the tumor edge is a particularly relevant indicator of malignancy (differences visible in Figure 1).

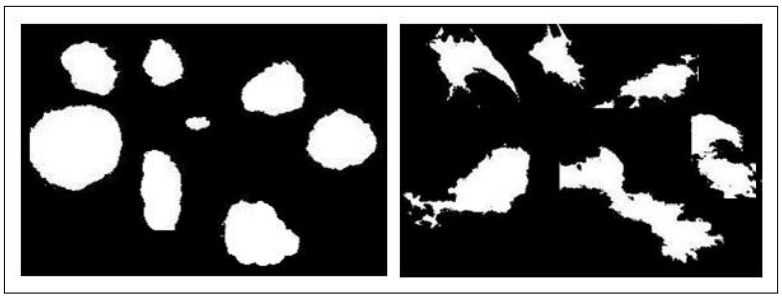

Figure 1: Benign and malignant tumors extracted from available mammographies

The evaluation of the spiculations of masses visible on the mammographic results implies form recognition techniques that extract numerical information usable in the process of differentiating between benign and malignant tumours. These techniques are continuously being developed and improved in order to make possible a more refined characterization of the particular morfological features and a higher classification performance. [3] computes a spiculation index that can classify tumours with 93% accuracy; [4] proposes three methods for morfological feature extraction and reaches 93% accuracy when classifying breast lesions; [5] explores the classification power of 6 contour algorithms on 349 masses using three popular classifiers (Bayesian Classifier, Fisher Linear Discriminant Analysis and Support Vector Machine) and shows that a big variation (14%) of the quality of the segmentation method influences only 4% of the classification performance given by the contour features.

Besides the current trend in technology and computer automation, the bioengineering interdisciplinary developments of the last years allowed the implementation of digital CAD (Computer Aided Diagnosis) aid tools to assist novice radiologists in making diagnostic and recommended treatments decisions, herewith providing a second opinion on the decision and playing the role of the second pairs of eyes in the analysis, certifying or not the quality and/or the choice. Although the computational CAD techniques used in determining a medical prognostic do not always provide the desired quality, their implementation using intelligent techniques (neural networks, fuzzy techniques, genetic algorithms and their hybrid variants) that are based on human experience and provide learning and adaptation abilities, demonstrates high performance in these kinds of tasks.

In this paper, we are trying to define new methods for extracting the spiculation feature set of a breast lesion identified on a mammographic result by analyzing the lesion contour on a number of contour regions. The methods have been tested by using a neural architecture integrated into a CAD that provides good classification performance when trained on the extracted spiculation feature sets of 96 breast cancer cases with known malignancy diagnostic. Thus, this neural CAD is able to distinguish, diagnose and classify breast cancer tumors in benign or malignant, highlighting the benefit and usefulness of both the methods and their neural CAD application in national breast cancer screening programs.

2 Materials and methods

In terms of imaging, the starry distortions visible on mammography are caused by the intrusion of cancer in surrounding tissue (invasion occurs in malignant tumors), so that the contour/outline form of the tumor is generally correlated to the degree of malignancy. The contour is thus an extremely valuable information in the differentiation between benign and malignant tumors. As stated above benign tumors usually have smooth, circumscribed, macrolobulate and well defined contours (Figure 1), while malignant tumors are characterized by vague, irregular,

microlobulate and spiculate contours (Figure 1). Based on these observations, researchers have defined certain objective and quantitative measures/indicators to characterize the contours in order to improve the imaging classification capability of the detected tumors. In terms of performance, among the most important and most frequent contour indicators found in the literature we count: the degree of compactness, the spiculation index, the fractional concavity, the Fourier factor and the fractal dimension, [6].

In our paper, the neural networks are used for classifying the tumours based on the extracted spiculation feature set of a breast lesion identified on a mammographic result. The neural networks (NNs) models are simplified structural and functional nervous systems, formed by a number of processing elements, the neurons, which are bound by weighted connections, similar to the neural synapses, [7]. The neural network architecture mainly used in the medical field is known as the multi-layer perceptron (or MLP), [8], Figure 2, which consists of neurons usually organized in three feed-forward interconnected layers (i.e. all neurons in one layer are fully connected to all neurons in the next layer, but there are no feedbacks to previous layers). A perceptron has the ability to learn, to self-organize and to generalize (i.e. it can have same output for similar sets of inputs). The most commonly algorithm used for training the neural network is the back-propagation algorithm, which calculates the error gradient of the network and adjusts each connection weight by minimizing the mean square difference and achieving convergence to a local minimum, [9]. Figure 2 shows a graphical representation of such a network, where, in the case of a medical system, the input layer neurons often corresponds to the clinical symptoms, the hidden layer simulates the medical inference process done by the doctor and the neurons from the output layer correspond to the medical diagnosis.

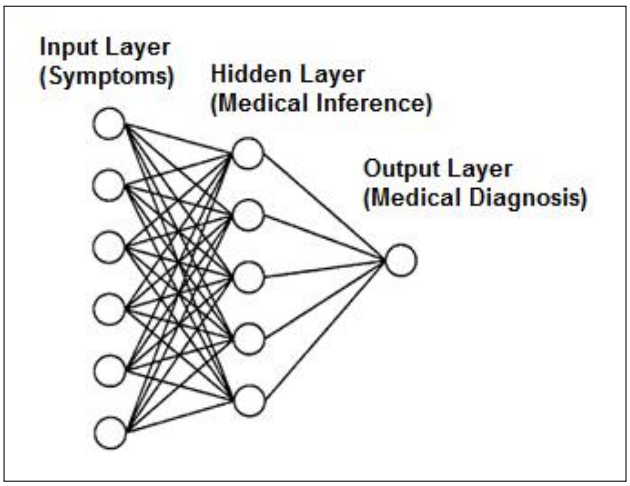

Figure 2: Graphical representation of a MPL neural network with one hidden layer

The focus in this paper is not to develop a novel MPL, but rather to apply it in the clinical relevant problem of breast cancer. Because many clinical scenarios can not be explained based on only one parameter, but as interaction of various clinical-pathological factors, [10], the inputs of the MPL may include any set of mammographic descriptors of the calcifications (distribution, number, description), of the detected masses (size, shape, density, margins, location) or of any other associated findings (asymmetries, distorsions), being able to include also inputs related to the patient history. The ouputs of the MPL are usually numbers between zero and one that may correpond to the prediction of the biopsy outcome (benign or malignant) as in [11], the stage of development for the analyzed lesion (in situ or invasive) or it may be correlated to the survival chance/rate of the patient (under 1 year, under 2 years, under 3 years, under 5 years, more than 5 years) as in [12].

3 New methods for lesion spiculation feature extraction

The mammographic lesions segmentation methods proposed below assumes that the spicules are visible on the mammography in the form of tumor infiltration or branches, usually narrow, in normal biological tissue. Therefore, the analysis of tumor contour on neighborhoods (or regions) of the contour and the measuring of the curvature change in each region offers an useful set of valuable information in determining the degree of spiculation in the analysed regions of the lesion contour and allowing subsequent CAD classification of tumors in benign or malignant.

For each of the neighborhoods of the lesion contour four spiculation indicators are computed, namely:

A. A Maximum Level Difference for every region of the contour, relative to the center of gravity of the lesion, according to the following figure (Figure 3):

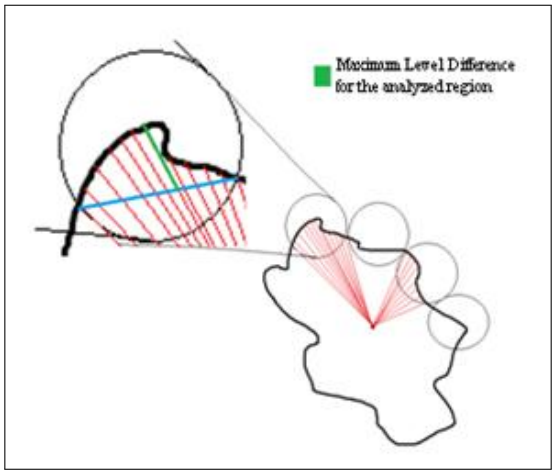

Figure 3: Calculation of the maximum level difference of for the regions of the tumoral contour

B. The Total Area of triangles in a neighborhood, calculated by adding the triangle areas formed by each three consecutive points along the contour, according to the following figure (Figure 4):

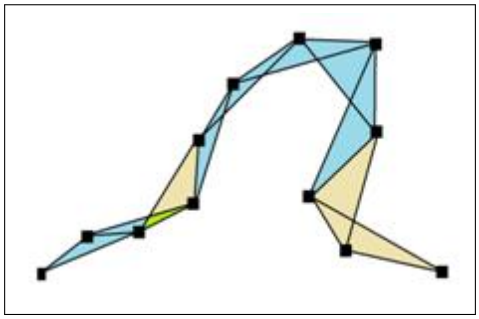

Figure 4: Calculation of the total area of the triangles formed along the contour for a contour region

C. The Total Angle in a neighborhood, calculated by adding all the angles formed by every three consecutive points along the contour, according to the following figure (Figure 5):

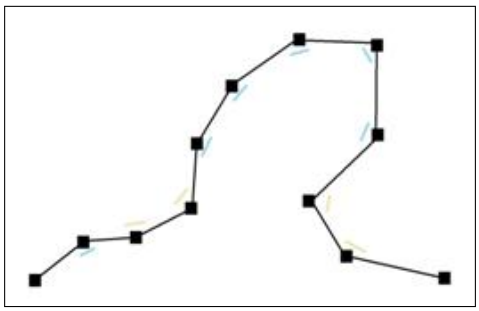

Figure 5: Calculation of total angle summed for the angles formed along a contour region

D. The Total Quadratic Curvature for each region, calculated by adding the curvatures of the circles passing through each three consecutive points along the contour, according to the following figure (Figure 6):

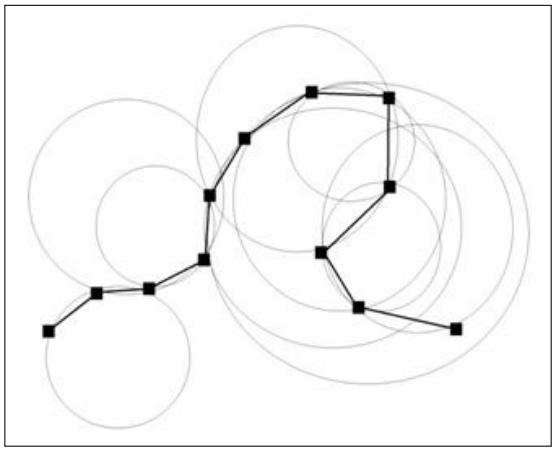

Figure 6: Calculation of the total quadratic curvature, by adding the curvatures of the circles passing through each three consecutive points of the analysed region of the contour

The main steps for the defined A, B, C and D methods are described as following:

i. The starting point of the method is an image of a detected mass (Figure 7 a),

ii. Calculate and plot the center of the mass based on the pixels that form the lesion (computing center of mass for lines and for columns) (Figure 7 b),

iii. Calculate and plot the marginal pixels of the tumor (Figure 7 b),

iv. Calculate and plot the distances between the center of mass and the pixels describing the edge of the tumor (Figure 7 c),

v. The distance vector is ascendently ordered according to the angle formed by these distances lines with one reference line,

vi. Depending on a relevant, experimentally determined, number of neighborhoods, X, for each angle Z = 360/X are done a number of operations specific for each algorithm. For each angle Z, for algorithm:

A. Is computed the maximum difference of the distances (= center of gravity - marginal pixels) that fall within the Z angle, thus identifying the characteristic vector of spiculation for the tumor. Table 1 shows an example of this vector for a malignant and a benign lesion).

B. Is computed the total area of triangles in the neighborhood described by the Z angle, by adding the areas of the triangles formed by every three consecutive points along the contour, according to the formula (1), [13]. Table 1 shows an example of this vector for a malignant and a benign lesion).

$$\sum_{i\epsilon Z} A_i, A_i = \frac{1}{2}[(X_i - X_{i+2})(Y_{i+1} - Y_i) - (X_i - X_{i+})(Y_{i+2} - Y_i)] \tag{1}$$

C. Is computed the total angle for the neighborhood described by the Z angle, by summing of all angles formed by every three consecutive points along the contour, according to the formula (2), [13]. Table 2 shows an example of this vector for a malignant and a benign lesion).

$$\sum_{i\epsilon Z} U_i, U_i = arcsin[2{\cdot}A_i/\sqrt{(X_i - X_{i+1})^2 + (Y_i - Y_{i+1})}{\cdot}\sqrt{(X_{i+1} - X_{i+2})^2 + (Y_{i+1} - Y_{i+2})}] \tag{2}$$

D. Is computed the total quadratic curvature for the neighborhood described by the Z angle, by adding quadratic curvatures of the circles passing through each three consecutive points along the contour, according to the formulas (3), (4), (5), [13]. Table 2 shows an example of this vector for a malignant and a benign lesion).

$$\sum_{i\epsilon Z} c_i, c_i = \frac{1}{R_i^2}, R_i = \sqrt{\frac{d^2 + e^2}{4a^2} - \frac{f}{a}}, where \tag{3}$$

$$a = \begin{vmatrix} X_i & Y_i & 1 \\ X_{i+1} & Y_{i+1} & 1 \\ X_{i+2} & Y_{i+2} & 1 \end{vmatrix}, d = \begin{vmatrix} X_i^2 + Y_i^2 & Y_i & 1 \\ X_{i+1}^2 + Y_{i+1}^2 & Y_{i+1} & 1 \\ X_{i+2}^2 + Y_{i+2}^2 & Y_{i+2} & 1 \end{vmatrix}, \tag{4}$$

$$e = \begin{vmatrix} X_i^2 + Y_i^2 & X_i & 1 \\ X_{i+1}^2 + Y_{i+1}^2 & X_{i+1} & 1 \\ X_{i+2}^2 + Y_{i+2}^2 & X_{i+2} & 1 \end{vmatrix}, f = \begin{vmatrix} X_i^2 + Y_i^2 & X_i & Y_i \\ X_{i+1}^2 + Y_{i+1}^2 & X_{i+1} & Y_{i+1} \\ X_{i+2}^2 + Y_{i+2}^2 & X_{i+2} & Y_{i+2} \end{vmatrix} \tag{5}$$

The spiculation features set computed with any of the four methods shows, after tests, a very good performance in terms of differentiating benign and malignant tumors and can be used to compute an objective measure/degree of spiculation for the examined lesions. Moreover, these methods are suitable for training a neural classifier of malignant or benign patterns of spicules that is able to make assessments in the presence of a new set of extracted mammographic spiculation features.

As observed, depending on the analyzed lesion, the nature of these sets of indicators show a large variation of values in each neighborhood which makes them very suitable to being analyzed with classification modules such as neural networks in order to determine patterns and nonlinear correlations. The following practical approach shows the great classification potential of these indicators, given the fact that the trained neural modules reached maximum performance after a very short training time.

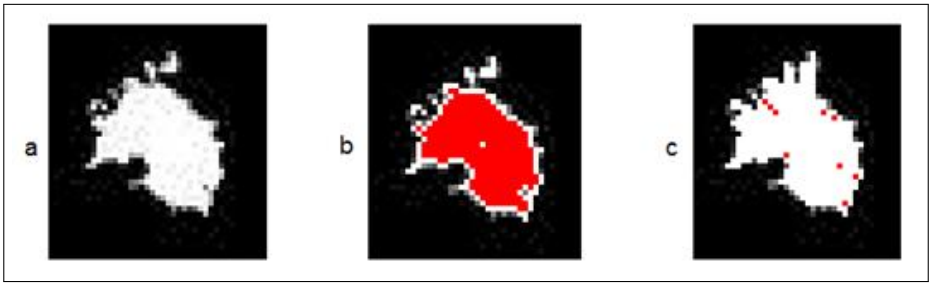

Figure 7: Lesion segmentation algorithm for computing the spiculation degree: a) a tumor identified on mammography, b) identification of the center of the mass and of the marginal pixels, c) calculating and sorting the angular distances from the center of the mass to the marginal pixels

Spiculation	Malignant	Benign
Region 1	0.029088023	0.002314645
Region 2	0.010393358	0.003456135
Region 3	0.013055199	0.010551446
Region 4	0.011486832	0.003844839
Region 5	0.012432602	0.024487918
Region 6	0.008171691	0.022505824
Region 7	0.008919256	0.004633745
Region 8	0.008129058	0.006751543
Region 9	0.004758858	0.005050591
Region 10	0.008588636	0.001135357
Region 11	0.005033413	0.023203568
Region 12	0.006881693	0.001615465
Region 13	0.012579647	0.007542353
Region 14	0.015354234	0.006765708
Region 15	0.032946416	0.005762422
Region 16	0.011897444	0.008253233
Region 17	0.00767037	0.014833624
Region 18	0.015423039	0.006765275
Region 19	0.011775156	0.002545662
Region 20	0.040558593	0.000563123

Total Area	Malignant	Benign
Region 1	-86	0
Region 2	969.5	-0.5
Region 3	26.5	-5.5
Region 4	2011	0
Region 5	2500.5	12
Region 6	2146.5	-152
Region 7	630.5	455.5
Region 8	809.5	263.5
Region 9	-1240.5	295.5
Region 10	-875	138.5
Region 11	574	-192
Region 12	2032.5	110.5
Region 13	-986.5	253
Region 14	-998	-463.5
Region 15	-925.5	3.5
Region 16	-1005.5	-12
Region 17	88.5	84.5
Region 18	-196.5	52.5
Region 19	-226	190.5
Region 20	-111.5	1

Table 1: The characteristical spiculation vectors for a malignant lesion and for a benign one for method A and method B

However, the efficient utilization of these methods may vary depending on the size and the quality of the imaging results (processed or unprocessed, noise filtered or unfiltered regions of interest, the quality of image binarization, etc.) and in what concerns the choice of the number of neighborhoods for the segmentation of the lesion contour. In this respect, one can successfully use a genetic algorithm to determine the optimal number of neighborhoods to achieve the maximum classification performance.

4 Neural networks trained for breast cancer diagnosis

The data sets obtained by applying the above methods can be used to train a neural intelligent module for the classification of the detected lesions on imaging results and determine the nonlinear correlations and the useful predictions. Thus, a feedforward neural network with one hidden layer, configurable in terms of the learning rate, of learning momentum, of the training epochs and of the minimum desired error, was trained using the backpropagation learning algorithm based on the extracted imaging spiculation feature sets determined with the above defined A, B, C and D methods (the feature sets will be noted as SetA, SetB, SetC and SetD). The

Total Angle	Malignant	Benign
Region 1	-158.9006115	10.30484647
Region 2	237.1041222	4.950272234
Region 3	170.4773613	-4.57392126
Region 4	105.8239209	0
Region 5	294.29397	-18.237718
Region 6	184.6354634	-14.2500327
Region 7	222.5665005	114.3045493
Region 8	156.3273605	57.12501634
Region 9	-169.667477	152.5138742
Region 10	-191.3721008	92.35031797
Region 11	84.80557109	-14.48976259
Region 12	362.1537249	6.441600099
Region 13	-176.3714678	152.8003632
Region 14	-66.65995455	-177.6626941
Region 15	-52.69605172	28.73979529
Region 16	-372.1805601	-1.708935032
Region 17	-48.36646066	65.11551647
Region 18	151.9275131	105.697576
Region 19	-101.3099325	86.37062227
Region 20	49.76364169	-22.87805803

Total Curvature	Malignant	Benign
Region 1	0.016552033	0.001116978
Region 2	0.019112517	0.001126586
Region 3	0.005208189	0.001130842
Region 4	0.002593499	0.001182075
Region 5	0.001063093	0.001469999
Region 6	0.001792455	0.001252206
Region 7	0.002036859	0.00123547
Region 8	0.002299495	0.001290132
Region 9	0.002999928	0.001390865
Region 10	0.002855358	0.001224238
Region 11	0.003950692	0.001623056
Region 12	0.003452697	0.001583039
Region 13	0.003150858	0.001771651
Region 14	0.004421394	0.001892085
Region 15	0.018709067	0.001960565
Region 16	0.006304613	0.002043145
Region 17	0.009259506	0.002107581
Region 18	0.008482187	0.002189537
Region 19	0.010724884	0.002172309
Region 20	0.02949604	0.002275411

Table 2: The characteristical spiculation vectors for a malignant lesion and for a benign one for method C and method D

general training and testing algorithm of the neural module is given below:

i. Having a selection of mammographies for which the diagnostic output is known, i.e. the diagnosis (benign or malignant),

ii. The spiculation set for each of the mammographies is extracted with one of the A, B, C, or D methods described above, for a number of neighborhoods,

iii. Both the input (the spiculation data set) and also the output (the diagnostic) are normalized,

iv. Based on the normalized data, the neural network is being trained and validated for the predicton of the output (the diagnostic),

v. The predicted output is compared with the actual output (truth values of malignancy) by calculating performance measures like: specificity (i.e. number of true negatives divided by the sum of true negatives and false positives), sensitivity (i.e. number of true positives divided by the sum of true positives and false negatives), accuracy (i.e. sum of true positives and true negatives divided by sum of true positives, false positives, true negatives and false negatives) and the Matthews Correlation Coefficient (MCC explained below).

The training, the testing and the validation of the neural modules are based on the information of 96 mammographic cases acquired from the Department of Medical Physics, University of FreeState, Bloemfontain, South Africa, of which 48 cases are benign and 48 are malignant, [14].

The practical experience has focused on the analysis of several selections of features in order to determine the training and classification performances of the neural networks. Rapid convergence of the training error and the classification and prediction power of the neural network indicate the correlation strength/weight between inputs and outputs, directly justifying the existence or the absence of non-linear correlations between them, in this case evaluated by Matthews Correlation Coefficient (MCC) - belonging to the interval [-1, +1], +1 representing a perfect correlation, 0 an arbitrary correlation and -1 inverse correlation.

Because the quality of the spiculation characteristics introduced in the previous section may vary depending on the number of neighborhoods set for segmentation of the lesions contour, the tests include also the variation of this value. Simultaneously, the regions of interest (ROI) processed and used in evaluating the imaging characteristics have the dimension of 335x436 pixels, an increase of the size being possible to the expense of the time needed for extracting data and for running the tests.

On average, 5 to 8 neural networks were trained for the same set of features in order to observe and determine the recorded performance variation. The performed tests (see Table 3) are not exhaustive, the results being obtained based on the currently available data sets.

5 Discussion of results

The performance results presented in Table 3 give a clear indication about the high potential of the introduced spiculation-feature extraction methods in what concerns the differentiation between benign and malignant tumors when using a neural classifier.

However, as shown in Table 4, the developed methods differ in terms of power and speed of convergence of the classifications and provide a different classification stability when changing the number of analyzed lesion contour neighborhoods. Thus, the method that calculates the maximum level difference on each region of the contour offers the optimal method for extracting the spiculation feature and the algorithm that calculates the total quadratic curvature for each region offers the most reliable measure of the lesion malignancy regardless of the neighborhoods number.

6 Conclusions

This paper introduces four new methods for the assessment of the tumor contour on a number of boundary neighborhoods. The Maximum Level Difference is calculated for every region of the analyzed contour, relative to the center of gravity of the lesion. The Total Area of Triangles in a neighborhood is calculated by adding the areas of each triangle formed by three consecutive points along the contour. The Total Angle for a neighborhood is calculated by adding up all the angles formed by every three consecutive points along the contour. The Total Quadratic Curvature for each region is calculated by adding the curvatures of the circles passing through each three consecutive points along the contour.

The spiculation feature extraction algoritms are tested on a selection of mammographies with known diagnostic by using a neural network that is trained on the extracted feature sets.

Following the performance tests, the spiculation feature sets computed with all of the four methods show a high potential in the differentiation of benign and malignant tumors and can be used to compute an objective measure/degree of spicularity for the analysed lesion. Moreover, these methods are suitable for training a neural classifier of malignant or benign patterns of spiculs that is able to make assessments in the presence of a new set of extracted mammographic spiculation features. However, as shown in the pages of the paper, the developed methods differ in terms of power and speed of convergence of the classifications and provide a different classification stability when changing the number of neighborhoods the lesion contour is segmented and analyzed.

These CAD extraction methods show high reliability and prove high implementation potential being currently used in an automated decision support systems for breast cancer designed for national mammography screening programs in Romania and South Africa.

ID	No. of neighborhoods	Inputs of the neural network	Outputs of the neural network	Malignity classification performances	MCC Correlation
1	5	SetA =5 inputs	Diagnostic	Sensitivity: [97 100 %] Specificity: [100 98.1 %] Accuracy: [98.9 %] For 50-200 training iterations	0.97
2	5	SetB =5 inputs	Diagnostic	Sensitivity: [86.3 100 %] Specificity: [96.2 83 %] Accuracy: [91.7 90.7 %] For 100-300 training iterations	0.83
3	5	SetC =5 inputs	Diagnostic	Sensitivity: [90.9 93.1 %] Specificity: [90.5 98.1 %] Accuracy: [90.7 95.8 %] For 100-300 training iterations	0.86
4	5	SetD =5 inputs	Diagnostic	Sensitivity: [97.7 100 %] Specificity: [98.1 98.1 %] Accuracy: [97.9 98.9 %] For 50-100 training iterations	0.98
5	5	The best sets: SetA,SetB =10 inputs	Diagnostic	Sensitivity: [100 %] Specificity: [100 %] Accuracy: [100 %] For 20-40 training iterations	1
6	5	SetA,SetB, SetC,SetD =20 inputs	Diagnostic	Sensitivity: [87.7 91.6 %] Specificity: [97.9 100 %] Accuracy: [92.7 95.8 %] For 100-300 training iterations	0.90
7	20	SetA =20 inputs	Diagnostic	Sensitivity: [100 %] Specificity: [100 %] Accuracy: [100 %] For 20-30 training iterations	1
8	20	SetB =20 inputs	Diagnostic	Sensitivity: [100 %] Specificity: [100 %] Accuracy: [100 %] For 50-150 training iterations	1
9	20	SetC =20 inputs	Diagnostic	Sensitivity: [100 %] Specificity: [100 %] Accuracy: [100 %] For 4-10 training iterations	1
10	20	SetD =20 inputs	Diagnostic	Sensitivity: [100 %] Specificity: [100 %] Accuracy: [100 %] For 150-200 training iterations	1
11	20	The best sets: SetA,SetC =40 inputs	Diagnostic	Sensitivity: [100 %] Specificity: [100 %] Accuracy: [100 %] For 3 training iterations	1
12	20	SetA,SetB, SetC,SetD =80 inputs	Diagnostic	Sensitivity: [100 %] Specificity: [100 %] Accuracy: [100 %] For 3-4 training iterations	1

Table 3: The trained neural networks and the achieved performances

Set ID	**Description of the Spiculations Feature Set**	**Observed features**	**Description**
SetA	Spiculation set for the A algorithm: The Maximum Level Difference for every region of the contour	Average convergence and avarage stability	Regardless of the neighborhoods number, the classification performance converges with average speed, and the obtain results vary very little.
SetB	Spiculation set for the B algorithm: The Total Area of Triangles in a neighborhood	Slow convergence and low stability	Regardless of the neighborhoods number, the classification performance converges with low speed. For a small number of regions, the results are much weaker compared with those obtained for a higher number of regions.
SetC	Spiculation set for the C algorithm: The Total Angle in a neighborhood	Fast convergence and low stability	Regardless of the number of neighborhood, the classification performance converges with high speed. For a small number of regions, the results are poor compared to those obtained for a larger number of regions.
SetD	Spiculation set for the D algorithm: The Total Quadratic Curvature for a region	Slow convergence but very high stability	Regardless of neighborhoods number, the classification performance converges with low speed, but the results are always powerful and do not vary.

Table 4: The efficiency of the spiculation feature extraction methods for a lesion

Bibliography

[1] Sultana, Alina (2010); *On Improving Image-Based Diagnosis Using Digital Image Processing*, Faculty of Electronics, Telecommunications and Information Technology, Bucharest.

[2] Feig, S.A.; Yaffe, M.J. (1995); Digital Mammography, Computer-Aided Diagnosis and Telemammography, *The Radiologic Clinics of North America*, Breast Imaging Press, 33(6):1205-1230.

[3] Guliato, D.; Rangayyan, R.M.; Carvalho, J.D.; Santiago, S.A. (2006); Spiculation-preserving Polygonal Modeling of Contours of Breast Tumors, *Proceedings of the 28th IEEE*, 2791-2794.

[4] Cheikhrouhou, I.; Djemal, K.; Sellami, D.; Maaref, H.; Derbel, N. (2008); New mass description in mammographies, *Image Processing Theory, Tools and Applications.*

[5] DomĂnguez, A.R.; Nandi, A.K. (2009); Toward breast cancer diagnosis based on automated segmentation of masses in mammograms, *Pattern Recognition*, 42(6):1138-1148.

[6] Rangayyan, R.M.; Nguyen, T.M. (2005); Pattern classification of breast masses via fractal analysis of their conturs, *International Congress Series*, 1281:1041-1046.

[7] Dumitrache, I.; Buiu, C. (1995); Hybrid geno-fuzzy controllers, *IEEE Intelligent Systems for the 21st Century*, 5:2034-2039.

[8] Pandey, B; Mishra, R.B. (2009); Knowledge and intelligent computing system in medicine, *Computers in Biology and Medicine*, 39:215-230.

[9] Alpaydin, Ethem (2010); Introduction to machine learning, *MIT Press*, 2010.

[10] Drew, P. J.; Monson, J. R.T. (2000); Artificial neural networks, *Surgery*, 127:3-11.

[11] Marcano-Cedeno, A.; Quintanilla-Dominguez, J.; Andina, D. (2011); Breast cancer classification applying artificial metaplasticity algorithm, *Neurocomputing*, 74:1243-1250.

[12] Mofidi, R.; Deans, C.; Duff, M.D.; Beaux, A.C.; Brown, S. P. (2006); Prediction of survival from carcinoma of oesophagus and oesophago-gastric junction following surgical resection using an artificial neural network, *European Journal of Surgical Oncology*, 533-539.

[13] Hazewinkel, M. (1994); *Encyclopaedia of Mathematics* (set), Kluwer, ISBN 1-55608-010-7.

[14] Balanica, V.; Rae, W.I.D.; Caramihai, M.; Acho, S.; Herbst, C.P. (2009); Integration of image and patient data, software and international coding systems for use in a mammography research project, *World Academy of Science, Engineering and Technology*, 58:1002-1005.

INT J COMPUT COMMUN, ISSN 1841-9836
8(3):366-374, June, 2013.

Efficient Data Organisation in Distributed Computer Systems using Data Warehouse

S. Cosma, M. Văleanu, D. Cosma, G. Moldovan, D. Vasilescu

Smaranda Cosma
Faculty of Business, Babeş-Bolyai University,
Cluj-Napoca, Romania, Tel/fax: 0040-264-599170
E-mail: smaranda.cosma@tbs.ubbcluj.ro

Mădălina Văleanu, Dan Cosma, Dana Vasilescu
Faculty of Medicine, "Iuliu Haţieganu" University of Medicine and Pharmacy,
Cluj-Napoca, Romania, Tel/fax: 0040-264-207043
Email: drvasilescu@yahoo.com

Grigor Moldovan
Faculty of Mathematics and Computer Science,
Babeş-Bolyai University, Cluj-Napoca, Romania
Tel/fax: 0040-264-405300
E-mail: moldovan@cs.ubbcluj.ro

Abstract:
Databases represent a highly developed form of data organisation. The efficient use of databases by their beneficiaries is a permanent and stringent concern. The first part of the article presents a short development of the way data are organised and of the ways distributed databases can be optimised in computer networks. Then, two means for the efficient operation of distributed databases are shown. The last part of the paper evaluations of the architectures of some data warehouses (DW) and of their building are made. Using the data warehouse, a beneficiary can prepare in advance the required support to get reports and then make the right decisions in specific situations.
Keywords: Database, Distributed Databases, Relational Databases, Optimization Algorithms, Data Warehouse, Data Marts.

1 Introduction

Computer science has had a large contribution to the solution of issues from technical, scientific and economic fields, mainly with regard to the processing and managing of large volumes of data, such as those from economy, health and other fields. After the Internet has appeared, more and more distributed data processing systems have been designed and built. The computer-based data processing performance increased and large data volumes processing have expanded.

The *data* concept represents a basic concept always in the attention of the computer science experts. Data, whatever their nature, are identified by their *name*. The data as a notion has changed in meaning together with the development of the computer-related instruments and tools, especially due to the memorisation and access of the data found in various information supports. An efficient processing of data has always required some kind of data organisation, mainly when the information support used by computers is discussed. At the beginning, *isolated data* and grouped data stored in the internal memory of the computers were considered. Later on, economy-related applications have extended together with the opportunity to memorise data on external information supports; data could be organised under the form of *files*.

The processing of isolated or grouped data and that of files is achieved with the help of some software programs written in various automated programming languages, usually oriented to the

application type (technical, scientific, economic etc.). The volume of processed data increased, together with the requirements of the users from various fields to receive reports and statements. Under such circumstances, there occurred the need to distinguish data from their subsequent processing, data being still stored on certain data supports. It is under this circumstance that the notion of *database* issued. Every database has a name, used whenever one wants to access data from the database in question. Data can be isolated or grouped or file or a database itself, as each and everyone has a name to be accessed with. The software applications have also diversified. Operational software appeared to manage certain data permanently; they are today called *operational data* (for example: in banking and medical systems) and are distinguished from *persistent data* which can also be stored in certain databases. To organise databases, various models have been used and consequently, various classifications of databases exist. The most known model of databases is the relational model. A relational database is a set of tables (that is relationships in the mathematical meaning of the word) with a relatively simple structure, where every table is defined with a set of attributes.

The Internet allowed the design and definition of *distributed databases*. Until today, we speak about more kinds of databases: relational databases, distributed databases, temporal databases, logic-based databases, object-based databases, object - relational databases or Web-based or XML-based databases. XML databases are defined by attributes to which documents interpreted as a sequence of characters are associated (that is, given as value). To create, manage and query databases, specific instruments have been achieved, and they are easy to use, powerful, and highly performing as they need to give answers to extremely complex situations and questions. One of these instruments to create and query relational databases is represented by the *SQL* language with its different extensions. The new generations of databases, mainly those based on the Web or XML, have the tendency of being NoSQL [14].

At this moment, databases constitute a high level form of data organisation. Relational databases are widely spread as they have a simple representation module of the component data under the shape of tables (that is relationships in the mathematical meaning of the word). If for $\forall$ i $\in$ *{1, ... ,m}* , A_i represent attributes of an instance of an r database, and D_i is the domain of attribute A_i , then r $\subseteq D_1 \times D_2 \times ... \times D_m$. We agree to note with R($A_1, A_2, ..., A_m$) or R=($A_1, A_2, ..., A_m$), the scheme of r database. When the Internet was developed, the move to distributed databases was a natural one. Various means to extend and particularise databases were developed, and the majority of them started from relational databases. The hardware infrastructure also became more diverse when more and more high performance computer networks were installed. Different systems such as *Database Management Systems (DBMS)* are known today, built mainly on the relational model, for instance: DB2, Ingres, Informix, SQL Server, Oracle. Now the concern has moved to the architecture of databases, so that the use of databases can lead to more performance, mainly in the operation of systems of databases (with main components: data, hardware, software and users) to *support decision-making processes*. The theoretical and practical research is oriented more to the internal structures of organising databases. The ANSI/SPARC architecture is reasonable for databases systems regarding three levels an internal level, a conceptual level and an external level (views of individual users).

2 Distributed databases

Distributed databases are part of a distributed system with a well-defined purpose. As a principle, a distributed database should be perceived by a user similarly to a non-distributed database. Processing data from distributed databases should consider the presence of a communications network which supposes new circumstances to be taken into account [2]. For this purpose, the Databases Management Systems have been extended to the distributed ones (DDBMS).

One of the most important issues, with respect to distributed databases, lies in minimising the number and volume of messages used in the network. That is why is significant to redistribute databases in the nodes of the communications network to get an efficient, if not optimal exploitation of the system. The query optimising process which requires distribution needs passing through two steps, a global and a local step. Also important are issues of propagating updates, recovery and concurrency control. Software making use of distributed databases are associated, in general, to a connecting graph defining the communications network. Be the network nodes *X={1,2,...,n}*, and the links among the nodes, respectively its arches, noted *U*, i.e. the connecting graph *G=(X,U)*. Let us note with B_i the database in node *i*, and with *B* the distributed database in all the nodes of the network considered, hence:

$$B = \{B_1, B_2, ..., B_n\}$$

Relational databases are defined by the relational schemes $B_i = (A_1^i, A_2^i, ..., A_m^i)$, where A_j^i, $j = \overline{(1, m)}$, $\forall$ i $\in$ *{1,2, ... ,n}* represent attributes.

The following refers to an operational distributed information system managing the databases in the nodes of the communications network defined by graph *G=(X,U)*. Through the DBMSs found in the nodes, computers are required services, respectively the databases in the network nodes are queried. Some of the nodes are under heavy stress, others are not so much under stress. To increase the efficiency of the information system a migration of the databases or of parts of them from the nodes under heavy stress to less stressful nodes could be useful. A balanced network nodes loading is a significant issue. The solving of the issue requires every node to send out and receive messages carrying information with respect to the number of queries in every node and to the number of nodes (databases) used. The number of these messages should be as small as possible. Every node *i* will contain information regarding the system loading. Let us suppose that for every node, the loading or request level or the number of queries is measured on a scale from *1*, that is *weak* load, to *p*, that is *heavy* load; we identify these pieces of information in node *i* with elements of the set Inc^i*=(1,2, ... ,p)* (Inc^i -node *i loading*). If *p=3*, we get the loadings: *weak, normal, heavy*, which some authors consider as sufficient.

Message migration together with databases (resources) always begins from the heavy loaded nodes towards the weak loaded nodes. A small number of messages exchange will occur in the nodes of the system under question until it reaches the desired equilibrium.

To make the distributed database exploitation more efficient, a balanced loading of the computer network should be provided, with some dynamic balance algorithms. The algorithm proposed by Suen and Wong [12] for distributed systems shall be adapted to the present situation.

In every node *i*, a piece of information regarding the nodes to which we *send out* query messages for the databases B_j in the nodes shall be preserved; the set of nodes is noted S^i . In the same node *i*, B_i database query messages *will be received* from a set of nodes noted R^i . It is obvious that $S^i \subseteq X, R^i \subseteq X$.

The two sets associated to node *i*, respectively S^i, R^i must satisfy some properties (constraints) to provide the operation of the efficiency algorithm of the database operated upon. These constraints, relative to S^i, are:

- Any of two distinct nodes $i, j \in X, i \neq j$ have at least one node to which they send messages, that is

$$S^i \cap S^j \neq \varnothing$$

- Whatever node *i*, this node is allowed to send a message to it and to receive a message from it, i.e. $i \in S^i \wedge i \in R^i$

- There is a property of equal responsibility for any $i \in X, i.e. |\{j/i \in S^j\}| = k$

- There is a property of equal work for any $i \in X$, i.e. $|S^i| = k$
- There is an optimal condition *N= k(k-1) + 1.*

The last two properties specify that every node i receives and sends out k messages to have an equal responsibility and work amount, so that the activities to be performed by the network nodes are in perfect balance.

The properties of R^i are written in the same manner, replacing S^i with R^i in the list above.

We will now present another approach regarding the efficient operation of a database distributed in the nodes of a computer network [10]. We consider that in graph *G=(X,U)*, we have a zoning made up of M components, if on the set of nodes X we have made a partition of M components noted $Z_i \subset X, Z_i \neq \varnothing, i = \overline{1,M}$ so that:

$$\bigcup_{i=1}^{M} Z_i = X \quad and \quad Z_i \cap Z_j = \varnothing, \forall i \neq j, i, j = \overline{1,M}.$$

We note $G_i = (Z_i, U_i),\ where\ U_i = \{u \in U | u \in Z_i \times Z_i\}, \forall i = \overline{1,M}$.

The purpose of this distribution of the databases on the M zones lies in getting a certain autonomy, as well as some constraints, hence a certain level of efficiency for their operation. We have in view the following properties:

- *equity;* following the loading in every node i, for a defined time interval, are determined statistically some weights h_i of services request offered in the nodes in question (for instance, a percentage of the number of queries of basis B_i, percentage of the number of messages received by node i, percentage of the use time for node i etc.). Hence, $\sum_{i=1}^{n} h_i = 1$.

Absolute equity for zone loading to fulfil the tasks will occur if the volume of the tasks for every zone will be $\frac{1}{M}$, i.e. $\sum_{j \in Z_i} h_j = \frac{1}{M}, i = \overline{1,M}$. A maximum deviation from the ideal value $\frac{1}{M}$ is accepted, though probably it will be difficult to meet, equal to $\alpha,\ 0 \leq \alpha \leq 1$. Hence, equity will exist if:

$$\left| \sum\nolimits_{i \in Z_j} h_i - \frac{1}{M} \right| \leq \frac{\alpha}{M}, \quad 0 \leq \alpha < 1, \quad 1 \leq j \leq M.$$

- *contiguity*; zone $G_i, i \in$ {1,2,...,M} is contiguous, if and only if this graph is connecting (there is a chain between any two of its nodes).

- *compactity*; zone G_i is compact if the shortest chain between any two nodes a and b from Z_j , $1 \leq j \leq M$, is smaller than or equal to a predefined constant, named exclusion distance.

- *exclusion of some enclaves;* an enclave is a node or a set of nodes that cannot form a zone if the criteria mentioned earlier are fulfilled.

We can achieve such zones with a not very complex algorithm and in the zones we can efficiently exploit the distributed database [11], [13].

3 Data Warehouse architecture and their efficiency

Data preservation without processing cannot be a purpose in itself. The applications of databases are numerous and for many domains. There are extremely many situations when databases are created as decision-making supports. Such situations can be encountered mainly when data refer to economy, though similar cases are applicable for health-related data or other fields. The volume of stored data on data supports has increased and continues to increase. During this development of information technology, the need to *restructure* data inside such supports for an efficient use has come up. The data collection sources are many-sided and their

structure is heterogeneous. This is due to the fact that the types of databases can vary and differ, as mentioned earlier.

The information systems designed many years ago showed to be unable to cope with such situations. Consequently, the reconsideration of the manner of data collection in a joint place and the processing of the mentioned data as decision making supports became a necessity. Such applications mainly appeared in the field of economics, as they could be used as two solutions to solve the difficulty. One of the solutions supposes the increase of computer technical performance, the other solution can be applied immediately and resorts to developing proper software for the purposes envisaged. The second direction underwent an avalanche of research and articles published in this domain.

The new concept regarding the management of large volumes of data as decision-making supports is represented by the *Data Warehouse* introduced by W.H. Inmon in 1992, which, in fact, is a special database, as also shown well in [3]. The simple idea consists in building warehouses as an intermediate form among various data sources, usually operational databases and selecting/extracting some subbases of special data of reasonable size from these warehouses. These special data subbases should serve as support for informing decision makers or for writing reports, research documents or other, in relation with the processed data. The decision in a company can be related to sales, customers, suppliers, finances, costs, profit, human resources, etc. [4]. In a hospital networks, they can refer to patients, medical staff, resources, medicines required, etc. This requires the division of the functional space of a data warehouse in three distinct areas: the data sources zone, in general, operational databases, but also other types of data received by means of other software, then the zone comprising data in the data warehouse, and the third area, the special data marts zone, which are used for analyses, reports drawing or forming the so-called data mining.

Data sources can be of different nature, different formats or different types. All the data will be subjected to significant preparation process before reaching the data warehouse. During the preparation process, through a well-defined selection - considering the objectives established for the use of the information system in question - there takes place *Data Cleaning, transformation and unification*. After *their loading*, they need to be refreshed and at each refreshing process, integrity, consistency and other constraints need to be provided to maintain a reasonable volume of data which are necessary to make a decision. We have mentioned earlier some of the features a data warehouse should possess. According to W.H. Inmon, a data warehouse is defined by enumerating its properties, that is:

Definition [8]: *Data warehouses are non-volatile data collections, oriented to the subject, integrated, variable in time and supporting the managerial decision making process.*

The creation of a *data warehouse* passes through the following:

{Data sours, ... , Data sours} → ECTL → Data Warehouse;

where *Data sours* represents operational databases or even data sources of other nature. Through a process of *Extraction, Cleaning, Transformation and Loading*, in brief *ECTL* (Extraction, Cleaning, Transformation and Loading) - a data base of uniform structure is developed, i.e. a *Data Warehouse* (DW). A *Data Warehouse* whose data cannot be modified (they can, however, be deleted) is formed of the following components: *(Heavily, slightly) Aggregated Data, Detailed data and Meta data*. A warehouse can be accessed only by repeated reading and can be used (distributed) to form some *views* representing data mart s to be used by decision makers.

Any standard architecture leading to the use of a data warehouse to make a decision in an organisation (for example, a company or a hospital) has the shape given in Fig.1.

When the data warehouse is distributed, then the middle part of the drawing above takes,

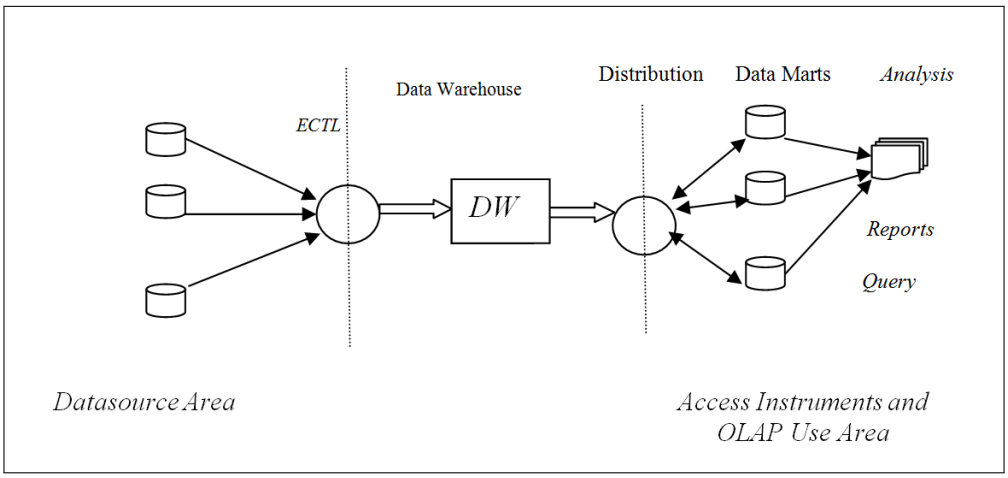

Figure 1: Architecture Standard Data Warehouse

in general, the shape below:

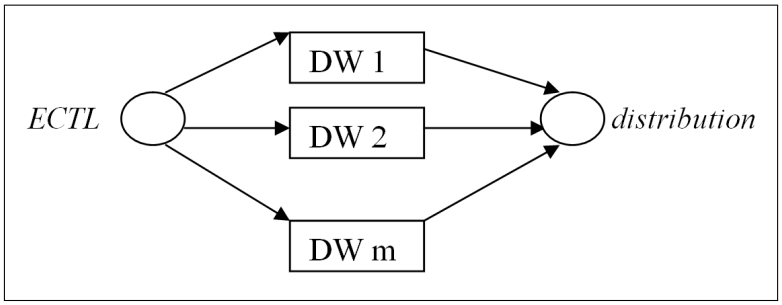

The loading of distributed data warehouses $DWi, i \in \{1,2, \ldots ,m\}$ uses any of the data sources to which some aggregation processes are applied, so that in Y, data will have a unitary structure. Let us note X the set of data sources, and Y the set of Data Warehouses $DW\ i$. The two sets have a application multivalued $f : X \to Y$.

For the destination area, in the drawing above, we can notice that the often mentioned data marts are highlighted. An analogous correspondence g exists between the Data warehouses set Y and the set Z of *Data Marts*, i.e. $g : Y \to Z$. It is possible to conceptually design directly a data mart from a source, such as *XML* as specified in [2], [7]. Though the term *data marts* is still disputed, we have chosen the definition below to be suitable for them:

Definition [2]: *We call a Data Mart a* ***specialised*** *data warehouse, oriented to the subject, including* ***volatile*** *integrated data, variable in time and being the subsupport for managerial decisions.*

In the destination area, specific technologies and instruments of processing data should be present. *OLAP (On-line Analytical Processing)* is the best known technology for the aggregation, access and use of data from a data warehouse, for the purpose of decision making. The term *OLAP* was proposed by Codd in 1993. *OLAP* operations with regard to multidimensional data (data cubes) are well-known. Let us mention the most significant of theme: *Roll-up, Drill-down, Slice, Slice-and-dice, Pivoting, Drill-across.*

In Fig. 1, a standard architecture of a Data Warehouse is given. The architectures are designed for organisations, having a well-defined purpose, and consequently, a specificity. It is always important that the architecture is less costly and more efficient for its users, possessing

certain hardware and software resources, while data, in general, are heterogeneous. Many authors (such as Jenning in 2011 [9]) specify that "the best solution for one enterprise is not necessarily the best for another". Optimal solutions are only for concrete situation. Anyway, the information systems designed for organisations for decision making purposes, based on Data Warehouse , have extended a lot. In Poland, for instance, as mentioned in [1] DW architectures are used in 20%, respectively 23% of cases for Data marts and only 7% Federal Architectures, from all the systems created in 2011.

The issue of preserving large volumes of data remains a constraint today, too. We will always want to use a smaller memory space. The model of *multidimensional tables* or *hypercubes* for data provides solutions to diminish the memory space. A *dimensional scheme* is made up of a factual table and more *dimensional tables* with connections established as keys. Such a multidimensional scheme can also be called *star-shaped scheme.* A theoretical example is illustrated in the drawing below.

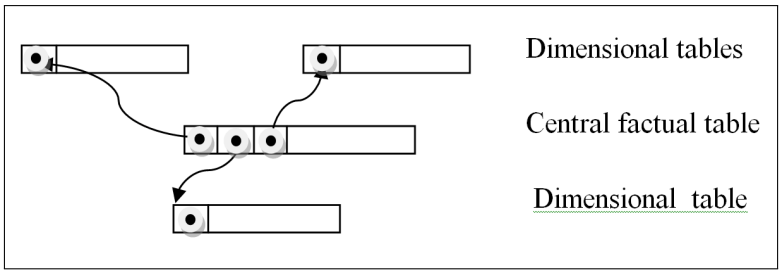

In the factual table given, at the beginning three attributes, in fact, keys, representing links to the three dimensional tables are found. The dimensional tables also contain keys under the same name of attribute, and the references are indicated by the three arrows. In the factual table, after the attributes-keys, other attributes are listed. The dimensional tables also contain a list of attributes after the key attribute.

In principle, when designing a DW, to produce factual schemes the following successive steps need to be followed: *building the attributes tree, cleaning and completing the attributes tree, specifying dimensions, measurements and hierarchies* [5]. When attributes are known from the operational databases schemes (dimensions, measurements, hierarchies), they are defined together with the final users. The conceptual factual scheme must be designed, definitely, before implementation. The effective scheme of a DW shall be a sum up of DM (Data Marts), data sources and profiles required by users. A DW design methodology such as the one based on the *Dimensional Fact Model* (DFM) should be useful as it proposes a formalisation of the diagrams E/R in a graph [5]. Using these elements, as the example above shows, one can built particular graphs, respectively *quasi-trees*, whose roots are facts; Golfarelli and Rizz acted in this manner in [5]. The majority of a DW elements, in our opinion, have a dynamic character and, in consequence, they should be considered cybernetic systems, where returns to the system under the form of feed-backs are admitted.

In order to select some options (actions) defining the conceptual schemes of data warehouses (DWs) and able to provide short time answers to queries made by users, some efficiency indicators can be used. Thus, such an evaluation used successfully in various domains is given below.

Be a set of options $A = \{a_1, a_2, ..., a_n\}$, their selection being made on the basis of well-defined criteria, forming set $C = \{c_1, c_2..., c_m\}$. Let us suppose that after evaluations, the level of influence of criterion c_i in the selection of option a_j with the value $q_i^{a_j}$, from a scale of values is known.

If we consider options a and b, in the mentioned order, from set A, we convene, to note with $p_i(a, b)$ the preference for option a versus b, a preference determined by criterion c_i. This degree

can be expressed as a percentage. If, for the two options a and b we take into account all the criteria c_i to select option a related to b, the result of the evaluation noted *r(a,b)* will be:

$$r(a,b) = \sum_{i=1}^{m} p_i(a,b) \cdot q_i^a$$

As every option a is compared to *n-1* options , a positive score for option a can be defined as $S^+(a)$ as well as a negative sc ore *S(a)*, as follows:

$$S^+(a) = \frac{1}{n-1} \sum_{x \in A} r(a,x) \quad ; \quad S^-(a) = \frac{1}{n-1} \sum_{x \in A} r(x,a)$$

The positive score of option a represents the maximum global influence of option a versus the rest of options, while the negative score of option a represents its minimal global influence. In this way, we will associate a *full degree* to each option a from set A as follows:

$$S(a) = S^+(a) - S^-(a)$$

Based on these indicators, we can define efficient conceptual schemes for DW and MS. For Data Marts constitution, option groupings following given criteria can also be useful.

4 Conclusions

It is obvious that high performance DW architectures are desired, as they could be capable to give answers at the shortest time and expense to various queries found in an organisation. As this paper shows, this optimisation can be performed only in exact and concrete environments, through successive improvements and applying various methods, among which those presented here. A high performance DW architecture depends on the computer network involved, on the concept schemes defined, including multidimensional tables, respectively hypercubes, on the quality of the software used as well as the *OLAP* processing.

Bibliography

[1] M. Alsqour, K. Matouk, M.L. Owoc, A survey of data warehouse arhitectures - preliminary results, *Proc.of the Federated Conference on Computer Science and Information Systems*, 1121-1126, 2011.

[2] C.J. Date, *On Introduction to Database Systems*, 8th Edition. Pearson Education Inc, Addison Wesley Higher Education, 2004.

[3] F.G. Filip, Decizie asistata de calculator. Concepte, metode si tehnici pentru deciziile centrate pe analiza datelor, *Rev. Informatica Economica*, 4(16):8-22, 2000.

[4] D. Fusaru, Z.Gherasim, I. Lungu, A. Bara, Tehnici si arhitecturi pentru micsorarea timpului de raspuns in sistemele cu depozite de date (Data Warehouse), *Analele Universitatii Spiru Haret. Seria Economie*, Ed. Fundatia Romania de maine, Bucuresti, 4(4):419-426, 2004.

[5] M. Golfarelli, S. Rizz: A Methodological Framework for Data Warehouse Design. In: *Proceedings ACM First International Workshop on Data Warehousing and OLAP (DOLAP)*, Washington, pp. 3-9, 1998.

[6] M. Golfarelli, S. Rizzi, E. Turricchia, Modern Software Engineering Methodologies Meet Data Warehouse Design: 4WD. In *13th International Conference on Data Warehousing and Knowledge Discovery (DaWaK 2011)*, pp. 66-79, Touluse, France, 2011.

[7] M. Golfarelli, S. Rizzi, B. Vrdoljak, Data warehouse design from XML sources, *Proceedings ACM Third International Workshop on Data Warehousing and OLAP (DOLAP'01)*, Atlanta, pp. 40-47, 2001.

[8] W.H. Inmon, *Building the Data Warehouse*, Third Edition. Pub. John Wiley&Sons, Inc. USA, 2002

[9] C.Jennings, L. Tristan, The Perils of Over Complicating Data Warehouses How Avoiding Unnecessary Complexity Con Provide Satisfaction and Savings, *Business Intelligence Journal*, 16(2):39-43, 2011.

[10] G. Moldovan, M. Valeanu, The Performance Optimization for Date Redistributing System in Computer Network, *INT J COMPUT COMMUN*, Vol.1, Supplementary Issue, 1(S):470-473, 2008.

[11] G. Moldovan, O problemă de redistribuire a serviciilor într-un sistem partiţionat în zone distincte după anumite criterii. "Babeş-Bolyai" University Cluj-Napoca, Fac. Math. and Computer Sci., *Res. Sem. Preprint*, no.5, 5-8, 1993.

[12] T.T.Y. Suen, J.S.K. Wong, Efficient Task Migration Algoritm for Distributed Systems, *IEEE Transactions on Parallel and Distributed Systems*, 3(4):488-499, July 1992.

[13] M. Valeanu, S. Cosma, D. Cosma, G. Moldovan, D. Vasilescu, Optimization for Date Redistributed System with Applications, *INT J COMPUT COMMUN*, 4(2):156-161, 2009.

[14] EG. Ularu, F. Puican, Noua generatie de baze de date NoSQL. *Rev. Romana de Informatica si Automatica*, Vol.22, no.4, 2012

INT J COMPUT COMMUN, ISSN 1841-9836
8(3):375-383, June, 2013.

Actuality of Bankruptcy Prediction Models used in Decision Support System

M. Crăciun, C. Raţiu, D. Bucerzan, A. Manolescu

Mihaela Crăciun, Dominic Bucerzan
"Aurel Vlaicu" University of Arad
Faculty of Exact Sciences
Department of Mathematics-Informatics
România, 310330 Arad, 2 Elena Drăgoi
E-mail: qbt@rdslink.ro, dominic@bbcomputer.ro

Crina Raţiu
DARAMEC srl, Arad
România, Sofronea FN
E-mail: ratiu_anina@yahoo.com

Adriana Manolescu
Agora University, Oradea, Romania
Piata Tineretului nr.8, 410526
E-mail: adrianamanolescu@univagora.ro

Abstract:
In the current conditions, the global economy is in a crisis situation. In terms of crisis management this article supports the Romanian companies. This article analyses some classical bankruptcy prediction models used in Decision Support Systems in order to validate or invalidate them in the actual Romanian economical conditions. It is essential to take the right decision at the right time, to help the company overcome an eventual moment of crisis, such as insolvency or even bankruptcy. Our study is based on the financial ratio of 60 Romanian companies, between 2005 and 2009. The firms are classified in two categories: bankrupted companies (B) and non-bankrupted companies (N-B).
Keywords: bankruptcy prediction models - BPM, multiple discriminant analysis - MDA, decision support system - DSS, crisis management

1 Introduction

The economic crisis initially appeared in 2007, in the United States of America and Japan. It expanded to almost every country, becoming a global phenomenon, whose negative outcomes are also present in the Romanian economy. The crisis is the consequence of an economic boom, which lasted over 25 years and it emerged when Japan and the United States began to reduce interest rates to avoid recession, measure that lead to the increase of the asset price worldwide.

This article analyses some classical bankruptcy prediction models used in Decision Support Systems in order to validate or invalidate them in the actual Romanian economical conditions.

Here are a few aspects that triggered the economic crisis of 2008:

- February 1, 2007 – The law of increasing the minimum wage was passed (Fair Minimum Wage Act of 2007) fact that blocked investments and by default, loans;
- February 17, 2007 – British bank Northern Rock is nationalized;
- September 7, 2008 – the largest mortgage banks in the United States - Freddie Mac and Fannie Mae - are placed under federal supervision;

- September 16, 2008 – U.S. central bank Federal Reserve and U.S. government nationalized the largest insurance group in the world, American International Group (AIG), threatened with bankruptcy, and brought in aid of 85 billion;
- September 28th – Fortis Group is nationalized by the authorities of Netherlands, Belgium and Luxemburg, to avoid closing down;
- October 13th – Great Britain nationalized three banks: Royal Bank of Scotland (HBS), Lloyds and HBOS;
- December 1, 2008 – U.S. announces that it was a year in recession.

The economic crisis in Romania is mainly a domestic crisis caused by bad macroeconomic policies mix from recent years. The economic growth appears to be unhealthy because the domestic growth relied on consumption financed by debt. The flax tax of 16% has stimulated consumption, which was assured by imports and did not lead to the increase of production capacity of Romanian companies. Variants had to be found to stimulate domestic production and exports. Most consumption credits went to imports [8]. Vulnerabilities of an unbalanced economy, with many delayed structural reforms have now become obvious. The risk of bankruptcy is present and it grows. Considering this aspect, analysis of 165 bankruptcy prediction studies published from 1965 till present reveals trends in bankruptcy prediction models development. [7].

It is important that the difficulties in discharging obligations and the economic and financial structural fragility should be determined at an early stage in order to avoid the bankruptcy by declaring insolvency. The state of insolvency can be defined as an inability of companies to deal with outstanding payments, i.e. their inability to repay the borrowed sums on time as determined by mutual agreement with third parties under an economical contract or credit [9].

Even if the terms bankruptcy or failure are used to describe the different situations of companies in difficulty, it should be noted that bankruptcy is a process that begins financially and ends legally. In the following we intend to tap the first part of the statement.

It is hard to say precisely when the bankruptcy occurs. Current experience in bankruptcy prediction is based on several studies beginning with the Anglo-Saxon School (1960 - 1999), continuing with the Continental School who has made his mark between the years 1976 - 1999 and last, but not the least, the Romanian Schools 1996 to 2000. A reference model of the Anglo-Saxon School is the "Altman Model" while the "Anghel Model" represents the Romanian School. There were several methods to detect financial difficulties of the company. Altman and Anghel Models are based on the starting rates method for detecting financial difficulties of the enterprise. One of the important reasons in using the rates method is linked to the theoretical and practical developments that found connections between analysis using financial ratios and statistical techniques [1]. With financial ratios, we can compare the profitability of different sized companies from different branches [2]. Risk of bankruptcy can be determined by the so-called method of scoring. This is based on statistical techniques of discriminant analysis (DA). The score, as final of discriminant analysis, represents a method of diagnosis that consists in measuring and interpreting the future economic risks for the company. The method uses a group of significant financial ratios, resulting mainly from the annual financial statements.

2 Description of the Altman model (1968)

Altman is a reference name cited in studies concerning the prediction of bankruptcy. The model proposed by Altman considers a number of 22 potential variables (based on annual financial statements) grouped into five categories: liquidity, profitability, debt, solvency and activity.

In an article published in 1968 [1], Altman commented upon the traditional indicators and concludes that the analysis made by the researchers were unable to establish the relevance of the indicators. Altman describes how he uses statistical techniques and discriminant analysis (DA) to develop a model of financial indicators that provide enterprise bankruptcy.

In the model development, Altman has selected a group of 33 companies with financial problems; the sample included industrial (manufacturing) companies. Healthy business group companies were selected by the principle of similarity, to each of the bankrupt companies (size, industry, etc.) corresponded a healthy firm. From the initial list of 22 indicators, the author chooses the five most significant.

The first model built by Altman includes five variables, each having attached weights.

$$Z = 1.2X_1 + 1.4X_2 + 3.3X_3 + 0.6X_4 + 1.0X_5 \tag{1}$$

Where :

- X_1 = working capital/total assets,
- X_2 = retained earnings/total assets,
- X_3 = earnings before interest and taxes/total assets,
- X_4 = market value equity/book value of total liabilities,
- X_5 = sales/total assets,
- Z = overall Index or Score.

To make the model operational, the two groups of companies were analyzed and classified by Z score size, setting the two limits and the uncertainty (area between the two limits).

Altman's model works based on the following decision rules:

- $Z \leq 1.8 \Rightarrow$ imminent bankruptcy situation, the company is likely headed towards bankruptcy;
- $1.8 < Z < 2.99 \Rightarrow$ uncertainty;
- $Z \geq 2.99 \Rightarrow$ good financial situation, solvent companies; the firm is most likely safe based on the financial data. Of course, mismanagement, fraud, economic downturns and other factors may cause an unexpected reversal.

Later, Altman refined the model, the aim was to reflect, through the financial information the economic reality of the companies. He modified the variable X_4 substituting the market value with the book values of equity [4].

The following score function was obtained:

$$Z\prime = 0.717X_1 + 0.847X_2 + 3.107X_3 + 0.420X_4 + 0.998X_5$$

The decision rules changed as followed:

- $Z\prime \leq 1.23 \Rightarrow$ imminent bankruptcy situation;
- $1.23 < Z\prime < 2.90 \Rightarrow$ uncertainty;
- $Z\prime \geq 2.90 \Rightarrow$ good financial situation.

Finally, from its previous models, which include a variable sensitive to the type of industry (X_5 = sales/total assets), Altman reviews the score function, retaining only four variables:

$$Z'' = 6.56X_1 + 3.26X_2 + 6.72X_3 + 1.05X_4 \ .$$

The decision rules became:

- $Z'' \leq 1.1 \Rightarrow$ imminent bankruptcy situation;
- $1.1 < Z'' < 2,6 \Rightarrow$ uncertainty;
- $Z'' \geq 2,60 \Rightarrow$ good financial situation.

3 Description of the Anghel model (2000)

The "Anghel Model" is the recent model developed by the Romanian School and it consist in building the function score model for the Romanian economy on multiple discriminant analysis (MDA). The score function consists of four variables, four parameters and one constant. To obtain the score function Anghel proposed the fallowing steps.

First step – Choosing the sample of companies divided in two groups: N-B group–companies without financial problems and B group - failed companies. His study is based on a sample of 276 companies from 12 branches of national economy. The companies were selected randomly. The information for each enterprize was taken from the annual financial statements for the period between 1994-1998.

Step 2 – A comparison is made over time period based on a set of significant indicators for the two groups of companies. Anghel analysis 20 financial indicators to see which of them covers a particular interest for the companies and divides them in: rates of activity, rates of liquidity, rate debt, rates of return and other economic and financial information.

Step 3 – Selecting indicators that make the best discrimination. Following the selection phase he chooses the following four financial variables: revenue performance, coverage of debt to cash flow, leverage the asset and period for payment of obligations.

- X_1 – earning after taxes/incomes;
- X_2 – Cash Flow/total assets;
- X_3 – liability/total assets;
- X_4 – (liability/sales)·360 .

Step 4 – Development through discriminant analysis technique of A linear combinations of relevant indicators X_i. In case of the two groups of previous assumptions there is a function representing the best discrimination B versus N-B. Based on economic and financial information since 1998 for a total of 276 Romanian companies it was build the A score function:

$$A = 5.676 + 6.3718X_1 + 5.3932X_2 - 5.1427X_3 - 0.0105X_4 \ . \tag{2}$$

Step 5 – Choosing a point (or points) of inflection which makes predictive classification of companies in the two groups. Computing the A score for each enterprize from the sample and sorting ascending the information obtained for the A score results a situation for all companies.

Step 6 – A-priori analysis of the success rate of A score by comparing the predictive classification with the known situation of companies in the sample. The assessment is based on the following classification:

- $A \leq 0 \Rightarrow$ imminent bankruptcy situation;
- $0 < A < 2.05 \Rightarrow$ uncertainty;
- $A \geq 2.05 \Rightarrow$ good financial situation.

Step 7 – A-posteriori analysis of the success rate of the function A by analyzing the degree of relevance for another sample of companies.

A sample of companies was considered, separated in the two groups B and N-B, and the subject of analysis was the prediction accuracy that the function A performs. The sample used to validate the proposed model includes 55 companies, 28 from the N-B and the other 27 from group B. Companies in the test sample were similar in size and industry sectors with the initial sample.

Under these conditions the prediction success rate similar to the a-priori, the author report a prediction with the value of 97.8%. This allowed the assessment that the score A was effective and could be applied to companies in the Romanian economy (retaining the limits in order to built the model).

4 The applicability of the Anghel and Altman models in the actual crisis conditions

In this paper we test the suitability of the statistical models in key economic context changes during the period between 2006 and 2010. Our hypothesis is that the functionality of the models of a previous period is questioned by the specific economic conditions in a time of crisis.

To test the applicability of the models in the actual economic conditions we proceed as follows.

First of all, we select groups of companies. Companies were chosen from a population of 200 Romanian companies, at random. The data collected is real; the Romanian companies used in our study exist and operate. We worked with a sample of 60 companies classified into two groups:

- Group 1 – non-bankrupt companies, see table position 1-30;
- Group 2 – bankrupt companies, see table position 31-60.

Analysis retains information for 2005-2009.

The second step is related to the classification of the companies presented in table. Classification was done according to the indicators resulting from the annual financial statements.

The next step consisted in computing the financial ratios of companies.

In the Anghel prediction model, we used the following indicators:

- X_1 – earning after taxes/incomes;
- X_2 – Cash Flow/total assets;
- X_3 – liability/total assets;
- X_4 – (liability/sales)·360 .

In the Altman prediction model we used as statistical indicators the following:

- X_1 = working capital/total assets,
- X_2 = retained earnings/total assets,

- X_3 = earnings before interest and taxes/total assets,
- X_4 = market value equity/book value of total liabilities,
- X_5 = sales/total assets

In this paper we test two models listed as: the Altman prediction model which is a reference model in the literature and the Anghel bankruptcy prediction model which is the latest Romanian model.

As a next step we calculated the score functions from the two prediction models, as follows:

- the Angel's score function (2);
- the Altman's score function (1).

Please note that the calculation of coefficients in the Anghel model was performed according to the author notes [5]. The model coefficients in Altman's model were calculated according to his details [1].

For the table the meaning of the heading table is the following:

- Year - represents the year for which the prediction is made;
- P - the current situation (related to year 2009) for the company: N-B or B;
- ET/I - represents the ratio Earning after Taxes / Incomes;
- CF/TA - represents the ratio Cash Flow / Total Assets;
- L/TA - represents the ratio Liability / Total Assets;
- (L/S)·360 - represents the ratio (Liability/Sales)·360;
- A - represents the results of the Anghel score function;
- AN - represents the prediction of Anghel's model;
- Z - represents the results of the Altman score function;
- ALT - represents the prediction of Altman's model.

In columns AN and ALT the symbol "U" represents uncertainty.

No.	Year	P	ET/I	CF/TA	L/TA	$(L/S) \cdot 360$	A	AN	Z	ALT
1	2006	N-B	0.356	0.029	0.765	777.708	-4	B	2	U
2	2009	N-B	0.001	0.205	0.786	181.925	1	U	2.4	U
3	2009	N-B	-0.026	-0.002	0.903	729.009	-7	B	2	B
4	2009	N-B	-0.444	0.008	1.168	1078.548	-14	B	0	B
5	2008	N-B	0.053	0.255	0.987	76.220	2	U	9	N-B
6	2009	N-B	-0.379	-0.006	1.342	1031.039	-15	B	0	B
7	2009	N-B	-0.562	0.019	1.403	855.857	-14	B	0	B

8	2008	N-B	0.307	0.987	0.107	13.907	12	N-B	11	N-B
9	2008	N-B	0.038	0.462	0.738	45.367	4	N-B	5	N-B
10	2009	N-B	-1.673	-0.047	0.997	2871.865	-41	B	0	B
11	2006	N-B	0.043	0.001	1.175	770.832	-8	B	2	B
12	2009	N-B	0.255	-0.002	0.142	214.982	4	N-B	4	N-B
13	2005	N-B	0.026	0.001	0.316	322.215	1	U	3	U
14	2009	N-B	-0.502	-0.006	1.590	1170.032	-18	B	0	B
15	2009	N-B	-1.410	-0.027	2.654	1219.977	-30	B	-4	B
16	2009	N-B	-0.039	0.000	1.166	692.457	-8	B	1	B
17	2009	N-B	0.013	0.011	1.474	533.522	-7	B	2	U
18	2009	N-B	-2.576	0.032	1.498	2710.456	-47	B	-1	B
19	2009	N-B	-0.492	0.139	1.675	425.326	-10	B	0	B
20	2009	N-B	-0.073	-0.005	1.550	266.427	-6	B	2	U
21	2009	N-B	0.011	-0.007	0.996	260.631	-2	B	2	U
22	2005	N-B	-0.947	0.165	0.575	16249.367	-173	B	1	B
23	2008	N-B	0.550	0.994	0.049	10.577	14	N-B	16	N-B
24	2006	N-B	0.030	0.149	0.474	41.178	4	N-B	5	N-B
25	2006	N-B	0.378	-0.047	0.356	331.038	3	N-B	3	U
26	2009	N-B	0.028	0.004	1.295	156.400	-2	B	4	N-B
27	2006	N-B	0.070	0.155	0.590	124.184	3	N-B	3	U
28	2006	N-B	0.012	-0.001	0.130	141.843	4	N-B	5	N-B
29	2009	N-B	-0.806	-0.113	5.977	935.200	-41	B	-7	B
30	2008	N-B	0.126	1.486	0.128	6.800	14	N-B	7	N-B
31	2006	B	0.204	0.108	0.757	546.183	-2	B	1	B
32	2008	B	-0.104	-0.005	1.078	497.157	-6	B	1	B
33	2008	B	-111.611	-0.036	1.404	227585.775	-3103	B	-1	B
34	2008	B	-0.564	0.108	13.052	745.531	-72	B	-6	B
35	2008	B	-0.304	-0.001	0.784	260.837	-3	B	0	B
36	2009	B	-0.082	-0.045	1.911	732.504	-13	B	-2	B
37	2008	B	-0.043	0.000	1.014	455.619	-5	B	1	B
38	2009	B	-0.086	0.157	1.086	336.851	-3	B	1	B
39	2007	B	-1.741	-0.001	1.294	2209.021	-35	B	-1	B
40	2009	B	-0.154	0.084	1.207	551.230	-7	B	1	B
41	2005	B	-4.503	0.277	4.306	1892.400	-64	B	-11	B
42	2008	B	-1.101	0.727	10.073	6276.031	-115	B	-10	B
43	2009	B	0.006	0.291	0.994	520.669	-3	B	1	B
44	2007	B	0.017	0.001	0.985	423.434	-4	B	1	B
45	2007	B	-0.478	-0.212	1.051	1921.361	-24	B	0	B
46	2008	B	0.136	-0.002	2.317	347.256	-9	B	0	B
47	2009	B	-3.694	-0.050	0.906	6164.473	-88	B	-1	B
48	2008	B	0.066	0.019	0.502	259.779	1	U	2	B
49	2008	B	-0.055	0.000	1.082	254.628	-3	B	1	B
50	2009	B	-0.121	-0.016	1.216	288.245	-4	B	1	B
51	2009	B	-0.359	-1.091	1.999	257.014	-15	B	-0.358	B
52	2008	B	-190.552	-3.129	9.518	60004.8	-1904	B	-36	B
53	2008	B	0.437	0.025	0.591	955.082	-4	B	1	B
54	2008	B	0.124	0.001	0.873	327.058	-1	B	2	B
55	2009	B	-1.997	0.000	1.428	3233.721	-48	B	-1	B
56	2006	B	-1.431	-0.022	6.249	3129.140	-69	B	-5	B

57	2007	B	-0.122	-0.093	2.037	843.028	-15	B	1	B
58	2009	B	-1.765	-0.021	1.135	770.342	-20	B	-2	B
59	2006	B	-4.244	0.004	2.467	2624.353	-62	B	-5	B
60	2009	B	-5.192	1.024	3.639	2469.939	-67	B	-7	B

After processing the data presented above, we obtained results about the success rates of the prediction models and types of errors that appear in the analysis. We processed the data in order to obtain the prediction both with Anghel's and Altman's model. We obtained the following success rates for the total sample: in Anghel's case we got a success rate of 63.33% and in Altman's model the success rate was 65%. Both rates are unsatisfactory when compared to the success rates reported in initial studies. Anghel's model report a success rate greater than 97% and in the Altman's model the success rates were: 93.9% for N-B companies and 97% for B companies.

Note that, due to the dynamic economy, the success rate obtained with Anghel's model drops from 97% to 63.33%. This leads to the idea that scoring function built in year 2000 cannot accurately predict the health of the company in the present.

In case of the success rates for N-B companies the rates obtained are unsatisfying. In the Anghel model the success rate is 30% while the Altman's model for N-B yields a success rate of 30%.

The next result is related to the analysis of error rates for the companies in the sample, by applying the two prediction models. Here we refer to "type I" errors (B companies classified as N-B) and "type II" errors (N-B companies classified as B). This error classification is done according to [9]. "Type II" errors are less significant. After the analysis, from Anghel's model we obtained "type I" errors 0%, "type II" errors 60% and total errors 30%. In the Altman model we obtained the following results: 0% for "type I" errors, 43.33% for "type II" errors and 21.67% for total errors.

5 Conclusion and Future Works

The changes from the economic and social life such as the inflationary phenomena, the increased competition, the technological progress, the political environment and the economic and financial crisis, more or less influence the business outcome that is always subjected to different risks: financial policy risk, operational risk, and the risk of bankruptcy.

Analysis of accuracy of the bankruptcy prediction models suggests that multivariate discriminant analysis and neural networks are the most promising methods for bankruptcy prediction models [7].

The Altman study included a sample of 66 companies, 33 in each group. The bankrupt group (group 1) recorded failure during 1946-1965. Average assets of the sample companies were $ 6.4 million, with values between $ 0.7 million and $ 25.9 million. The non-bankrupt group (group 2) includes companies with assets between $ 1-25 million, which continued to operate in year 1966, too. The period considered for analysis was 1946 - 1965 (20 years) [3]. The source of information was Moody's Industrial Manual.

The Anghel study of building A score for the Romanian economy is based on a sample of 276 companies from 12 branches of national economy. Companies were selected randomly. The information for each company was taken from the annual financial statements for the period between 1994 and 1998. In the verification sample the success rate was 97.8%.

The models presented in this paper obtained a satisfying result for the economic period in which the models were developed. But taking into consideration our study on a sample of

companies from the present unstable economic environment we cannot recommend to use the two models mentioned above as a tool for predicting bankruptcy.

A well designed decision support system is a must have tool in the success of any enterprise. This aspect is very important considering the current economic crisis. For this purpose, our article analyses some classical bankruptcy prediction models used in Decision Support Systems in order to validate or invalidate them in the actual Romanian economical conditions.

Taking into consideration the conclusions of this study, our future work will focus on updating the score function proposed by Anghel and Altman to the current economic conditions. The purpose is to obtain an external diagnostic method that predict the risk to which the investor, the creditor and the company are exposed and ensures an optimal relation between outcome and risks on the Romanian economic market environment.

Bibliography

[1] Altman, E.I.: Financial Ratios, Discriminant Analysis and the Prediction of Corporate Bankruptcy, *Journal of Finance*, September, 589-609, 1968.

[2] Pinches G., Eubank A., Mingo K. and Caruthers K.: The Hierarchical Classification of Financial Ratios, *Journal of Business Research*, 1975.

[3] Altman, E.I.: *Credit Rating: Methodologies, Rationale and Default Risk*, London Risk Books, 2002.

[4] Altman E.I., Haldemon R. and Narayama P.: Zeta Analysis, *Journal of Banking and Finance*, 89-108, June 1977.

[5] Anghel, I.: *Falimentul - Radiografie şi Predicţie*, Ed. Economică, Bucureşti, 2002.

[6] Szenteşi, S., Lile, R., Rusu, S., Csorba, L. and Bălan, L.: *Statistică Economică*, ediţia a III-a, Ed. Universităţii Aurel Vlaicu, Arad, 2011.

[7] Bellovary J., Giacomino D., Akers M. :A Review of Bankruptcy Prediction Studies: 1930 to Present, *Journal of Financial Education*, Vol. 33 (Winter 2007).

[8] Voinea, L.: *Criza economica interna: cauze si solutii 23 nov 2008* http://www.zf.ro/opinii/criza-economica-interna-cauze-si-solutii-3544642.

[9] Pisleag, A.: The Importance of Assessing the Risk of Bankruptcy Under the Current Global Crisis, *Bulletin of the Transilvania University of Brasov*, Vol. 3 (52) - 2010 Series V: Economic Sciences http://but.unitbv.ro/BU2010/Series%20V/BULETIN%20V%20PDF/291%20Pisleag.pdf.

INT J COMPUT COMMUN, ISSN 1841-9836
8(3):384-394, June, 2013.

An Agent-Based Solution for the Berth Allocation Problem

C. Cubillos, R. Díaz, E. Urra, D. Cabrera-Paniagua, G. Cabrera, G. Lefranc

Claudio Cubillos, René Díaz, Enrique Urra,
Guillermo Cabrera, Gastón Lefranc
Pontificia Universidad Católica de Valparaíso
Av. Brasil 2241, Valparaíso, Chile
claudio.cubillos@ucv.cl, imrede@gmail.com, enrique.urra@gmail.com,
guillermo.cabrera@ucv.cl, glefranc@ucv.cl

Daniel Cabrera-Paniagua
Escuela de Ingeniería Comercial
Universidad de Valparaíso
Pasaje La Paz 1301, Viña del Mar, Chile
daniel.cabrera@uv.cl

Abstract: This work presents the development of MABAP, a decision support system based on the agent technology that helps in solving the problem of berth allocation for ships within a port. The Berth Allocation Problem (BAP) regards the logistics involved in planning and controlling the berthing of vessels. A software architecture in terms of agents is presented; Berths and Ships representing the actors in the system, BerthRequest and BerthPlanner as representatives of ships and berths in the planning process, and finally the Dock and Central agents representing the dock or pier. The architecture modeling was done using PASSI methodology for the design of agent-oriented systems, and the implementation was done in JADE, a Java-based development environment for multiagent systems. To validate the resulting support system, tests were carried out in which the user can choose different port-policy scenarios, ranging from maximizing vessels throughput to maximize berths use.
Keywords: Artificial Intelligence, Decision support system, Multiagent architecture, Ports planning.

1 Introduction

Maritime traffic is of significant importance to our country and the world, as reported by the United Nations Conference on Trade And Development (UNCTAD) [1], which places Chile in the Top 20 of container traffic. However, while container traffic has increased, the percentage of change from year to year has been declining and it is expected that this trend will continue. The latter, is largely due to the world economical state. Under such settings, an enormous potential can be developed through the optimization of related processes, obtaining competitive advantage in the market. The operations involved in maritime traffic and more precisely the activities carried out in ports are one of the most complex ones within the transportation industry. Such complexity is due to three reasons: 1) the wide variety of involved actors, 2) the interaction under a highly dynamic environment and 3) the distributed nature of the problem. Of the vast number of problems present in port logistics, there is one referred as the Berth Allocation Problem (BAP), which can be defined as a tactical planning problem, where the objective is to assign, ideally optimally, the position of ships inside the port for loading and unloading, so as to minimize the costs of container movements within the port. The problem, in the most complete form, involves two stages: A first stage of assigning the ships to each section of the port, and then a second stage of sequencing each vessel in the temporary space of the different sections. This work focuses on the second stage, considering the presence of only one big section in the

port and its further division into berths. Given the complex, distributed and dynamic nature of the problem, the use of multi-agent technology reveals useful to build a distributed software architecture and get a flexible, adaptable and robust decision support system solution capable to deliver a better quality of service together with attempting to obtain competitive results close to the pareto-optimal frontier. The main contributions of the present work are 1) to provide the design of a decision support system based on agent technology for the berth allocation planning, 2) provide a distributed planning process based on a greedy insertion heuristic solver [15] and the contract net protocol [4], and 3) provide an implementation of such and its validation through tests that show how diverse port policies can be chosen.

2 Multiagent Technology

In literature there is no exact definition of what an agent is. However, one of the most cited is Wooldridge's definition [2]: "An agent is a computer system located in an environment that is capable of performing actions independently to achieve its design goals". While this definition identifies some characteristics of an agent, it is not clearly distinguishable from a conventional distributed system. However, the main mentioned feature in which there is a consensus is autonomy. In the rest, there is often little agreement as many of the features have different relevance depending on the domains. For example, the characteristic of learning can be desirable for a certain application, while for another one it would not only be unimportant, but even undesirable. Despite the differences, one can forget about a precise definition in order to identify certain common properties, such as [2]:

- Autonomy: agents are capable of task selection, prioritization, goal-oriented behavior, and decision making without human intervention.
- Social ability: they can "contract" other components through some communication and coordination, and cooperation in solving any given task.
- Reactivity: they can perceive the context in which they operate and react appropriately.

Multiagent Systems

Multiagent architectures arise from the need to develop advanced complex applications consisting of a number of subsystems that interact to achieve distribute intelligence among various actors, giving rise to the creation of multi-agent systems (MAS). The use of a multiagent architecture appears as an appropriate solution when dealing with physically distributed problems, or where experience is required for integrating heterogeneous technologies or where the problem in question is defined on a computer network. The use of a multiagent architecture features in these cases as the most suitable alternative to leverage a distributed solution, adaptable to changes in structure and environment. In addition, an associated approach will build a total system from different autonomous units.

In a MAS, subsystems are defined with absolute local decision-making, and therefore a definition of policies to cooperate, negotiate and coordinate their actions is necessary. Therefore we can find different types of agents according to their capabilities [8].

The PASSI Methodology

PASSI (a process for Agent Societies Specification and Implementation) [3] is a step-by-step methodology that allows to go from the requirements to the system code. Aimed at designing

and developing multi-agent societies, it integrates design models and concepts from software engineering and object-oriented multi-agent systems using UML notation. Thus allows providing the engineering formalism required in such systems' design. The PASSI methodology consists of five phases at various design levels, and twelve steps in the process of building a multi-agent system. Examples of its use can be found in literature devoted to the design of a bookstore system [3], a virtual enterprise for transportation [16] and an open agent system [17], among others.

3 The Berth Allocation Problem

In container shipping, the Hub and Spoke model is widely adopted. The ocean-going ships, also called mother ships (mother vessels) operate between a limited number of transfer terminals (hubs). Smaller vessels (feeders) link the hubs to the other ports (spokes). In recent years, the mother vessels have increased markedly in size making transport up to 8000 TEU (Twenty foot Equivalent Units) and larger sizes are planned. Transshipment ports are large intermodal platforms and only a limited number of them handle a significant part of world traffic. However, when a ship arrives at a port, it must wait for a space to tie up to the dock. For this reason it has different sections, mooring points or Berths. In addition, there are Gantry Cranes available for loading/unloading and smaller vehicles for the rest of the transportation work, such as forklifts. Once docked at the berth, containers destined to the port must be unloaded and new containers directed to other ports must be loaded before the ship can continue its course. The demand on those ports for the load/unload procedure to run with maximum efficiency will become greater, as the shipping companies will continue to increase their fleet size and the capacity of new ships. The logistics involved in planning and controlling the docking of ships is called the Berth Allocation Problem (BAP). In the BAP, the port management should try that:

- The ships dock as soon as possible to ensure a rapid turnover.
- The forklifts load/unload the required containers in the shortest time possible.
- The cost of transshipment of containers is minimal.

A frequent problem associated with the latter has to do with the allocation of forklifts to each of the arriving ships, which is directly associated with the handling time and has a strong impact on the BAP, known as the Crane Scheduling Problem [5]. The problem can be represented in a two-dimensional space as shown in Figure 1, where the rectangles represent the ship whose dimensions are its length, including a safety margin and the handling time. These rectangles are positioned in the decision space without overlapping and meet certain restrictions. In the spatial dimension, there are restrictions on water depth (draft allowance) and the maximum distance in relation to the most favorable location along the pier, calculated considering the outbound-containers location and the space reserved for the inbound containers. In the temporal dimension, restrictions are expressed as time windows. Some of them are soft and can be relaxed by an appropriate penalty cost.

Related Work

In literature, many studies on the problem can be found. First, the BAP can be modeled in a discrete case if the dock is seen as a finite set of berths. In this case, the berths are described as fixed length segments or if the spatial dimension is ignored, as dots. When considering that the length of vessels is very variable, one could divide the dock in sections to make the assignment,

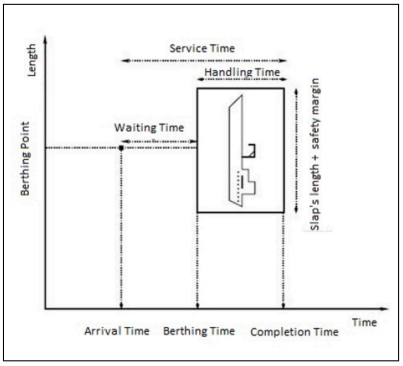

Figure 1: BAP two-dimensional (space vs. time).

although it would be difficult because the requirements vary dynamically. If large segments are used, space sub-use will happen in some cases, while smaller segments will make it difficult to find feasible solutions. To overcome this, a dynamic model is considered which defines that the ships can tie up anywhere in the dock. For the discrete case, the BAP can be modeled as an Unrelated Parallel Machine Scheduling problem [10], where each boat is seen as a work and each docking point as a machine. The time of arrival of each vessel is the release time of the work. In the continuous case, the BAP is a two-dimensional problem of the Cutting Stock Problem with additional constraints. In either case, BAP complexity turns out to be NP-hard [11]. In [12] has been proposed a dynamic formulation of the BAP or Dynamic Berth Allocation Problem (DBAP), which is represented as a finite set of docking berths and the arrival of the ships is considered random. In other words, the spatial dimension of the ships and berths is not considered. This formulation is called "dynamic" compared to the previous one called Static Berth Allocation Problem (SBAP) [13] which considers that all the ships are already in port when the berths are available. The SBAP can be solved in polynomial time with the Hungarian method proposed in [14], since it can be reduced to an assignment problem. For the DBAP, the authors take advantage of this feature and propose a Lagrange relaxation for reaching a desirable allocation sub problem. The computational results show that DBAP is relatively easy to solve while the cases are "close" to the static case, in the sense that most of the ships are already in port when the berths are becoming available. The objective function is the sum of service times of the ships and do not consider the existence of certain vessels priority over others. On the other hand, in literature there is no much research covering the BAP from a software architecture perspective, nor using agent technology as modeling paradigm. In the following are mentioned the two most relevant works in the area for the present research. The first is MADARP [6], an agent software architecture for the Dial-a-Ride Problem (DARP), because BAP can be seen as a Passenger Transportation Problem, in which ships correspond to passengers and the berths to the vehicles. MADARP architecture identifies different layers: interface, planning, service and ontology and agents associated with each of the actors involved: customers and vehicles. In [9] the work was further advanced and a novel solver for DARP was leveraged based on Genetic Algorithms. A second alternative found tackling partially BAP is [7], which proposes a multiagent architecture as solution to a port terminal operations automation problem. The system architecture divides the problem into sub-problems, which are determined by specific agents. However, the above solutions do not provide enough details on the solvers used and on how the resulting planning & control support systems aid port decision-makers to implement diverse planning policies according to their needs.

4 The MABAP Planning System

This chapter presents the functional specification of the multiagent decision support system and its technical design, in terms of software engineering artifacts. Regarding the BAP, some of the specifications for the requirements and restrictions considered for the problem are described in the following:

- It is considered the discrete case of the problem, in which the docking points are considered fixed in size and number.
- Each ship must have its ETA (Estimated Time of Arrival), the estimated processing time and allowed time windows for its processing.
- The berthing points have time windows that limit their availability.
- The implementation must consider the existence of dynamism, due to events that may occur, such as a ship's cancellation of arrival, delays and/or closure of any berth.
- The length of the ship must not exceed the length of the largest section in the dock.
- A section can only process the ships one by one, and as we know they should not overlap in the time-space diagram.

Proposed Multiagent Architecture

Figure 2 shows the proposed conceptual architecture, based on the MADARP architecture [6]. Therefore, the paper considers making an adaptation of this architecture to the particular problem of BAP maintaining its structure, leading agents to have similar functions, i.e. the vessels are considered as "clients" that request a service, not of transportation in this case but of a docking point assignment. On the other hand, berthing points or its subsections are considered as "vehicles" that offer a service, not of transportation but of vessels stowage. The following Figure 2 depicts the main agents of the MABAP architecture. In the first layer, Berth agents and Ship agents leverage as interface agents, plus the BerthPlanner and BerthRequest agents tackling the planning & scheduling tasks.

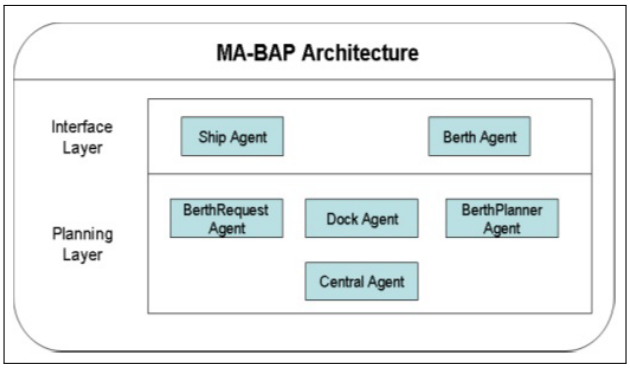

Figure 2: Multiagent Architecture for BAP.

There is also another agent called Dock agent, representing the management of the port company to act as intermediary between Berths and Ships. The Central Agent is a matchmaker, responsible for delivering the list of Berth agents that meet the requirements of a given Ship agent. The agents participating in the system and their main responsibilities are described in the following:

- Ship Agent: It is the one who communicates with the operator and takes the tasks of ship registering and the reporting of events that take place with the ship. It also initiates the docking process with a request, being entitled to cancel and change such request. The created requests are sent to the BerthRequest agent.
- BerthRequest Agent: This agent represents each ship in the negotiation process when requesting a new berthing point. It is responsible for receiving orders to process a new request and terminate its execution. Together with the Ship agent, they embody each of the vessels requiring stowage.
- Berth Agent: Represents each docking point or berth in the system, creating its corresponding BerthPlanner agent. It also manages the berth registration with the Central agent.
- BerthPlanner Agent: It corresponds to the planner agent for each docking point or berth. It keeps track of the ships stowage sequence and it is involved in the process of allocation of new docking points, evaluating the diverse berth requests from ships as they arrive. It also provides its actual schedule to other agents in the society upon request.
- Central Agent: Together with the Dock agent, this agent embodies the third main actor, the dock or pier. It keeps up a registry of the berths available at the dock and is responsible for providing the list of berths that happen to be candidates for a particular request coming from a ship.
- Dock Agent: This agent is devoted to manage the process of allocation of berthing points, handling incoming requests and initiating negotiations with the various berths of the dock.

The main interaction scenario (Figure 3) is when a ship calls for the allocation of a new docking point. The sequence starts with the ship which sends a docking request through the BerthRequest agent to the Dock agent. Such request has a profile, wherein the information includes the ship's name, its approximate time of processing and estimated dates (time) of arrival and departure.

The Dock agent sends the request to the Central agent, requesting a list of candidate sections that meet the profile of the request. The latter generates the list and sends it back to the Dock agent. The Dock initiates a contract-net [4] with the BerthPlanner agents; therefore, it sends a request for berthing to all the BerthPlanner agents from each of the sections in the matching list. These latter agents perform a greedy algorithm for evaluating the insertion of the new ship in its space-time diagram and send back a proposal profile.

From the arrived proposals, the Dock agent selects the best alternative according to its objective function (e.g. minimum total time of stay of the ship in port). Then, the agent communicates to the selected BerthPlanner agent to insert the ship in its sequence and informs the other BerthPlanner agents the rejection of its proposals. Finally reports the ship agent on the result of its request.

5 Insertion Algorithm

Within the MABAP system, the evaluation of the inclusion of a new ship into a berth sequence and to choose within the proposals from each berth which is most suitable, are the fundamental objectives of the problem and, therefore, a key aspect of the application implementation. The algorithm used in the application is based on the insertion heuristic proposed by Jaw et al. [15] for the DARP problem, and used on a past research [9] which has been adapted to fit the BAP

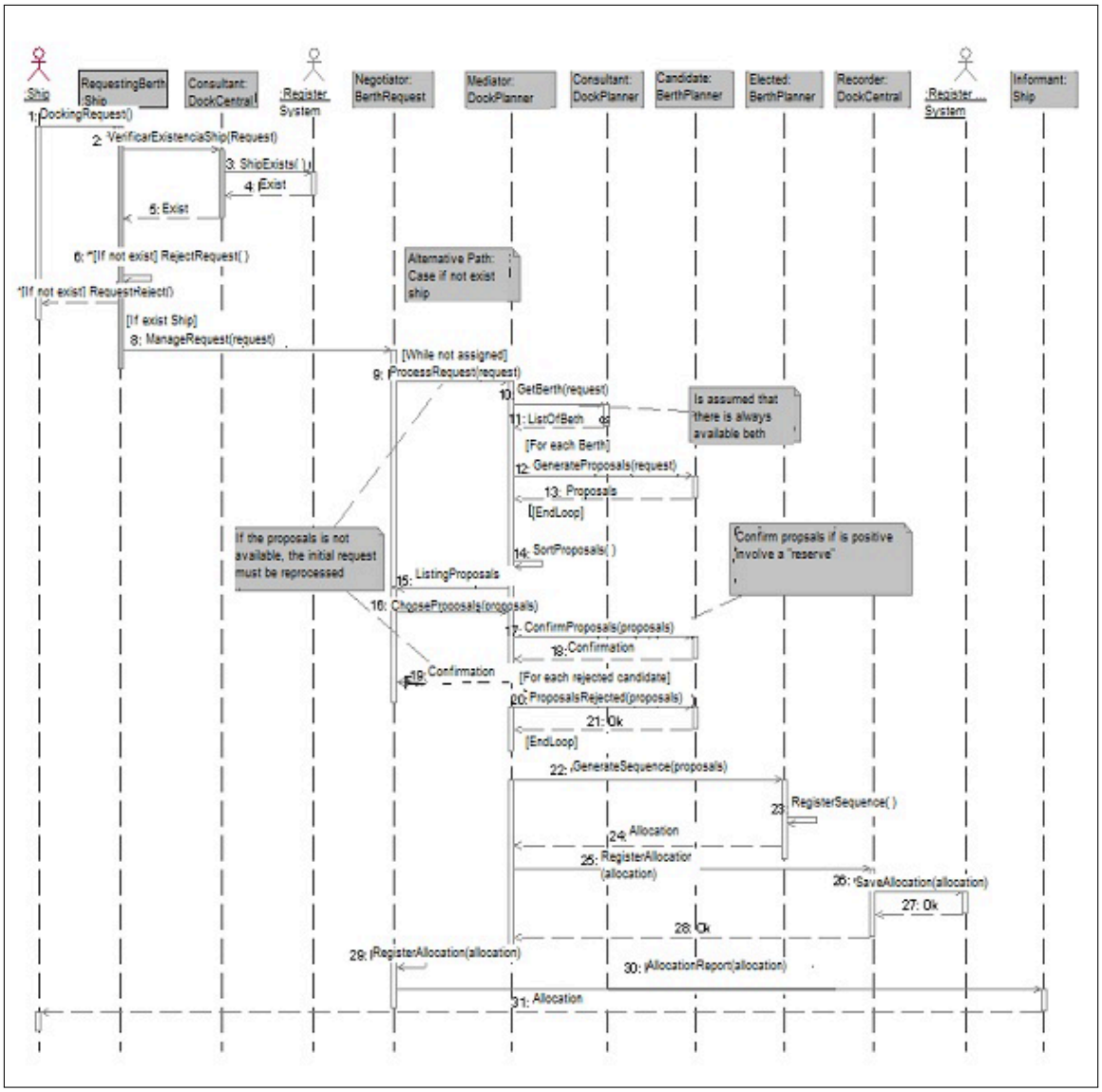

Figure 3: Role Identification Diagram for Berth request scenario.

problem. These changes consider using a single event that is associated with the ship service at the dock, which involved working with a single time window. In the case of DARP are considered two events; one for the pickup of the passenger and another for his delivery. The creation of the initial time window for each ship is related to the processing time associated with it, as shown in Figure 4a. For the ship A, with estimated arrival and departure times of ET and LT respectively, and processing time N, its maximum time window corresponds to [ET, LT] and the feasible initial time to [ET, LT-N]. The idle time or "slack" in DARP is associated with the time in which the vehicle is idle; either stopped or traveling without having to go to pickup or deliver a passenger. In the case of BAP, it is determined by the difference of the time the berth is ready to receive a new ship and the time of the ship actual arrival to the berth.

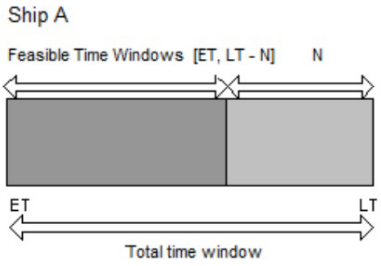

(a) Time Windows.

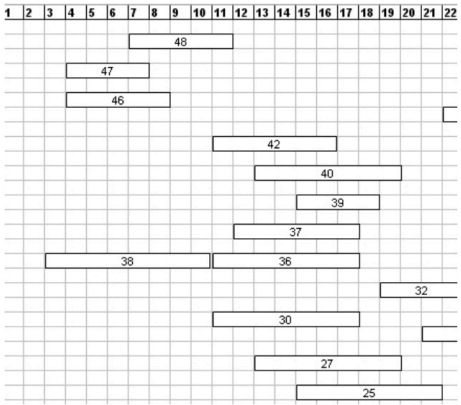

(b) Input file example with distribution of ships arrival.

Figure 4: Initial parameters of MABAP.

Therefore, unless the port has a very high ship arrival rate, there will always be idle times at the berthing points of the port. Hence, it was decided to remove the restriction of the original heuristic as to allow slack times between ship arrivals, providing a more realistic scenario. Furthermore, slack times will also allow discriminating better solutions among the proposals provided by each of the berths.

6 Tests and Results

This section presents the results obtained from the tests. To gather data a typical scenario that considers a dock with 10 berthing points has been considered together with the arrival of 50 ships within a time horizon of 60 time units. Each docking point takes 1 time unit to be ready to serve the arrival of a new ship (getReadyTime). No space restrictions are considered as any docking place can attend any ship.

The generation of instances was performed by an automated process, generating ships data with random time windows of 5 time units maximum. Figure 4b shows a graphical representation of the ships arrival within the time horizon for a sample input file. Each box represents a ship and its time windows width. The objective function considered the weighted sum of two factors: on one hand, the number of processed ships and on the other hand, the idle time (slack) of berths between ships services.

Results

The tests were carried out under two scenarios for planning the distribution of ships on berths, which considered different values for weighting the two factors of the objective function; the ShipsNumberFactor and the SlackFactor. A first scenario had weights of 80% - 20% and a second scenario had weights of 20% - 80% respectively. To obtain the results on each scenario, 10 input files were used and 20 runs were made under each scenario for a total of 200 executions. The graphics show the total estimated cost of the ten sequences under the two scenarios. By starting with the scene of strong restriction on the number of ships (Figure 5), the total cost is in principle almost a straight line and keeps controlled equally for each docking point.

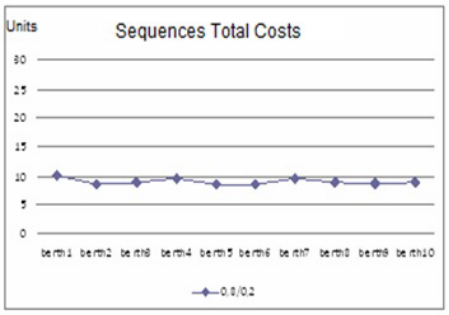

(a) Graphic of total costs for scene 80%-20%.

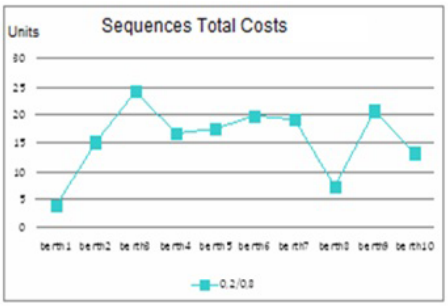

(b) Graphic of total costs for scene 20%-80%.

Figure 5: Graphical results.

Discussion

The following graphics show how the multiagent system can be tuned according to the policies of the port decision-maker. In a first case, the user can prefer solutions in which a higher number of ships are served per berth (80%-20%) while in another case the user may prefer to minimize the idle time of berths (20%-80%). Of course the proposed solution can consider other performance measures either for the operator (e.g maximizing throughput) or for the ships it serves (e.g. minimizing ships' stay).

Other aspect to analyze refers to the distributed nature of the planning. In this case the planning process involves two steps: 1) the assignment of ships to available berths and 2) the scheduling of the assigned ships inside each berth. Our actual prototype of support system provides a distributed solution by using the Contact-Net Protocol [4] as coordination/connection mechanism. Other protocols can be used, such as Dutch or English auctions, however in a general case no significant improvement should be obtained as in such cases there is no bids selection process. As early described, for each berth request coming for a ship the Dock agent makes a call-for-bids to the available BerthPlanner agents in charge of managing the ships' schedule of each berth. The underlying optimization problem is known to be NP-Hard, hence the actual prototype uses a greedy insertion heuristic which ensures less than a second per request. Such solver used inside the BerthPlanners can be changed according to the given needs (by incorporating soft computing techniques) for best solutions alternatives at a cost of more processing time. Finally, from a more political perspective, the ship arrival into a port and its berth allocation triggers a transversal process that involves diverse entities and decision-makers (port operator, port authority, berth operators, etc.). Therefore, a centralized system is unrealistic. The multiagent system for berth allocation enables such integration of the different actors involved in the berth planning process. In addition, the resulting software architecture is flexible enough to permit

the inclusion of other actors (e.g. Customs Authority, customs brokers, crane & floor/yard operators, etc.) in a transparent way. In this sense, an interesting approach would be to make it an open agent system by incorporating what developed in [17]. The integration of the diverse port enterprises through a multiagent system capable of wrapping the diverse enterprises' systems, leverages as a feasible alternative in port operations in general and in the berth planning process in particular.

7 Conclusion

This paper has tackled one of the many problems that can be found in the daily operation of a port, the berth allocation problem (BAP). The complexity of the problem, its mathematical modeling and its variants have been reviewed. A multiagent system has been presented which solves the underlying optimization problem by making use of a greedy insertion heuristic. Good results were obtained, allowing the decision-maker to choose solutions according to the port authority policies.

Further research considers refining the events to be managed by the system (e.g. delays, cancels, breakdowns), introducing multi-objective optimization, thus providing a curve of solutions, and the incorporation of a 3D graphical interface to show the planned solution.

Acknowledgments

This work has been partially funded the Pontifical Catholic University of Valparaíso (www.pucv.cl), through Regular Project No. 037.425

Bibliography

[1] United Nations Conference on Trade And Development (UNCTAD), *Review Maritime Transport*, Cap V, pp. 73-74, Cap VII. 2005.

[2] Wooldridge, M., *An Introduction to Multiagent Systems*, Dept. of Electronic Engineering, Queen Mary & Westfield College, 2002.

[3] Burrafato, P., Cossentino, M. Designing a Multi-Agent Solution for a Bookstore With the PASSI Methodology, In *Fourth International Bi-Conference Workshop on Agent-Oriented Information Systems (AOIS-2002)*, 2002, pp. 27-28.

[4] FIPA, Contract Net Interaction Protocol Specification. Available at: www.fipa.org/specs/fipa00029/SC00029H.pdf

[5] Daganzo, C., The Crane Scheduling Problem, *Transportation Research B 23B*, 1989, 159-175.

[6] Cubillos, C., Crawford, D., Rodríguez, N., MADARP: A Distributed Agent-based System for On-Line DARP. In: *I. Stojmenovic et al. (Eds.): ISPA 2007, Springer Heidelberg LNCS*, Vol. 4742, 160-169, 2007.

[7] Botti, V.J. Multi-Agent System Technology in a Port Container Terminal Automation, *European Research Consortium for Informatics and Mathematics News*, Vol. January, No 56, 37-39, 2004.

[8] Nwana, H.S., Ndumu, D.T., *An Introduction to Agent Technology*, Re-Drawn by Mobile Computing, Dept. of IECS, Feng Chua University, R.O.C., 2003.

[9] Cubillos, C., Urra, E., Rodríguez, N., Application of Genetic Algorithms for the DARPTW Problem, *INT J COMPUT COMMUN* , ISSN 1841-9836, 4(2):127-136, 2009.

[10] Pinedo, M. Scheduling: *Theory, Algorithms and Systems*, Prentice-Hall, Englewood Cliffs, NJ. 1995.

[11] Garey, M. R., Johnson, D. S., *Computers and Intractability: A guide to the Theory of NP-Completeness*, Freeman, San Francisco. 1979.

[12] Imai, A., Nishimura, F., Papadimitriou, S., The dynamic berth allocation problem for a container port, *Transportation Research 35B*, 401-417. 2001.

[13] Imai, A., Nagaiwa, K. Chan, W. T., Efficient planning of berth allocation for contenedor terminals in Asia, *Journal of Advanced Transportation*, 31, 75-94. 1997.

[14] Papadimitriou, C. H., Steiglitz, K., *Combinatorial Optimization; Algorithms and Complexity*, Prentice-Hall, Englewood Cliff, NJ. 1982.

[15] Jaw, J. Odoni, A. R. Psaraftis, H. N. Wilson, N.M.H. A heuristic algorithm for the Multi-Vehicle Advance-Request Dial-a-Ride Problem with Time Windows, *Transportation Research B*, 20B(2): 243 - 257, 1986.

[16] Cabrera-Paniagua, D., Herrera, G., Cubillos, C., Donoso, M. Towards a Model for Dynamic Formation and Operation of Virtual Organizations for Transportation, *Studies in Informatics and Control*, ISSN 1220-1766, 20 (3): 255-264, 2011.

[17] Cubillos, C., Donoso M., Rodríguez N., Guidi-Polanco F., Cabrera-Paniagua D., Towards Open Agent Systems Through Dynamic Incorporation, *INT J COMPUT COMMUN*, ISSN 1841-9836, 5(5):675-683, 2010.

INT J COMPUT COMMUN, ISSN 1841-9836
8(3):395-406, June, 2013.

An Approach to Fuzzy Modeling of Electromagnetic Actuated Clutch Systems

C.-A. Dragoş, R.-E. Precup, M.L. Tomescu, S. Preitl, E.M. Petriu, M.-B. Rădac

Claudia-Adina Dragoş, Radu-Emil Precup,
Stefan Preitl, Mircea-Bogdan Rădac
"Politehnica" University of Timişoara
Department of Automation and Applied Informatics
Bd. V. Parvan 2, 300223 Timisoara, Romania
claudia.dragos@aut.upt.ro, radu.precup@aut.upt.ro,
stefan.preitl@aut.upt.ro, mircea.radac@aut.upt.ro

Marius L. Tomescu
Aurel Vlaicu University of Arad
Romania, 310330 Arad, Elena Dragoi, 2
tom_uav@yahoo.com

Emil M. Petriu
University of Ottawa
School of Electrical Engineering and Computer Science
800 King Edward, Ottawa, ON, K1N 6N5 Canada
petriu@eecs.uottawa.ca

Abstract: This paper proposes an approach to fuzzy modeling of a nonlinear servo system application represented by an electromagnetic actuated clutch system. The nonlinear model of the process is simplified and linearized around several operating points of the input-output static map of the process. Discrete-time Takagi-Sugeno (T-S) fuzzy models of the processes are derived on the basis of the modal equivalence principle; the rule consequents of these T-S fuzzy models contain the state-space models of the process. Three discrete-time T-S fuzzy models are suggested, compared and validated by simulation results.
Keywords: Discrete-time Takagi-Sugeno fuzzy models, electromagnetic actuated clutch system, linearization, operating points, simulation results.

1 Introduction

The process taken into consideration and modeled in this paper is an electromagnetic actuated clutch system as a representative nonlinear system application. Therefore the derivation of accurate models is a challenging problem. Several approaches to fuzzy modeling of nonlinear servo systems are given in the literature. They belong to the general framework of nonlinear process models [1], [2], [3], [4], [5]. A parallel distributed compensation scheme is proposed in [6] with focus on fuzzy reference models; the linear matrix inequalities are formulated and solved in order to linearize the errors between the feedback system and the nonlinear reference model. The nonlinear system behavior is modeled in [7] by the division of the phase plane into sub-regions and a linear model represented either in state-space or ARX model form is assigned for each regions; the linear models are next expressed as fuzzy models. A DSP-based fuzzy-linear-model robust tracking control is developed in [8] for a piezoelectric servo system with dominant hysteresis in terms of the weighted combination of N fuzzy linear pulse transfer functions; the fuzzy model is included in a dead-beat control system. An ANFIS-based neuro-fuzzy model for a low inertia servomotor is suggested in [9], and several comparisons between the performance of the system with the standard motor model and its neuro-fuzzy model are carried out in the framework of

adaptive control. Fuzzy feedback linearization and fuzzy sliding mode control applications are given in [10] and [11].
This paper offers discrete-time dynamic Takagi-Sugeno (T-S) fuzzy model of an electromagnetic actuated clutch system. The computation of the T-S fuzzy models starts with the derivation of the continuous-time models which are obtained on the basis of the local linearization of the process models at five operating points (o.p.s). The local models are next discretized accepting a zero-order hold, and these local models are placed in the rule consequents of the T-S fuzzy model of the process.

Our approach is advantageous because it is relatively simple and it can be incorporated in many fuzzy control structures [12], [13], [14], [15], [16], [17], [18], [19]. Three fuzzy models are offered and compared using simulation results.
The paper is organized as follows: Section 2 is dedicated to the mathematical modeling of the process, the computation of T-S fuzzy models is synthesized in Section 3. Simulation results are presented in Section 4 to validate the new T-S fuzzy models. The concluding remarks are highlighted in Section 5.

2 Process Modeling

The mathematical modeling of the electromagnetic actuator as part of electric drive clutches is based on the schematic structure of a magnetically actuated mass-spring-damper system presented in Figure 1 [20]. The state-space model of the nonlinear servo system is:

$$\begin{aligned}
&\dot{x}_1 = x_2,\\
&\dot{x}_2 = -\tfrac{k}{m}x_1 - \tfrac{c}{m}x_2 + \tfrac{k_a x_3^2}{m(k_b+d-x_1)^2},\\
&\dot{x}_3 = -\tfrac{R(k_b+d-x_1)}{2k_a}x_2x_3 + \tfrac{1}{k_b+d-x_1}x_2x_3 + [(k_b+d-x_1)/2k_a]V,\\
&y = 1000x_1,
\end{aligned} \tag{1}$$

where x_1 is the position, i.e., the mass position, x_2 is the mass speed, x_3 is the current, V is the control signal, y is the measured position (output), k is the stiffness of the spring, c is the coefficient of the damper, R is the electromagnetic coil resistance, and k_a, k_b are the constants in the relation between the magnetic flux and the current. The numerical values of the process parameters are listed in [21].

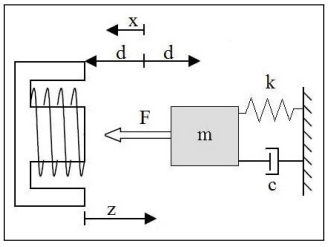

Figure 1: Schematic structure of a magnetically actuated mass-spring-damper system [20].

The linearization of the nonlinear servo system model (1) at five o.p.s $A_j(x_{10}, x_{20}, x_{30}, x_{40})$ (with j-the index of the o.p. $j = \overline{1,5}$, and 0-the index of the coordinates of the o.p.s, i.e., the state variables) leads to the linearized state-space models:

$$
\begin{aligned}
&\dot{\mathbf{x}}(t) = \mathbf{A}\mathbf{x}(t) + \mathbf{b}\Delta V(t),\\
&\Delta y(t) = \mathbf{c}^T\mathbf{x}(t),\\
&\mathbf{x} = [\ x_1 = x \quad x_2 = \dot{x} \quad x_3 = i]^T,\\
&\mathbf{A} = \begin{bmatrix} 0 & 1 & 0 \\ -\frac{k}{m} + \frac{2k_a x_{30}^2}{m(k_b+d-x_{10})^3} & -\frac{c}{m} & \frac{2k_a x_{30}}{m(k_b+d-x_{10})^2} \\ \frac{Rx_{30}-V_0}{2k_a} - \frac{x_{20}x_{30}}{(k_b+d-x_{10})^2} & -\frac{x_{30}}{k_b+d-x_{10}} & -\frac{x_{20}}{k_b+d-x_{10}} - \frac{R(k_b+d-x_{10})}{2k_a} \end{bmatrix},\\
&\mathbf{b} = \begin{bmatrix} 0 \\ 0 \\ \frac{k_b+d-x_{10}}{2k_a} \end{bmatrix}, \mathbf{c}^T = [\ 1000 \quad 0 \quad 0\ ].
\end{aligned}
\tag{2}
$$

where $\mathbf{x}(t)$ is the system state vector, $\mathbf{A}$, $\mathbf{b}$ and $\mathbf{c}^T$ are the linearized system matrices, and t is the continuous time variable. The matrices of the discrete-time systems developed from (2) will be presented in the sequel.

3 Approach to Takagi-Sugeno Fuzzy Modeling

In order to capture both the static nonlinearity and the linear dynamics of the process, the derivation of a discrete-time dynamic T-S fuzzy model of the process is presented as follows. Figure 2 illustrates the structure of the T-S fuzzy model identification process.

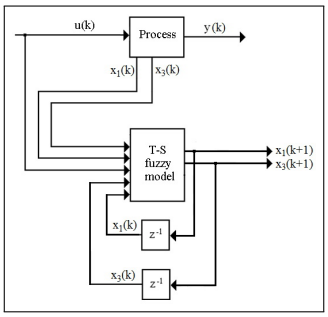

Figure 2: Structure of the discrete-time dynamic Takagi-Sugeno fuzzy model identification process.

The steps of our modeling approach are:

Step I. The definition of the membership functions of the input variables x_1 and x_3.

Step II. The choice of the settling time and the discretization of the continuous-time state-space models of the process which result in the discrete-time state-space models with the matrices $\mathbf{A}_{d,i}$, $\mathbf{B}_{d,i}$ and $\mathbf{C}_{d,i}$ and $\mathbf{C}_{d,i}$, $i = \overline{1,5}$.

Step III. The derivation of the T-S fuzzy model of the process, which has the state variables x_1 and x_3 as input variables, and the discrete-time state-space models of the process in the rule consequents.

The step I starts with the setting of the largest domains of variation of the two state variables used in all electromagnetic actuated clutch system operating regimes:

$$0 \leqslant x_1 \leqslant 0.004,\ 0 \leqslant x_3 \leqslant 10. \tag{3}$$

The fuzzification part of the T-S fuzzy model consists of the linguistic terms assigned to the input variables and defined as follows.

Three cases were considered for the input variable x_1 . The first two cases employ five linguistic terms, $LT_{x_1,j},\ j=\overline{1,5}$, with trapezoidal membership functions defined and referred to as $LT_{x_1,1}$, with the universe of discourse $[0.0019, 0.0023]$, $LT_{x_1,2}$, with the universe of discourse $[0.0021, 0.0027]$, $LT_{x_1,3}$, with the universe of discourse $[0.0023, 0.003]$, $LT_{x_1,4}$, with the universe of discourse $[0.0027, 0.0033]$ and $LT_{x_1,5}$, with the universe of discourse $[0.003, 0.004]$. The expressions of these trapezoidal membership functions are:

$$\mu_{TL_{x_3,j}}(x)=\begin{cases}0, & x<a_{x_1,j}\\ 1+\frac{x-b_{x_1,j}}{b_{x_1,j}-a_{x_1,j}}, & x\in[a_{x_1,j},b_{x_1,j})\\ 1, & x\in[b_{x_1,j},c_{x_1,j})\\ 1-\frac{x-c_{x_1,j}}{d_{x_1,j}-c_{x_1,j}}, & x\in[c_{x_1,j},d_{x_1,j})\\ 0, & x\geqslant d_{x_1,j}\end{cases},\ a_{x_1,j}<b_{x_1,j}\leqslant c_{x_1,j}<d_{x_1,j},\ j=\overline{1.5} \tag{4}$$

The modal values of the membership functions are the parameters $a_{x_1,j},\ j=\overline{1,5}$, $b_{x_1,j},\ j=\overline{1,5}$, $c_{x_1,j},\ j=\overline{1,5}$ and $d_{x_1,j},\ j=\overline{1,5}$. The values of these parameters are given in Table 1 for the first case and in Table 2 for the second case.

Table 1
Parameters of input membership functions in the first case

Linguistic terms,	Trapezoidal membership functions			
$LT_{x_1,j},\ j=\{1,5\}$	$a_{x_1,j},\ j=\overline{1,5}$	$b_{x_1,j},\ j=\overline{1,5}$	$c_{x_1,j},\ j=\overline{1,5}$	$d_{x_1,j},\ j=\overline{1,5}$
$LT_{x_1,1}$	0.0019	0.0019	0.0021	0.0023
$LT_{x_1,2}$	0.0019	0.0021	0.0023	0.0027
$LT_{x_1,3}$	0.0021	0.0023	0.0027	0.003
$LT_{x_1,4}$	0.0023	0.0027	0.003	0.00384
$LT_{x_1,5}$	0.003	0.00384	0.004	0.004

Table 2
Parameters of input membership functions in the second case

Linguistic terms,	Trapezoidal membership functions			
$LT_{x_1,j},\ j=\{1,5\}$	$a_{x_1,j},\ j=\overline{1,5}$	$b_{x_1,j},\ j=\overline{1,5}$	$c_{x_1,j},\ j=\overline{1,5}$	$d_{x_1,j},\ j=\overline{1,5}$
$LT_{x_1,1}$	0.0019	0.0019	0.0021	0.0023
$LT_{x_1,2}$	0.0021	0.0023	0.0025	0.0027
$LT_{x_1,3}$	0.0025	0.0027	0.003	0.0033
$LT_{x_1,4}$	0.003	0.0033	0.0035	0.00384
$LT_{x_1,5}$	0.0035	0.00384	0.004	0.004

Five linguistic terms, $LT_{x_1,j},\ j=\overline{1,5}$, with trapezoidal and triangular membership functions are defined and employed in the third case, and referred to as $LT_{x_1,1}$, with the universe of discourse $[0.0019, 0.0023]$, $LT_{x_1,2}$, with the universe of discourse $[0.0021, 0.0027]$, $LT_{x_1,3}$, with the universe of discourse $[0.0023, 0.003]$, $LT_{x_1,4}$, with the universe of discourse $[0.0027, 0.0033]$, and $LT_{x_1,5}$, with the universe of discourse $[0.003, 0.004]$. The modal values of the trapezoidal membership functions are the parameters $a_{x_1,j},\ j\in\{1,5\}$, $b_{x_1,j},\ j\in\{1,5\}$, $c_{x_1,j},\ j\in\{1,5\}$ and $d_{x_1,j},\ j\in\{1,5\}$ given in Table 3.

Table 3
Parameters of trapezoidal input membership functions in the third case

Linguistic terms,	Trapezoidal membership functions			
$LT_{x_1,j},\ j=\{1,5\}$	$a_{x_1,j},\ j\in\{1,5\}$	$b_{x_1,j},\ j\in\{1,5\}$	$c_{x_1,j},\ j\in\{1,5\}$	$d_{x_1,j},\ j\in\{1,5\}$
$LT_{x_1,1}$	0.0019	0.0019	0.0021	0.0023
$LT_{x_1,5}$	0.0033	0.00384	0.004	0.004

The expressions of the triangular membership functions are:

$$\mu_{TL_{x_1,j}}(x)=\begin{cases}0, & x<a_{x_1,j}\\ 1+\frac{x-b_{x_1,j}}{b_{x_1,j}-a_{x_1,j}}, & x\in[a_{x_1,j},b_{x_1,j})\\ 1-\frac{x-b_{x_1,j}}{c_{x_1,j}-b_{x_1,j}}, & x\in[b_{x_1,j},c_{x_1,j})\\ 0, & x\geqslant c_{x_1,j}\end{cases},\ a_{x1,j}<b_{x1,j}<c_{x1,j},\ j=\overline{2,4} \tag{5}$$

where the modal values of the membership functions are the parameters $a_{x_1,j}$, $b_{x_1,j}$, and $c_{x_1,j}$, $j=\overline{2,4}$ presented in Table 4.

Table 4
Modal values of linguistic terms in the third case

Linguistic terms,	Trapezoidal membership functions		
$LT_{x_1,j},\ j=\overline{2,4}$	$a_{x_1,j}$	$b_{x_1,j}$	$c_{x_1,j}$
$LT_{x_1,1}$	0.0021	0.0023	0.0027
$LT_{x_1,3}$	0.0023	0.0027	0.003
$LT_{x_1,4}$	0.0027	0.003	0.0033

Figure 3 shows the membership functions of x_1 in these three cases: the first case in Figure 3 (a), the second case in Figure 3 (b) and the third case in Figure 3 (c).

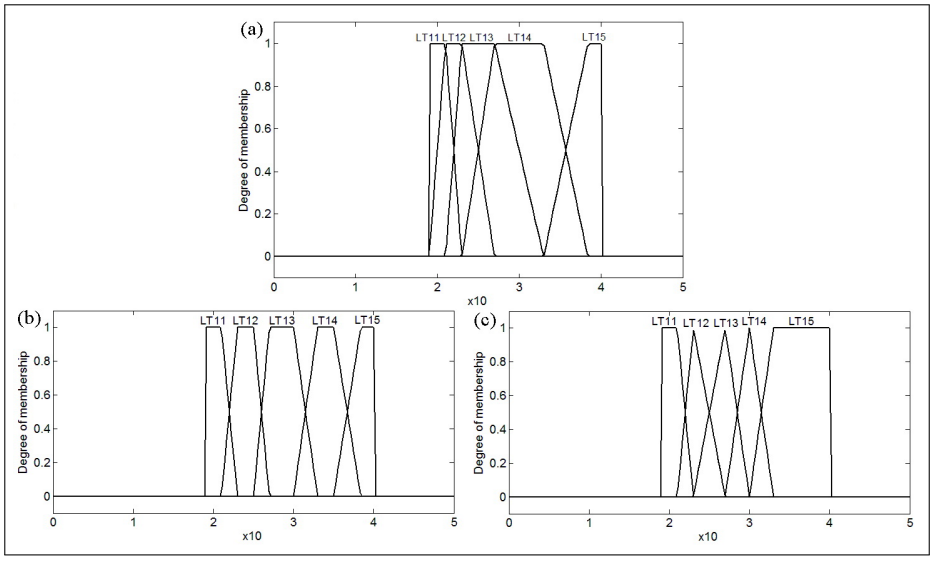

Figure 3: Membership functions of the input variable x_1 in the first case (a), in the second case (b) and in the third case (c).

Five linguistic terms, $LT_{x_3,j},\ j=\overline{1,5}$, are defined for the input variable x_3 . The first and the fifth one are modeled by trapezoidal membership functions, and the second, the third and the fourth one are modeled by trapezoidal membership functions. The universes of discourse of the

membership functions of these linguistic terms are: $[4,8]$ for $LT_{x_3,1}$, $[5,9]$ for $LT_{x_3,2}$, for $[6,10]$, $LT_{x_3,3}$, $[7,11]$ for $LT_{x_3,4}$, and $[8,12]$ for $LT_{x_3,5}$. The expressions of the trapezoidal membership functions are:

$$\mu_{TL_{x_3,j}}(x)=\begin{cases}0, & x<a_{x_3,j}\\ 1+\frac{x-b_{x_3,j}}{b_{x_3,j}-a_{x_3,j}}, & x\in[a_{x_3,j},b_{x_3,j})\\ 1, & x\in[b_{x_3,j},c_{x_3,j})\\ 1-\frac{x-c_{x_3,j}}{d_{x_3,j}-c_{x_3,j}}, & x\in[c_{x_3,j},d_{x_3,j})\\ 0, & x\geqslant d_{x_3,j}\end{cases},\ a_{x_3,j}<b_{x_3,j}\leqslant c_{x_3,j}<d_{x_3,j},\ j\in\{1,5\} \quad (6)$$

The modal values of the membership functions are the parameters $a_{x_3,j},\ j\in\{1,5\}$, $b_{x_3,j},\ j\in\{1,5\}$, $c_{x_3,j},\ j\in\{1,5\}$, and $d_{x_3,j},\ j\in\{1,5\}$, given in Table 5.

Table 5
Parameters of trapezoidal linguistic terms

Linguistic terms,	Trapezoidal membership functions			
$LT_{x_3,j},\ j=\{1,5\}$	$a_{x_3,j},\ j\in\{1,5\}$	$b_{x_3,j},\ j\in\{1,5\}$	$c_{x_3,j},\ j\in\{1,5\}$	$d_{x_3,j},\ j\in\{1,5\}$
$LT_{x_3,1}$	4	4	6	8
$LT_{x_3,5}$	8	10	12	12

The expressions of the triangular membership functions are:

$$\mu_{TL_{x_1,j}}(x)=\begin{cases}0, & x<a_{x_1,j}\\ 1+\frac{x-b_{x_1,j}}{b_{x_1,j}-a_{x_1,j}}, & x\in[a_{x_1,j},b_{x_1,j})\\ 1-\frac{x-b_{x_1,j}}{c_{x_1,j}-b_{x_1,j}}, & x\in[b_{x_1,j},c_{x_1,j})\\ 0, & x\geqslant c_{x_1,j}\end{cases},\ a_{x1,j}<b_{x1,j}<c_{x1,j},\ j=\overline{2,4}, \quad (7)$$

where the modal values of the membership functions are the parameters $a_{x_3,j}$, $b_{x_3,j}$, and $c_{x_3,j}$, $j=\overline{2,4}$, given in Table 6.

Table 6
Modal values of linguistic terms

Linguistic terms,	Trapezoidal membership functions		
$LT_{x_3,j},\ j=\overline{2,4}$	$a_{x_3,j}$	$b_{x_3,j}$	$c_{x_3,j}$
$LT_{x_3,1}$	5	7	9
$LT_{x_3,3}$	6	8	10
$LT_{x_3,4}$	7	9	11

Figure 4 shows the membership functions of the input x_3.

The rule consequents of the T-S fuzzy models correspond to the discrete-time state-space models characterized by the matrices $\mathbf{A}_{d,i}$, and $\mathbf{B}_{d,i}$, $\mathbf{C}_{d,i}$, $i=\overline{1,5}$, detailed in Table 7. These models are obtained by discretization of the continuous-time state-space linearized models (1) using the sampling period $T_s=0.001$ s.

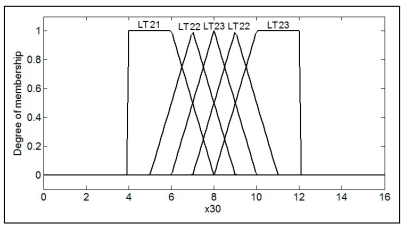

Figure 4: Membership functions of the input variable x_3.

Table 7
Numerical values of matrices of discrete-time state-space models

O.p.s	Numerical values of the matrices
1	$\mathbf{A}_{d1} = \begin{bmatrix} 0.9864 & 0.0007 & 0.0000062 \\ -24.3234 & 0.4847 & 0.011 \\ 3.018 & -0.1579 & 0.9816 \end{bmatrix}, \mathbf{B}_{d1} = \begin{bmatrix} 0.000000031 \\ 0.000088 \\ 0.0142 \end{bmatrix},$ $\mathbf{C}_{d1} = [1000 \quad 0 \quad 0]$
2	$\mathbf{A}_{d1} = \begin{bmatrix} 0.9869 & 0.0007 & 0.0000073 \\ -23.352 & 0.4847 & 0.013 \\ 3.4059 & -0.1856 & 0.9811 \end{bmatrix}, \mathrm{B}_{d1} = \begin{bmatrix} 0.000000036 \\ 0.000088 \\ 0.0142 \end{bmatrix},$ $\mathbf{C}_{d1} = [1000 \quad 0 \quad 0]$
3	$\mathbf{A}_{d1} = \begin{bmatrix} 0.9876 & 0.0007 & 0.0000086 \\ -22.0872 & 0.4847 & 0.0153 \\ 3.7379 & -0.2153 & 0.9807 \end{bmatrix}, \mathbf{B}_{d1} = \begin{bmatrix} 0.000000042 \\ 0.00012 \\ 0.0139 \end{bmatrix},$ $\mathbf{C}_{d1} = [1000 \quad 0 \quad 0]$
4	$\mathbf{A}_{d1} = \begin{bmatrix} 0.9885 & 0.0007 & 0.0000101 \\ -20.4072 & 0.4847 & 0.018 \\ 3.9765 & -0.2479 & 0.9801 \end{bmatrix}, \mathbf{B}_{d1} = \begin{bmatrix} 0.000000049 \\ 0.000139 \\ 0.0135 \end{bmatrix},$ $\mathbf{C}_{d1} = [1000 \quad 0 \quad 0]$
5	$\mathbf{A}_{d1} = \begin{bmatrix} 0.9897 & 0.0007 & 0.0000101 \\ -18.3864 & 0.4847 & 0.0209 \\ 4.1934 & -0.2814 & 0.9793 \end{bmatrix}, \mathbf{B}_{d1} = \begin{bmatrix} 0.000000055 \\ 0.000158 \\ 0.0132 \end{bmatrix},$ $\mathbf{C}_{d1} = [1000 \quad 0 \quad 0]$

The modal equivalence principle guarantees the equivalence between the fuzzy models and the nonlinear state-space models. That is the reason to express the rule base of the discrete-time dynamic T-S fuzzy models in the following general form:

$$R^i : \mathrm{IF}x_{1,k}\mathrm{IS}LT_{x_1,j}\mathrm{AND}x_{3,k}\mathrm{IS}LT_{x_3,j}\ \mathrm{THEN}\begin{cases} \mathbf{x}_{k+1} = \mathbf{A}_{d,i}\mathbf{x}_k + \mathbf{B}_{d,i}u_k \\ y_{k,m} = \mathbf{C}_{d,i}\mathbf{x}_k \end{cases}, \quad (8)$$
$$i = \overline{1, nR},\ j = \overline{1, nLT},$$

where k is the index of the current sampling interval, i is the index of the current rule, j is the index of the current linguistic term, nR is the number of rules, nLT is the number of linguistic terms, $nR = nLT = 5$ in our discrete-time dynamic T-S fuzzy models.

The fuzzy controller employs the SUM and PROD operators and the weighted average defuzzification method. Other operators can be used [22], [23], [24], [25], [26], [27].

4 Experimental Results

The modeling approach presented in the previous sections is applied and exemplified in this section in order to obtain fuzzy models for the electromagnetic actuated clutch system. Three T-S fuzzy models were developed for this nonlinear process. Some comparisons were done to illustrate the difference between them. A part of the results is presented as follows. The simulation results include the evolutions of the position versus time (in Figure 5), the evolution of the measured position versus time (in Figure 6), the evolution of the modeling error versus time (in Figure 7), and the evolution of the current versus time (in Figure 8).
Figure 5 and Figure 6 present the evolution of both position and measured position y in four cases: nonlinear model (1) of the process, first T-S fuzzy model, second T-S fuzzy model and third T-S fuzzy model. These evolutions point out in all cases an aperiodical evolution with a small overshoot, but the fuzzy modeled responses exhibit a delay of 0.1 s and they exceed the steady-state values of the nonlinear model. The modeling error versus time is highlighted in Figure 7 to outline the difference between the nonlinear model and the fuzzy models.

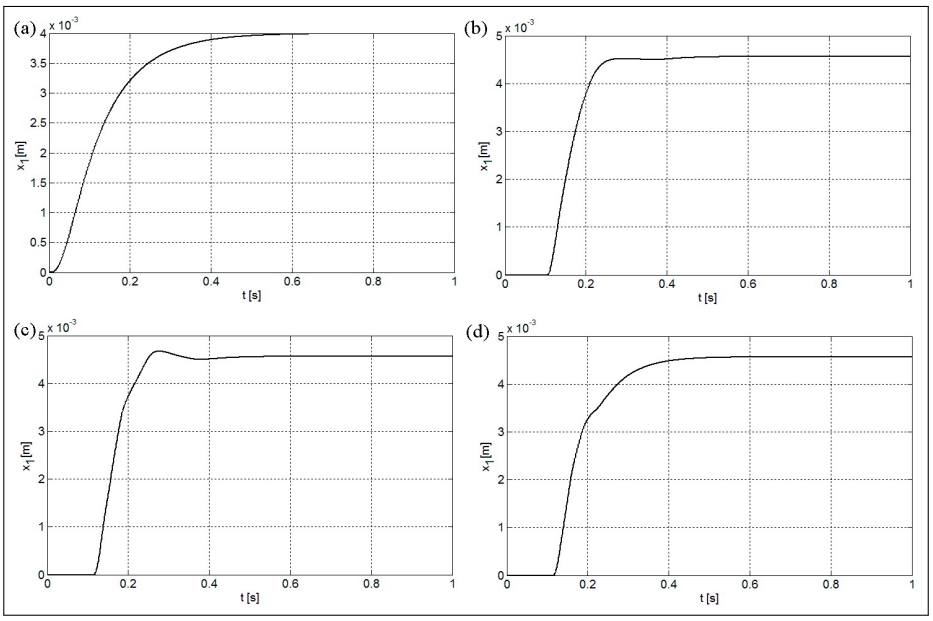

Figure 5: Position of nonlinear model (a), of first T-S fuzzy model (b), of second T-S fuzzy model (c) and of third T-S fuzzy model (d) versus time.

Figure 8 points out the evolution of the current in the same four cases: nonlinear model (1) of the process, first T-S fuzzy model, second T-S fuzzy model and third T-S fuzzy model. Figure 8 illustrates that the current exhibited by the T-S fuzzy models has a delay, but it reaches the steady-state value in approximately 0.5 s and with aperiodical response as that of the model (1). All responses point out a delay of 0.1 s which must be reduced. Moreover, the convergence of the modeling error to zero can be achieved by the optimization of the parameters of several parameters of the fuzzy models including input membership functions or parameters in the rule consequents. Various optimization algorithms can be implemented in this context [28], [29], [30], [31], [32], [33], [34], [35], [36].

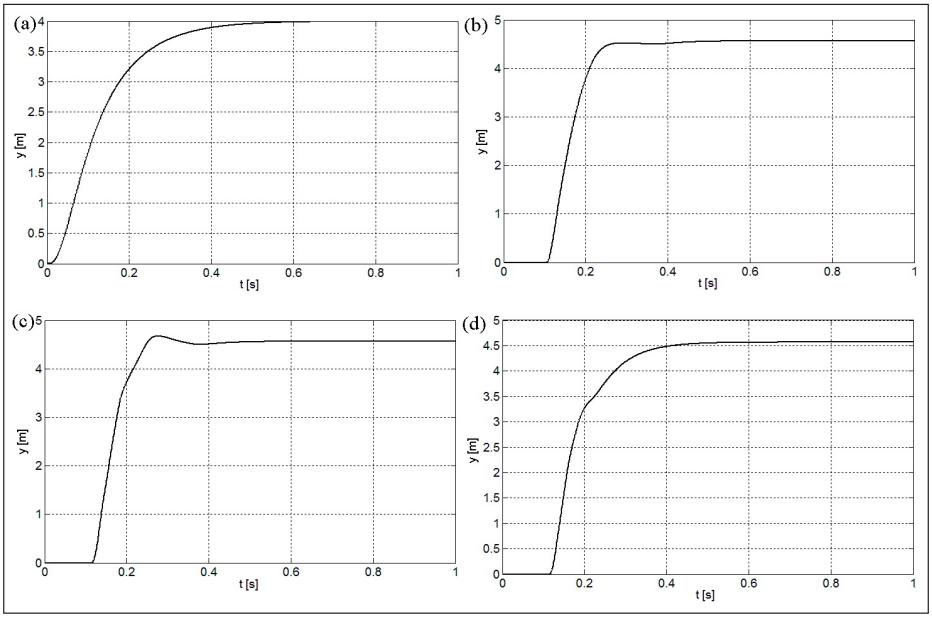

Figure 6: Measured position of nonlinear model (a), of first T-S fuzzy model (b), of second T-S fuzzy model (c) and of third T-S fuzzy model (d) versus time.

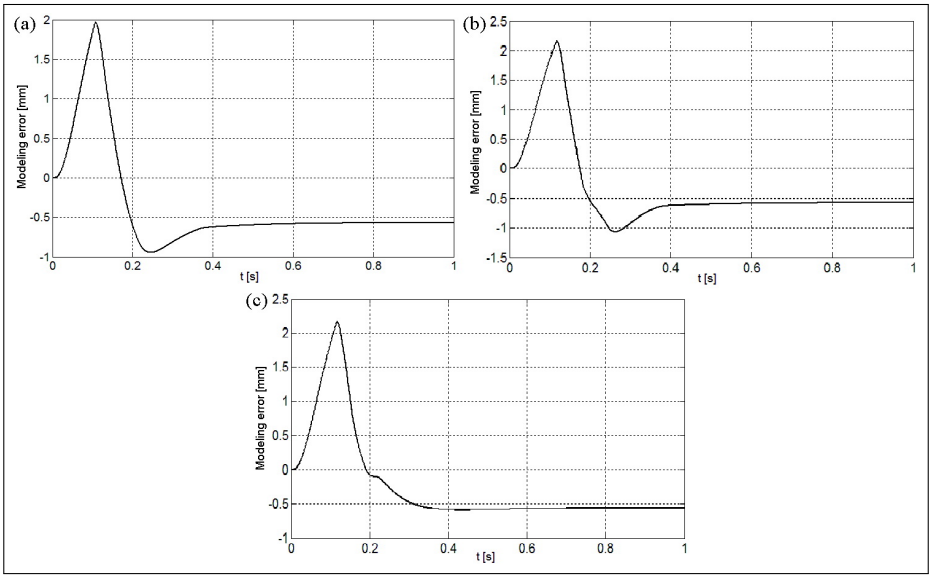

Figure 7: Modeling error of first T-S fuzzy model (a), of second T-S fuzzy model (b) and of third T-S fuzzy model (c) versus time.

5 Conclusions

The paper has proposed an approach to the fuzzy modeling of an electromagnetic actuated clutch system. This approach is important because it is easily applicable with adequate but not complicated generalizations to a wide category of industrial applications. Other similar T-S fuzzy models can be obtained in order to be further used in the T-S fuzzy controller design and tuning.

The future work will be dedicated to separating a part of the parameters of the input membership functions. These parameters will be obtained by different optimization algorithms which

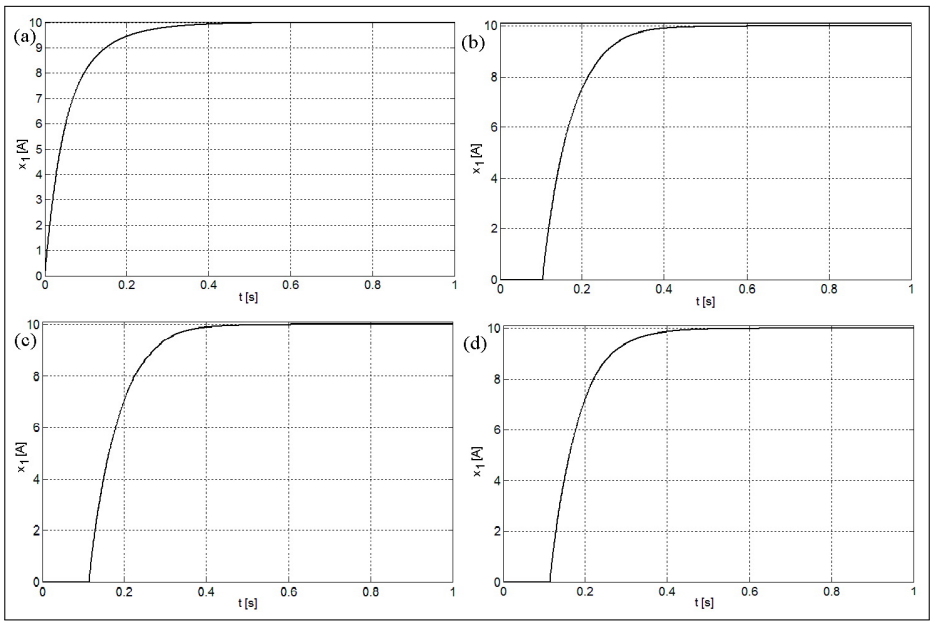

Figure 8: Current of nonlinear model (a), of first T-S fuzzy model (b), of second T-S fuzzy model (c) and of third T-S fuzzy model (d) versus time.

will solve the optimization problems with objective functions that depend on the modeling errors. The reduction of the modeling errors will be thus ensured.

Acknowledgements

This work was supported by a grant in the framework of the Partnerships in priority areas - PN II program of the Romanian National Authority for Scientific Research ANCS, CNDI - UEFISCDI, project number PN-II-PT-PCCA-2011-3.2-0732.

Bibliography

[1] Škrjanc, I.; Blažič, S.; Agamennoni O. (2005); Identification of dynamical systems with a robust interval fuzzy model, *Automatica*, 41(2):327-332.

[2] Johanyák, Z.C. (2010); Survey on five fuzzy inference-based student evaluation methods, in: Computational Intelligence in Engineering, I. J. Rudas, J. Fodor, J. Kacprzyk, Eds., *Studies in Computational Intelligence*, Springer-Verlag, Berlin, Heidelberg, 313:219-228.

[3] Vaščák, J.; Madarász, L. (2010); Adaptation of fuzzy cognitive maps-a comparison study, *Acta Polytechnica Hungarica*, 7(3):109-122.

[4] Babu Devasenapati, S.; Ramachandran, K. I. (2011) Hybrid fuzzy model based expert system for misfire detection in automobile engines, *Int. J. of Artificial Intelligence*, 7(A11):47-62.

[5] Dzitac, I; Vesselényi, T; Tarcă, R. C. (2011) Identification of ERD using fuzzy inference systems for brain-computer interface, *INT J COMPUT COMMUN*, ISSN 1841-9836, 6(3):403-417.

[6] Taniguchi, T; Tanaka, K.; Yamafuji, K.; Wang, O.H. (1999) A new PDC for fuzzy reference models, *Proc. of 1999 IEEE Int. Conf. on Fuzzy Systems*, Seoul, Korea, 2:898-903.

[7] Eksin, I.; Erol, O.K. (2000) A fuzzy identification method for nonlinear systems, *Turkish Journal of Electrical Engineering and Computer Sciences*, 8(2):125-135.

[8] Hwang, V.-L.; Jan (2002) A DSP-based fuzzy robust tracking control for piezoelectric servosystems, *Proc. of 2002 IEEE International Conference on Fuzzy Systems*, Honolulu, HI, USA, 2:1410-1415.

[9] Mihai, D. (2004) Discrete fuzzy control loops based on a motor neuro-fuzzy model. Pushing too far a continuous logic?, *Proceedings of 2004 IEEE International Conference on Fuzzy Systems*, Budapest, Hungary, 2:587-592.

[10] Chien, T.-L.; Chen, C.-C.; Tsai, M.-C.; Chen, Y.-C. (2010) Control of AMIRA's ball and beam system via improved fuzzy feedback linearization approach, *Applied Mathematical Modelling*, 34(12):3791-3804.

[11] Cerman, O.; Hušek, P. (2012) Adaptive fuzzy sliding mode control for electro-hydraulic servo mechanism, Expert Systems with Applications, 39(11):10269-10277.

[12] Precup, R.-E.; Preitl, S. (1999) Fuzzy Controllers, *Editura Orizonturi Universitare Publishers*, Timişoara.

[13] Orlowska-Kowalska, T.; Szabat, K.; Jaszczak, K. (2002) The influence of parameters and structure of PI-type fuzzy-logic controller on DC drive system dynamics, *Fuzzy Sets and Systems*, 131(2):251-264.

[14] Precup, R.-E.; Preitl, S.; Faur, G. (2003) PI predictive fuzzy controllers for electrical drive speed control: Methods and software for stable development, *Computers in Industry*, 52(3):253-270.

[15] Precup, R.-E.; Preitl, S.; Korondi, P. (2007) Fuzzy controllers with maximum sensitivity for servosystems, *IEEE Transactions on Industrial Electronics*, 54(3):1298-1310.

[16] Angelov, P.; Lughofer, E.; Zhou X. (2008) Evolving fuzzy classifiers using different model architectures, *Fuzzy Sets and Systems*, 159(23):3160-3182.

[17] Precup, R.-E.; Preitl, S.; Petriu, E.M.; Tar, J.K.; Tomescu, M.L.; Pozna, C. (2009) Generic two-degree-of-freedom linear and fuzzy controllers for integral processes, *Journal of The Franklin Institute*, 346(10):980-1003.

[18] Linda, O.; Manic, M. (2011) Interval ypype-2 fuzzy voter design for fault tolerant systems, *Information Sciences*, 181(14):2933-2950.

[19] Khanesar, M. A.; Teshnehlab, M.; Kaynak, O. (2012) Control and synchronization of chaotic systems using a novel indirect model reference fuzzy controller, *Soft Computing*, 16(7):1253-1265.

[20] Di Cairano, S.; Bemporad, A.; Kolmanovsky, I.V.; Hrovat, D. (2007) Model predictive control of magnetically actuated mass spring dampers for automotive applications, *International Journal of Control*, 80(11):1701-1716.

[21] Dragoş, C.-A.; Preitl, S.; Precup, R.-E.; Petriu, E.M.; Stînean, A.-I. (2011) A comparative case study of position control solutions for a mechatronics application, *Proc. of 2011 IEEE/ASME International Conference on Advanced Intelligent Mechatronics*, Budapest, Hungary:814-819.

[22] Angelov, P.; Buswell, R. (2003) Automatic generation of fuzzy rule-based models from data by genetic algorithms, *Information Sciences*, 150(1-2):17-31.

[23] Precup, R.-E.; Tomescu, M.-L.; Preitl, S. (2007) Lorenz system stabilization using fuzzy controllers, *INT J COMPUT COMMUN*, ISSN 1841-9836, 2(3):279-287.

[24] Johanyák, Z.C. (2010) Student evaluation based on fuzzy rule interpolation, *Int. J. of Artificial Intelligence*, A10(5):37-55.

[25] Vaščák, J.; Madarász, L. (2010) Adaptation of fuzzy cognitive maps-A comparison study, *Acta Polytechnica Hungarica*, 7(3):109-122.

[26] Sadighi, A.; Kim, W.-J. (2011) Adaptive-neuro-fuzzy-based sensorless control of a smart-material actuator, *IEEE/ASME Transactions on Mechatronics*, 16(2):371-379.

[27] Ho, T.H.; Ahn, K.K. (2012) Speed control of a hydraulic pressure coupling drive using an adaptive fuzzy sliding-mode control, *IEEE/ASME Transactions on Mechatronics*, 17(5):976-986.

[28] Precup, R.-E.; Preitl, S. (2004) Optimisation criteria in development of fuzzy controllers with dynamics, *Engineering Applications of Artificial Intelligenc*e, 17(6):661-674.

[29] Blažič, S.; Matko, D.; Škrjanc, I. (2010) Adaptive law with a new leakage term, *IET Control Theory & Applications*, 4(9):1533-1542.

[30] Sánchez Boza, A.; Haber-Guerra, R.; Gajate, A. (2011) Artificial cognitive control system based on the shared circuits model of sociocognitive capacities. A first approach, *Engineering Applications of Artificial Intelligence*, 24(2):209-219.

[31] Liu, T.; Hu, Z. (2011) Immune algorithm with memory coevolution, *Int. J. of Artificial Intelligence*, 7(A11):189-197.

[32] Niu, B.; Fan, Y.; Wang, H.; Li, L.; Wang, X. (2011) Novel bacterial foraging optimization with time-varying chemotaxis step, *International Journal of Artificial Intelligence*, 7(A11):257-273.

[33] Damanafshan, M.; Khosrowshahi-Asl, E.; Abbaspour, M. (2012) GASANT: An ant-inspired least-cost QoS multicast routing approach based on genetic and simulated annealing algorithms, *INT J COMPUT COMMUN*, ISSN 1841-9836, 7(3):417-431.

[34] Rankovic, V.; Radulovic, J.; Grujovic, N.; Divac, D. (2012) Neural network model predictive control of nonlinear systems using genetic algorithms, *INT J COMPUT COMMUN*, ISSN 1841-9836, 7(3):540-549.

[35] Bacanin, N.; Tuba, M. (2012) Artificial Bee Colony (ABC) algorithm for constrained optimization improved with genetic operators, *Studies in Informatics and Control*, 21(2):137-146.

[36] Ben Omrane, I.; Chatti, A.; Borne, P. (2012) Evolutionary method for designing and learning control structure of a wheelchair, *Studies in Informatics and Control*, 21(2):155-164.

INT J COMPUT COMMUN, ISSN 1841-9836
8(3):407-415, June, 2013.

Automatic Growth Detection of Cell Cultures through Outlier Techniques using 2D Images

P.A. Gagniuc, C. Ionescu-Tîrgovişte, C. H. Rădulescu

Paul Aurelian Gagniuc
Department of Genetics, University of Bucharest, Romania
E-mail: paulgagniuc@yahoo.com

Constantin Ionescu-Tîrgovişte
National Institute of Diabetes,
Nutrition and Metabolic Diseases "N.C. Paulescu", Romania
E-mail: cit@paulescu.ro

Clara Hortensia Rădulescu
National R&D Institute for Textile and Leather, Romania
E-mail: clarabios@yahoo.com

Abstract:
Using conventional statistics, we have developed a new method for cell culture analysis through outlier detection techniques. Statistical methods enable researchers in microbiology to identify experimental parameters that are critical for colony growth and inhibition. This paper reports a method for analysing 2D images of cell cultures in Petri dishs, such as fungi, bacteria or yeast. The aim of this study was to obtain a sensitive and robust method for detection of growth rate, surface coverage and the approximate number of cells in the colony. For testing we have implemented a software application called MoldATRIX. This software generates useful statistics and displays critical information about the cell colony area. Our results were obtained by analyzing a series of digital images of *Aspergillus niger* cultures at different time intervals. Moreover, our results show the behavior of *Aspergillus niger* on leather.
Keywords: outliers, cell cultures, biodegradation, growth detection.

1 Introduction

New textile materials are conceived in order to increase their biodegradability properties [1]. For research, small quantities of bacteria or fungal cells are usually grown in a petri dish on a solid support that contains embedded nutrients (agar gel with a particular mix of nutrients), and new textile samples. Molds extract energy from organic matter in which they live and some of them play an important role in biodegradation [3, 4], food production, antibiotics [2] or enzyme synthesis. These microorganisms can be found in divisions such as Ascomycota, Deuteromycota or Zygomycota. Usually, molds secrete hydrolytic enzymes [4–6] which degrade complex biopolymers [8] such as cellulose [2, 3] or starch into simpler substances. Therefore, molds play a major role in decomposition of organic material. There are many known species of molds (eg. pathogens, aquatic species, thermophiles), but their impact is not known for new products (ie. new textile materials). Accordingly, their behavior should be measured quickly by different laboratories. The criteria for evaluation of the behavior of some leather samples [8] toward the fungi [1, 6] is represented by the percentage of the surface coverage with mycelium. Nevertheless, the EN 14 119 standard provides a table of correspondence for this percentage. Yet, there is no indication in this standard of a technique for measuring the coverage of the mycelium surface. The immediate option of the laboratory operator is a subjective visual approximation of the mycelium percentage from the total surface of the sample. Yet, this remains an empirical evaluation. Biodegradation process is currently studied for textile industry [7, 14]. Many leather

materials are tested with different mold cultures in order to characterize the type of fabric and the impact it has on the environment or the behavior in special conditions [16] (eg. extreme temperatures, long-term resistance). Parameters such as rate of growth, surface coverage or the number of cells are very difficult to quantify. We have developed an algorithm based on outlying observations [17, 18] which can extract data from pictures (photos) of the mold culture surface [19], made at different time intervals. An outlying observation is defined as an anomaly that appears to deviate from other members of the sample. Outliers may indicate data points that belong to a different population than the rest of the sample set. Identifying an observation as an outlier depends on the underlying distribution of the data. For testing we have implemented a software application called MoldATRIX (Supplementary material 1), which can work with bitmap or JPEG (Joint Photographic Experts Group) files taken from a digital camera. The aim of this paper is to provide a method of measurement for biodegradation, in order to certify the integration of new materials. Continuing the work presented in [20] with additional results and several refinements, we show a novel method for detection of colony area, growth rate and the approximate number of cells in the colony.

2 Materials and Methods

The European standard EN 14 119:2003 "Testing of textiles - Evaluation of the action of microfungi" was used in order to test the behavior of some leather samples towards the action of the philamentous fungus *Aspergillus niger* IMI 045551 [21]. Agar plates are frequently used in microbiology. Agar medium with mineral salts and a carbon source (glucose) was used as a culture medium. The medium was sterilized in an autoclave at $115°C$ for 30 minutes. In order to obtain the inoculum (cell suspension), a fresh culture tube was used. The surface of the culture was gently scraped, and then the spores were washed and centrifuged twice in a EBA 21 centrifuge. Next, the medium was held at $50°C$ in a waterbath. The inoculum was mixed with the medium and then was poured in Petri dishes (of 90 mm diameter, with a depth of maximum 5 mm) for cooling at room temperature for 20 minutes. The leather samples were cut in 25 mm square form and placed in the center of the Petri dish. Next, all Petri dishes were incubated at a temperature of $28 \pm 2°C$ for 14 days. Throughout this period, the cell cultures were photographed at 3, 7 and 14 days.

2.1 Implementation

In order to detect the surface coverage on leather materials we designed an algorithm consisting of five main loops. First, we consider a digital image (of the mold sample - 255x255 pixels) as a square matrix A (Figure 1A). Each pixel color can be represented by a 24-bit or 32-bit RGB value. Therefore, each pixel can be considered an element with a value between 0 and 32 million. We then consider a void square matrix B (255x255 pixels) that stores the outlier values (Figure 1B). Initially, the algorithm requires a traversal through every pixel of the image (matrix A) in order to store the pixel values inside variable e. The mean is obtained by dividing variable e to the total number of elements (pixels) from matrix A. Next, the algorithm calculates the variance, standard deviation and the Z-score for all pixels of matrix A. Outlier values are listed in matrix B depending on the Z-score value for each pixel of matrix A. If the Z-score for a pixel of matrix A exceeds a threshold value (user specified parameter), the program copies the pixel position and value into matrix B. Next, the algorithm calculates the density of pixels from matrix B and displays the results. The growth rate of the cell culture is calculated based on photographs taken at various time intervals. The program can store the results of tests carried out for other pictures of the same cell culture. Accordingly, surface coverage can be calculated by:

$$C = \left(\frac{100}{E}\right) \times OL \tag{1}$$

where C represents the surface coverage, E represents the total number of elements from matrix A and OL represents the number of outliers found. For our experiment, we used three intervals, namely C_1=3 days, C_2=7 days and C_3=14 days.

In our test, a total of four pictures were analyzed. The first picture represents a control sample used to verify the average pixel color before the cell culture growth. The other three images are taken from C_1, C_2 and C_3 intervals. In order to detect the culture growth rate, we used the difference between two images of the mold surface taken at different time intervals ($G = C_{n-1} - C_n$). Nevertheless, the number of photos and the intervals between photo shots can be chosen by the user. The approximative number of cells is estimated by converting the number of pixels into millimeters. Thus, the result is multiplied by the number of outliers found and by cell density/millimeter (eg. yeast size can vary depending on the species, typically measuring $3\mu m$ up to $40\mu m$),

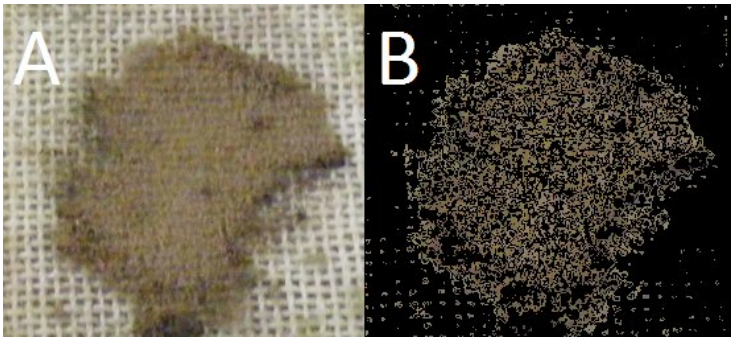

Figure 1: Textile material analysis. (**A**) a textile material image containing a mold culture (**B**) outlier pixels.

$$NC = \left(OL \times \left(\frac{P}{M}\right)\right) \times CM \tag{2}$$

where NC represents the total number of cells, OL represents the number of outliers found, P stores the number of pixels on $y - axis$ or $x - axis$ (number of rows or colums on the square matrix A), M represents the size of the sample (millimeters) and CM represents the number of cells/millimeter. Depending on the chosen yeast or fungal species, the density of cells/millimeter is a parameter left to the user appreciation. Yeasts are unicellular, although some species may become multicellular through the formation of pseudohyphae or false hyphae (ie. molds). These unicellular and pseudohyphae yeasts lead to different densities of cells/millimeter, due to a different spatial positioning inside the colony (ie. formation of 3D structures that can not be neglected in some cases). For these special cases, a calculation of the colony surface is not an adequate solution.

2.2 Algorithm implementation

We aimed at assessing the effectiveness of the proposed algorithm by implementing a GUI application (Figure 3). Below we show the source code implementation of the algorithm, syntactically compatible with VBA, VBScript, Visual Basic 4,5,6, Visual Basic .NET and 2005.

```
1 Dim Mean, Variance, SD, Background_Mean, pixel As Double
2
3 Dim X, Y, X1, Y1, e, p1 As Double
4 Matrix_B.Cls
5
6 X1 = Matrix_A.ScaleWidth - 1
7 Y1 = Matrix_A.ScaleHeight - 1
8 e = 0
```

```
9
10 For x = 0 To X1
11     For Y = 0 To Y1
12         e = e + 1
13         Mean = Mean + Matrix_A.Point(X, Y)
14     Next
15 Next
16
17 Mean = Mean / e
18
19 e = 0
20 For x = 0 To X1
21     For Y = 0 To Y1
22         e = e + 1
23         pixel = control_pic.Point(X, Y)
24         Background_Mean = Background_Mean + pixel
25     Next
26 Next
27
28 Background_Mean = Background_Mean / e
29
30 e = 0
31 For x = 0 To X1
32     For Y = 0 To Y1
33         e = e + 1
34         pixel = Matrix_A.Point(X, Y)
35         Variance = Variance + (pixel - Mean) ^ 2
36     Next
37 Next
38
39 Variance = Variance / e
40 SD = Sqr(Variance)
41
42 For x = 0 To X1
43     For Y = 0 To Y1
44         p1 = Matrix_A.Point(X, Y)
45         zP = zP + p1
46         z = (p1 - Background_Mean) / SD
47
48         If (Abs(z) >= (1/100) * Int(Lim.LowerValue) And Abs(z) <= (1/100) * _
49             Int(Lim.UpperValue)) Then
50             Matrix_B.PSet (X, Y), p1
51         End If
52     Next
53 DoEvents
54 Next
55
56 zMare = (zP - Mean) / SD
57
58 For x = 0 To X1
59     For Y = 0 To Y1
60         q1 = q1 + 1
61         If Matrix_B.Point(X, Y) <> 0 Then q2 = q2 + 1
62     Next
63 Next
64
65 total_elements = (100 / q1)
66 procentage = total_elements * q2
67 CM = val(CM_txt.Text)
68 M = val(M_txt.Text)
69 P = Matrix_A.ScaleHeight
70 pm = P / M
71 NC = (q2 * pm) * CM
```

Variable `Background_Mean` represents the average pixel color of the control sample and `Mean` variable represents the average pixel color of the matrix A. The input objects, such as `CM_txt.Text` or `M_txt.Text`, are responsible for taking user input parameters. `CM_txt.Text` object stores the side length of a square (fabric size from the petri dish) and `M_txt.Text` object stores the amount of cells/millimeter. For the `Background_Mean` value, the user can also click with the mouse on the matrix A object to choose the cell culture approximative color value.

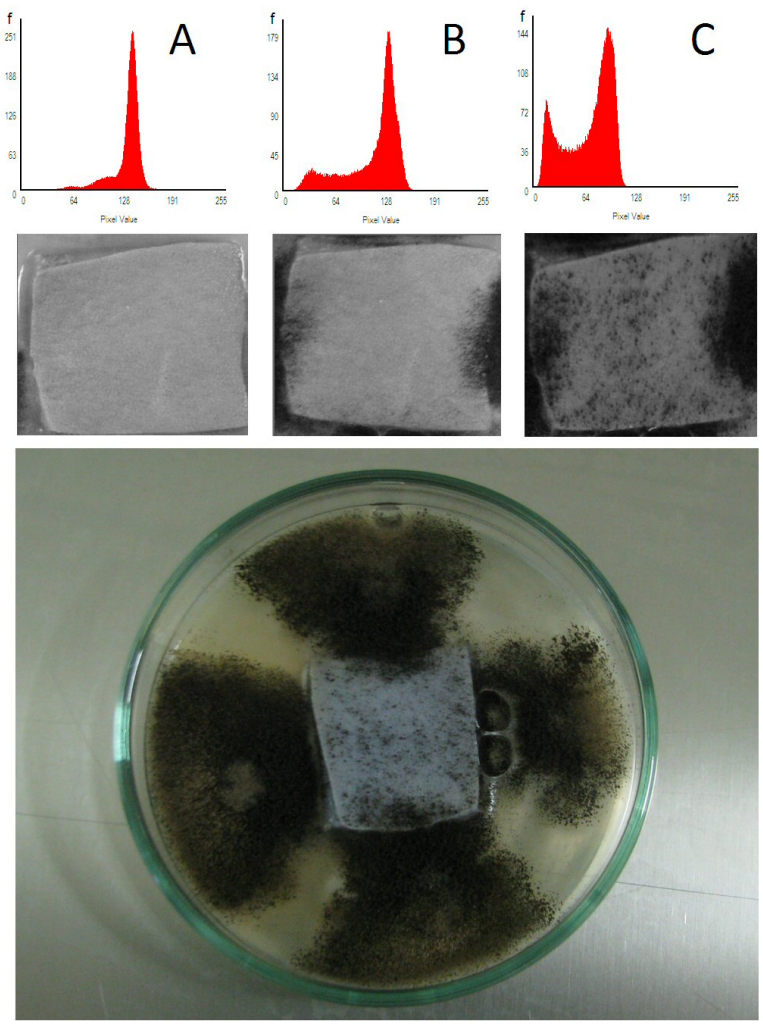

Figure 2: Results from the analysis of leather materials against *Aspergillus niger* cultures. The alignment of cell culture images following (**A**) C_1 phase, (**B**) C_2 phase and (**C**) C_3 phase. Their corresponding histograms are presented at the top of the figure. The petri dish is shown at the bottom of the figure.

2.3 Equipment

We used a digital camera connected to a tripod. The distance between the petri dish and the digital camera was set to 25 centimeters (9.84 inch). Initially, for calibration reasons, the petri dish contained a ruler (the measuring unit was the centimeter) next to the sample. The ruler is important for further image processing on MoldATRIX software. The leather sample was cut from the picture at 25 mm by using the ruler from the image. Next, the sample area (of 25x25 mm) is stretched to 255x255 pixels and is processed by MoldATRIX program. However, the ruler is not a mandatory criteria. Another method consists of cutting a square-shaped sample (25x25 mm), thus avoiding the use of the ruler from the petri dish. An alternative method is to find the size of the sample directly from the photo by performing a pixel to millimeter transformation using dots or pixels per inch (dpi, 1 inch = 25.4 mm),

$$mm = \frac{(pixel \times 25.4)}{dpi} \tag{3}$$

MoldATRIX runs on all Windows operating systems, no installation required and the complete package has 9.44Mb (Supplementary material 1). MoldATRIX memory requirements are between 1.9Mb and 5Mb, depending on Windows OS version. MoldATRIX was tested on a computer equipped with an Intel P4 - 2800 MHz and 512 MB DDR dual channel.

3 Results and Discussion

An outlier is an observation that is numerically distant from the rest of the data. A common method for outlier detection is to look for observations that deviate more than three times ($3\sum$ edit rule) the standard deviation from the mean. However, this is not the only criterion that could be used. Is also common practice to use Z-scores to identify possible outliers [22]. The proposed algorithm uses Z-scores and is tested on various images with different characteristics.

We also made additional tests to verify the correctness of the algorithm. Perhaps the most useful tool available in digital photography is the histogram [23, 24]. We generate histograms from a gray image sample of the cell culture by plotting the number of pixels for each color value. As shown in Figure 2, once the cell culture increases, the second peak appears in the histogram (Figure 2(A,B,C)). On the $x - axis$, the histogram shows color variations of the sample, while on the $y - axis$ shows the number of pixels of that particular color. The left side of the histogram represents the black areas of the square sample, whereas the middle represents medium grey and the right side represents the pure white areas. For tests we used leather against *Aspergillus niger*. In C_1 phase the mold coverage accounted for approximately 2%. In C_2 phase the mold coverage increased to 7% and in the last phase, C_3, the mold coverage has reached 22% (Figure 4). Growth rate is calculated according to each pre-final phase ($G = C_{n-1} - C_n$). Table 1 shows the results of $C_1 \ldots C_3$ phases, where MC represents the mold coverage and MG represents the mold growth rate. $MaxPV$ stands for the maximum pixel value, whereas $MinPV$ represents the minimum pixel value (Supplementary material 2).

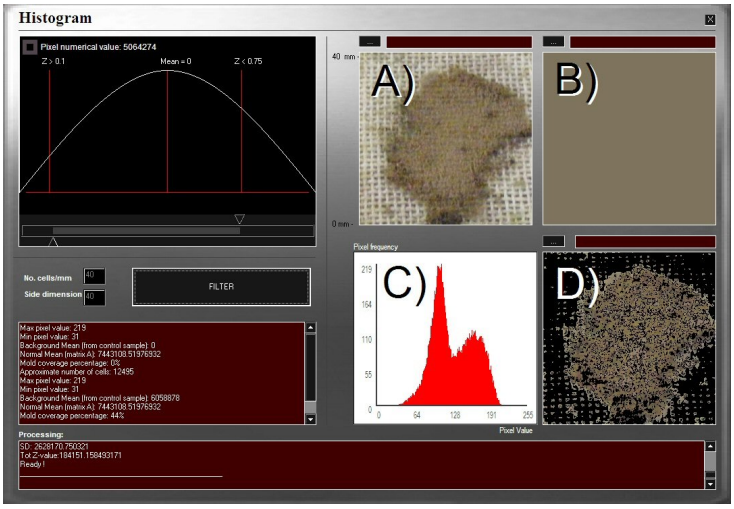

Figure 3: MoldATRIX program. On the right we show four matrices, (**A**) matrix A that contains the picture of the cell culture at a certain stage of growth (C_1, C_2 or C_3), (**B**) represents the control sample, (**C**) represents the histogram of matrix A, (**D**) represents matrix B. On the left panel are the control parameters, results window and the status window.

Table 1: *Aspergillus niger* on leather

C_n	MC	MG	$MinPV$	$MaxPV$
C_1	2%	2%	32	251
C_2	8%	6%	11	179
C_3	22%	14%	3	144

In MoldATRIX, users can define specific parameters, such as color differentiation (outlier pixels), sample size or number of cells/millimeter. For a better implementation of an experiment, users can create particular camera settings allowing different environments, such as illumination or color intensity. Nevertheless, in order to obtain clear and reliable results, the same initial settings must be preserved for each experiment.

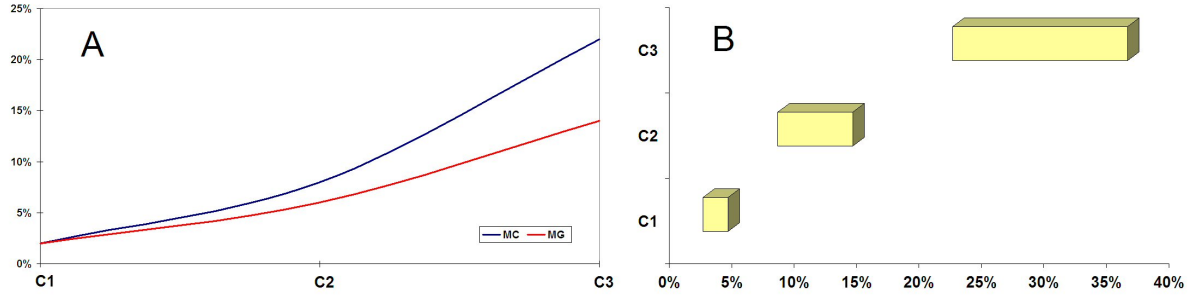

Figure 4: *Aspergillus niger* growth rate on leather. Two visualization methods are used: (**A**) blue line represents the mold coverage (MC) and the red line represents the mold growth rate (MG), (**B**) light yellow bars start from the MC value and show the mold growth for each phase.

Different methods, algorithms and automated systems have been proposed for cell culture studies. The outlier data detection may also be a potential solution for numerous studies performed on diabetes-related issues [25–28], such as electron microscopy images of b-cells or adipocyte cells. Some other possible applications are in the area of genomic signal processing [29–31], where outlier data usually exhibits biological significance.

Notice: Part of this paper was presented in a preliminary version as [20].

4 Conclusion and Future Works

Mold species within the genus Aspergillus have a large chemical range. Among scientists working on molds, there is an endless fascination with their biodeterioration potential. In this work, a new method was proposed in order to improve the quality of results for cell culture (ie. fungi, bacteria or yeast) studies on textile materials. Our immediate step is to use this method in cooperation with a neural network in order to detect different cellular structures on electron microscopy images. Future applications may include other areas, such as antibiotic research, hygiene research, contamination control or bioinformatics.

5 Acknowledgments

This research was partially funded by *Ministry of Education, Youth and Sports* through the PN2IDPCE2011-30429 project.

Bibliography

[1] J.W. Raymond, T.N. Rogers, D.R. Shonnard, A.A. Kline, A review of structure-based biodegradation estimation methods, *J Hazard Mater*, 84(2-3):189-215, 2001.

[2] K.N. Bharath, R.P. Swamy, G.C. Mohan Kumar, Experimental studies on biodegradable and swelling characteristics of natural fibers composites, *International Journal of Agriculture Sciences*, Vol.2, No.1, pp. 01-04, 2010.

[3] K.B. Raper, C. Thom, *A Manual of the Penicillium*, The Williams & Wilkins Co., Baltimore, 1949.

[4] S. Moularat, E. Robine, O. Ramalho, M.A. Oturan, Detection of fungal development in closed spaces through the determination of specific chemical targets, *Chemosphere*, 72, pp. 224-232, 2008.

[5] S. Lehrer and A. Nowotny, Isolation and Purification of Endotoxin by Hydrolytic Enzymes, *Infection and immunity*, Vol. 6, No. 6, pp. 928-933, 1972.

[6] W.E.S. Carr et al., The role of degradative enzymes in chemosensory processes, *Chem. Senses*, 15(2):181-190, 1990.

[7] S.P. Vinogradova and S.N. Kushnir, Biosynthesis of Hydrolytic Enzymes during Cocultivation of Macro- and Micromycetes, *Applied Biochemistry and Microbiology*, Vol. 39, No. 6, pp. 573-575, 2003.

[8] N. Lucas et al., Polymer biodegradation: Mechanisms and estimation techniques, *Chemosphere*, 73, pp. 429-442, 2008.

[9] D. Montegut, N. Indictor, R.J. Koestler, Fungal Deterioration of Cellulosic Textiles: a Review, *Intern. Biodet. Bull.*, 28, pp. 209-226, 1991.

[10] C. Aranyank, Microscopical Study of Fungal Growth on Paper and Textiles, *Proceedings of the 3rd International Conference on Biodeterioration of Cultural Property*, 4-7, Bangkok, Thailand, pp. 83-102, 1995.

[11] C.H. Xue et al., Preparation of superhydrophobic surfaces on cotton textiles, *Sci. Technol. Adv. Mater*, Vol. 9, No.3, pp. 1-7, 2008.

[12] K.H. Domsch et al., *Compendium of soil fungi*, Vol. 1 and 2, Academic Press, London, 1980.

[13] J.C. Gilman, *A Manual of Soil Fungi*, Second Edition, U.S.A., 1975.

[14] J. Szostak-Kotowa, Biodeteration of Textiles, *Int. Biodeter. Biodegrad.*, 53, pp. 165-170, 2004.

[15] D. K. Setua, G. D. Pandey, R. Indusekhar, G. N. Mathur, Biodeterioration of coated nylon fabric, *Journal of Applied Polymer Science*, 75(5):685-691, 2000.

[16] E.D. Weil and S.V. Levchik, Flame Retardants in Commercial Use or Development for Textiles, *Journal of Fire Sciences*, 26(3):243-281, 2008.

[17] M. Agyemang, K. Barker, and R. Alhajj, A comprehensive survey of numeric and symbolic outlier mining techniques, Intell. *Data Anal.*, 10:521-538, 2006.

[18] V. Barnett and T. Lewis, *Outliers in Statistical Data*, John Wiley & Sons., 3rd edition, 1994.

[19] D. J. Watts and J. M. Ashworth, Growth of Myxamoebae of the Cellular Slime Mould Dictyostelium discoideum in Axenic Culture, *Biochem. J.*, Vol. 119, pp. 171-174, 1970.

[20] P. Gagniuc et al., Automatic growth detection of cell cultures through outlier techniques, GSP 2011, *2nd International Workshop on Genomic Signal Processing*, pp. 143-147, 2011.

[21] K.A. Powell, A. Renwick, and J.F. Peberdy, *The Genus Aspergillus from taxonomy and genetics to industrial application*, Plenum Press in New York, 1994.

[22] Richard J. Larsen and Morris L. Marx, *An Introduction to Mathematical Statistics and Its Applications*, Third Edition, Prentice Hall, Upper Saddle River, USA, 2000.

[23] H.O. Lancaster, *An Introduction to Medical Statistics*, John Wiley and Sons, 1974.

[24] D.W. Scott, On optimal and data-based histograms, *Biometrika*, 66(3):605-610, 1979.

[25] C. Ionescu-Tîrgovişte and F. Despa, Biophysical alteration of the secretory track in b-cells due to molecular overcrowding: the relevance for diabetes, *Integrative Biology*, 3(3):173-179, 2010.

[26] C. Ionescu-Tîrgovişte, A short personal view on the pathogenesis of diabetes mellitus, *Proc. Rom. Acad., Series B*, 12(3):219-224, 2010.

[27] A. Constantin & G. Costache, The emerging role of adipose tissue-derived leptin in inflammatory and immune responses in obesity: an update, *Proc. Rom. Acad., Series B*, (1):3-12, 2010.

[28] N. Milici, A short history of the metabolic syndrome definitions, *Proc. Rom. Acad., Series B*, (1):13-20, 2010.

[29] P.D. Cristea, R. Tuduce, *Use of Nucleotide Genomic Signals in the Analysis of Variability and Inserts in Prokaryote Genomes*, BIOCOMP 2008, pp. 241-247, 2008.

[30] P.D. Cristea, Large scale features in DNA genomic signals, *Signal Processing*, 83(4):871-888, 2003.

[31] P. Gagniuc et al., A sensitive method for detecting dinucleotide islands and clusters through depth analysis, *RJDNMD*, 18(2):165-170, 2011.

INT J COMPUT COMMUN, ISSN 1841-9836
8(3):416-424, June, 2013.

Erosion based Method for Quantification of Facial Palsy

M. Găianu, G. Cristescu, D. M. Onchiş

Mihail Găianu
West University of Timişoara
România, 300223 Timişoara, Vasile Pârvan No. 4,
E-mail: mgaianu@info.uvt.ro

Gabriela Cristescu
Aurel Vlaicu University of Arad
România, 310130 Arad, Bd. Revoluţiei, Nr. 77,
E-mail: gcristescu@inext.ro

Darian M. Onchiş
University of Vienna
Austria, Nordbergstrasse 15, A-1090, Vienna
E-mail:darian.onchis@univie.ac.at

Abstract:
This paper presents a novel 3D face recognition method developed by means of erosion of a contractible topological space. The procedure was is involved in the quantification of facial palsy using pre-marked points. The recognition is done in two steps: in the first step a detection of the pre-marked mimic points on a human face is performed and in the second step the mutual distances between points are calculated. A procedure of deducing the mobility or the immobility of points and the amplitude of mimic points movement follows.
Keywords: distance, deletable point, interest point of mimic, Univalue Segment Assimilating Nucleus.

1 Introduction and main results

Face recognition is a challenging task, that has been extensively investigated during the last years by many authors (e.g. [1, 2]). While most of the previous has face recognition works based on 2D images, the development of 3D scanning techniques moved the domain towards the 3D face recognition. In a controlled environment, the actual 2D face recognition techniques can achieve acceptable accuracy, but inadequate for more challenging applications, especially in the presence of variation of lighting conditions and positions. Therefore, the approach using 3D recognition, by including the complete geometrical information, provides potential to alleviate the impact of lightening and position and may improve the recognition performance.
Detecting and tracking markers on the 3D human face is a challenging task. A standard procedure in this field is to use the level set algorithm ([1]). An important aspect is to measure the geodesic distances between markers applied on the 3D human face in order to emphasize the interest points of mimic and to evaluate the improvement of the face mobility. The purpose of this paper is to elaborate a method of detecting the interest points of face mimic, followed by computing the mutual distances between them together with a method of deducing the movement and its amplitude. Nowadays physicians use to measure these distances by means of the classical rule, which is an operation affected by considerable error. A computer aided procedure of points detecting and distance computing benefits of the possibility of increasing the resolution, which diminishes the error size.

The patient is placed in a two mirror system, which was developed by Frey, Jenny, Giovanoli and Stussi in ([2]). In the first step, the interest points of mimic are marked with a water-resistant pen on the patient's face (see Figure 1), obtaining a mask. The mimic interest points are:

- Central points: Central Nose (CN), Philtrum (PH=CM);
- Left side points: Left Ala of the Nose (LAN), Left Brow (LBP), Left Lower Eyelid (LLE), Left Mouth Corner (LMC), Left Midlateral Point of the Lower Lip (LML), Left Midlateral Point of the Upper Lip (LMU), Left Tragus (LTR), Left Upper Eyelid (LUE);
- Right side points: Right Ala of the Nose (RAN), Right Brow (RBP), Right Lower Eyelid (RLE), Right Mouth Corner (RMC), Right Midlateral Point of the Lower Lip (RML), Right Midlateral Point of the Upper Lip (RMU), Right Tragus (RTR), Right Upper Eyelid (RUE).

In a computer image each interest point of the mimic, i.e. each marked point of the mask, is represented by an area consisting in a set of pixels colored by the marker called Univalue Segment Assimilating Nucleus (usually denoted by USAN) [14]. Marking is necessary, because otherwise the points cannot be identified at the same place, especially on the side views of the face of the two mirror images.

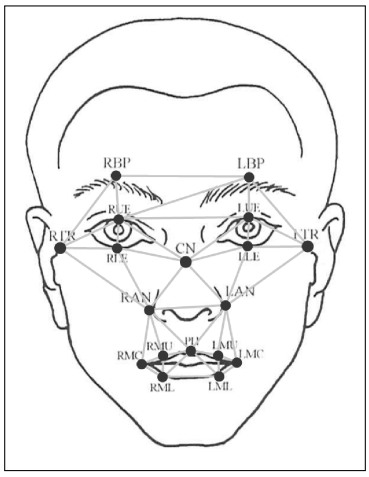

Figure 1: Pattern of the markers

Phases of diagnose computer aided process presented in this paper are:

- Operation 1: Marking interest points of mimic on patient's face;
- Operation 2: Acquiring the image of patient's face from video camera;
- Operation 3: Selecting a restricted area including one interest point of mimic;
- Operation 4: Detecting the contour of USAN (Univalue Segment Assimilating Nucleus);
- Operation 5: Determining a representing pixel of USAN by erosion and detecting a marker with the algorithm 1;
- Operation 6: Preserving the coordinates of the representing pixel;

- Operation 7: Decision: If all interest points are detected:
  - No - Repeat from Operation 3 to Operation 6;
  - Yes - Go to Operation 8;
- Operation 8: Computing mutual distances between pixels representing interest points of mimic and introducing them into the database;
- Operation 9: Repeating Operations 2 - 7 and computing the maximum variation of each distance;
- Operation 10: Decision on the mobility by comparing the variation of distances;
- Operation 11: Presenting the result to the physician.

The paper is structured as follows. In the second section the algorithm used during the proposed procedure of the computational diagnose aid is described. In the third section, after the detection (see Figure 2), we calculate the mutual distances between the markers on the face and use them to describe the face mobility. Some numerical results are included.

2 Active contours models and interest points detection

There are two main approaches in active contours models based on the mathematic implementation: snakes and level sets. Snakes explicitly move predefined snake points based on an energy minimization scheme, while level set approaches move contours implicitly as a particular level of a function.
As image segmentation methods, there are two kinds of active contour models according to the force evolving the contours: edge- and region-based. Edge-based active contours use an edge detector, frequently based on the image gradient, to find the boundaries of sub-regions and to attract the contours to the detected boundaries.

The first model of active contour was proposed by Kass, Witkin and Terzopoulos in ([5]) and named snakes due to the appearance of contour evolution. This method originates in various erasing techniques, which started with the algorithms of Rosenfeld ([8]). The same class of chain techniques are used in linear programming, for example in fast solving a class of transportation problems ([4]). The snake method consists in selecting a set of points, called snake points, which is connected and defines the contour. The snakes points are initially placed at further distance from the boundary of the object. Then, each point moves towards the optimum coordinates, according to some specific rule. The snake points eventually stop on the boundary of the object. The classic snakes provide an accurate location of the edges only if the initial contour is given sufficiently closed to the edges because they make use only of the local information along the contour. Estimating a proper position of initial contours without prior knowledge is a difficult problem. Also, classic snakes cannot detect more than one boundary simultaneously because the snakes maintain the same topology during the evolution. That is, snakes cannot split into multiple boundaries or merge from multiple initial contours.

For that reason more authors discuss approach using the level set method, which was first proposed by Osher and Sethian [7], [13]. A formulation to implement active contours in this way, was proposed by Osher and Sethian ([11], [7]). Level sets represent a contour implicitly via a two-dimensional Lipschitz-continuous function $\phi(x, y) : \Omega \to \mathbb{R}$ defined on the image plane Ω. This function results by solving a differential equation. This equation is digitized into a finite

differences equation, which describes the frontier of the domain by level sets.

The model we use in this paper takes into account the pixel by pixel description of the image, originating in the fundamental image analysis literature ([8]). Each image is represented as a $n \times m$ matrix, where n is the number of pixels on horizontal and m is the number of pixels on the vertical of the screen. So, the image is a subset of a network $\mathbb{Z}^2(h) = \{(ih, jh) | i, j \in \mathbb{Z}^2\}$ over a rectangle from $\mathbb{R}^2$, of sides equal to the dimensions of the computer screen. The number h is given by the selected resolution, representing the length of the side of a pixel (without loss of generality, a pixel is considered to be a square). So, the structure in which we work is that of a totally bounded metric space embedded into the linear space $\mathbb{R}^2$. Also, we consider it as a topological space, with the topology induced by the metric. The number h is considered to be the measurement unit for computing and decision making and it is finally converted into the desired unit according to the requirement of the user.

A subset of an image, which is the object of our computation procedure, is the digitization of a contractible topological space from mathematical point of view, i.e. a topological space that reduces to a point by means of a homotopy. The following concepts and properties are necessary in order to describe the procedures. Let $X \subseteq \mathbb{R}^2$ a contractible topological space. We consider, without loss of generality, the digitization of the space X by means of the method of digitization, $f : \mathbb{R}^2 \to \mathbb{Z}^2$,

$$f(x, y) = ([x + \frac{1}{2}], [y + \frac{1}{2}]), (x, y) \in \mathbb{R}^2.$$

If $x(ih, jh) \in \mathbb{Z}^2(h)$ is a grid point then its 4-neighborhood is the set $V_4(x) = \{x, (ih, (j - 1)h), (ih, (j+1)h), ((i-1)h, jh), ((i+1)h, jh)\}$ and its 8-neighborhood is the set $V_8(x) = V_4(x) \cup \{((i - 1)h, (j - 1)h), ((i + 1)h, (j - 1)h), ((i - 1)h, (j + 1)h), ((i + 1)h, (j + 1)h)\}$. The concepts of connectivity used in this paper are the 4-connectivity (i.e. defined using $V_4(x)$ by horizontal and vertical lines) and the 8-connectivity (i.e. defined using $V_8(x)$ by horizontal, vertical, at 45° and at 135° lines) by means of arcs, as defined in [8].

Proposition 1. *The digital image $f(X)$ of a contractible topological space $X \subseteq \mathbb{R}^2$ is a 8-connected set.*

Proof. If X is contractible then it is path connected. Denote by $S = f(X) \subset \mathbb{Z}^2(h)$ and consider the 8-connectivity in S. Suppose that S has an isolated point $a = (kh, lh)$, $k \in \mathbb{N}$, $l \in \mathbb{N}$. Let us consider the pixel having the center $(kh, lh) = f(a)$, i.e. the square $D = [kh - h/2, kh + h/2) \times [lh - h/2, lh + h/2)$. There is at least a point from X situated in the rectangle D, say point b. Therefore $f(b) = a$. Since a is an isolated point of S, The squares of side h and centers $((k-1)h, (l-1)h)$, $((k-1)h, lh)$, $((k-1)h, (l+1)h)$, $(kh, (l-1)h$, $(hk, (l+1)h)$, $((k+1)h, (l-1)h)$, $((k+1)h, lh)$, $((k+1)h, (l+1)h)$, i.e. the 8-neighbors of a, are not in $S = f(X)$. So, none of these squares contain points of X. Therefore, X is not connected, which contradicts the hypothesis that space X is contractible. ◇

Let $S \subset \mathbb{Z}^2$ a finite subset. After removing a point $x = (i, j) \in S$ from S the number of connected components of S or of $\mathbb{Z}^2 \setminus S$ may increase or decrease. Let us suppose that S is 4-connected (the case of the 8-connectivity is similar). A. Rosenfeld proved in [8] that if $S \subset \mathbb{Z}^2$ is a finite subset, $S \setminus \{x\}$ does not have less 4-connected components than S if and only if $V_4(x) \cap S \neq \emptyset$. Also, $\mathbb{Z}^2 \setminus (S \setminus \{x\})$ has not more 8-connected components than $\mathbb{Z}^2 \setminus S$ if and only if $V_8(x) \cap (\mathbb{Z}^2 \setminus S) \neq \emptyset$. If $x \in S$ such that $V_4(x) \cap S$ is contained in a 4-connected component of $V_8(x) \cap S$, then $S \setminus \{x\}$ does not have more 4-connected components than S. More, if $\mathbb{Z}^2 \setminus S$ does not have more 4-connected components than S, then $V_4(x) \cap S$ is included in a 4-connected component of $V_8(x) \cap S$. As consequence, the following concept is introduced in [8].

Definition 2. An element $x \in S$, which verifies the conditions: 1) $V_4(x) \cap S \neq \emptyset$, 2) $V_8(x) \cap (\mathbb{Z}^2 \setminus S) \neq \emptyset$, and 3) $V_4(x) \cap S$ is included in a 4-connected component of $V_8(x) \cap S$, is called a 4-deletable element.

As consequence of the above mentioned properties, Rosenfeld has proven in [8] that:

Theorem 3. *Let $S \subset \mathbb{Z}^2$ a finite set with the property that $\mathbb{Z}^2 \setminus S$ has only one 8-connected component. Then $S \setminus \{x\}$ has the same number of 4-connected components as S and $\mathbb{Z}^2 \setminus (S \setminus \{x\})$ has an unique 8-connected component if and only if x is 4-deletable.*

In [8] the deletable elements of a set are classified into two classes: extremities and corners. A point $x \in S$ is called extremity if $card(V_4(x) \cap S) = 1$. A point $x \in S$ is said to be a corner if $V_4(x) \cap S$ has exactly two neighbors of x in S. Every simple 4-connected set S having more than one element has at least two deletable elements.
In case of the 8-connectivity, a point $x \in S$ is said to be an extremity if $V_8(x) \cap S$ has either exactly one element, or two 4-neighboring elements, or three 4-neighboring elements out of which only one is in $V_4(x)$. A point $x \in S$ is said to be a corner if $V_8(x) \cap S$ has exactly three, four or five 4-neighboring elements, out of which only two are in $V_4(x)$.
The Diagnose Procedure consists in a succession of computer programs, as it follows:

i. *Program for frames acquiring* divides the succession of pictures taken from the face of the patient into frames, called images. The film is of AVI (Audio Video Interleaved) format, divided into frames having PNG (Portable Network Graphics) format, in order to allow procession. The resolution of the film is 720×576 pixels, with $25fps$ (frames per second). The frames are coded either on 8 bits (PNG-8) or on 24 bits (PNG-24), including the transparency on 256 levels. The result is a collection of 4150 images, indexed by $i \in \{1, 2, ..., 4150\}$.

ii. *Program for detection of the mimic interest centers on patient's face, and computation of mutual distances between them.* The pixel by pixel erosion algorithm below presents the manner of processing each image in order to detect the coordinates of each central pixel representing each marker on patient's face. Also, the manner of validation and storage of each marker is included. The search of these points is optimized in the algorithm we cut the margins, which do not offer relevant information. In this manner we reduce the number of color tests. Each center of marker is the center of an USAN area, which is approximately ellipse (circle) shaped. The USAN area is detected based on pixel by pixel color tests, detecting the contour and erasing each USAN area following the contour. The erosion means changing the color from the artificial USAN area color into face color. After determining the coordinates of centers of all USAN areas from an image, the mutual distances between these pixels is computed and stored into a database. The database contains all these distances taken from all the 4150 images from our collection.

iii. *Program for computing the difference between an image and the initial one.* Initially the patient's face is in relaxed position, which gives the so called initial image. In order to take the other images from the collection, the patient is asked to perform various movements of the face. The differences between the corresponding distances between the mimic interest centers give the information on the existence of a displacement on the face from an image to another one. The maximum positive difference and the minimum negative difference are chosen from the database, together with the images in which they appear. These images are presented to the physician, together with the numerical results, converted into required units.

iv. *Decision on the movement variability* is taken by analyzing the mutual distances and comparing them from an image to the next one. If the distance from a center, for example CN to another one, for example RAN does not change and the rest of the distances from LAN to LTR, CN, RAN are variable, then it follows that LAN is the moving point. It means that the patient moved ones face. The decision is also stored for further investigations and comparisons in order to assess the evolution of patient's face mobility in various stages of the treatment.

Algorithm 1: Detecting a point on the patient's face

```
Data: imagine, contour, x, y, area, detect
Result: detection of the markers on the patient face
initialization;
eps=2;
ok=0;
cnt;
while ok<25 do
    ok=0;
    cnt=contor;
    for j=x-20;j<=x+20;j++ do
        for i=y-30;i<=y+30;i++ do
            pixel=(rgb*)(data+i*width+j);
            is[cnt]=i;
            js[cnt]=j;
            vals[cnt]=area;
            if valid(imagine,pixel,i,j,eps)==1 then
                vals[cnt]=detect;
                ok++;
            end
            cnt++;
        end
    end
    eps+=3;
end
printf("%d\n ",eps);
contor=cnt;
```

The algorithm 1 detects the markers LTR, RTR, CN and others. The marker is being searched in a area of 40×60 pixels.

3 Numerical results

As a result of Operation 6 one obtains a collection of distinct points on the face of the patient.

Usually physicians measure the distance between each pair of these points using the rule, i.e. using the Euclidean distance in two dimensions. This is the reason we use this distance in our experiment. Increased accuracy may occur if another kind of metric is used, for example the Earth Mover's Distance. The Earth Mover's Distance was introduced in the computer vision

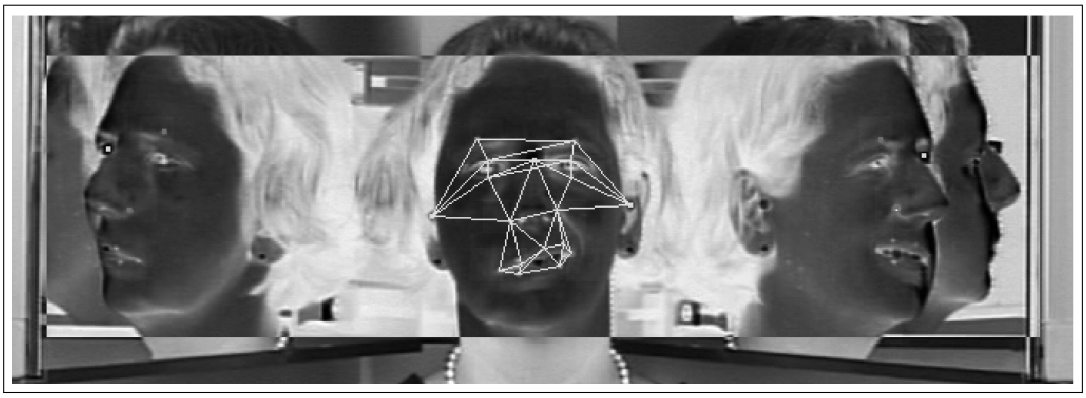

Figure 2: Detection of the points on the patient's face

Table 1: Mutual distances between the interest points of face mimic from figure 2

Location of interest points	**Mutual distance**
RTR↔RBP	55.569776
RTR↔RUE	49.497475
RTR↔RLE	42.438190
RTR↔RAN	49.091751
LTR↔LBP	53.150729
LTR↔LUE	46.400431
LTR↔LLE	40.718546
LTR↔LAN	46.097722
CN↔RUE	29.000000
CN↔RLE	31.016125
CN↔RAN	40.853396
CN↔LUE	23.000000
CN↔LLE	25.495098
CN↔LAN	34.014703
RBP↔LBP	61.008196
RBP↔RUE	14.764823
RUE↔LBP	55.317267
RUE↔RLE	11.000000
RLE↔RAN	30.413813
RLE↔LUE	53.150729
LBP↔LUE	12.165525

community in 1997 by Rubner, Guibas and Tomasi [10], [9] to overcome inconsistencies with perceptual similarity observed in (weighted) L_p -norms and quadratic forms.
The innovation of the paper consists in a more elaborated face model which allows quantification of facial palsy. Based on this model, a new scoring system for mimic function recovery is developed. More accurate results which are relevant for plastic surgery as well as for face models in computer vision are obtained. Another advantage of the method described in this paper is the real time data acquisition and processing. A fast high resolution real time 3D video system is used to acquire data from patients. They are filmed and analyzed before and after any kind of treatments in a standardized pre-treatment and follow-up scheme. If a patient is repeatedly analyzed in the above described manner, a database is constructed, which exactly document and visualize the recovery course of facial palsy. The system is able to recognize shape, texture, movements and illumination conditions of the face and is automatic in acquiring and processing patient's data. This simplifies the process of measuring and - at the same time - enhance the clinical methodology in terms of diagnostic and prognostic accuracy and convenience for patients. For example, the mutual distances between the mimic interest points on the face from figure 2 are in table 1. They are presented to the physician to be used in medical diagnose process. In this case the color to detect, i.e. the markers' color, is green and the function to maximize is a three dimensional vectorial one, obtained based on a normalized RGB description, in which the first coordinate refers to green. The order relation in $\mathbb{R}^3$ is the lexicographic one.
An important consequence of the technique described in this paper is the automatic evaluation of the facial palsy's degree of the patient. The system is able to directly perform a 3D face recognition thus supporting medical staff in exact planning the patient's medical procedures. The models allow to determine the position and movements of facial features with high accuracy, avoiding model bias in fitting to particularities of individual faces and diseases. The procedure described in this paper is setting up a high-end up to date standardized 3D facial palsy grading system, which is been used to monitor and document post-treatments course for facial palsy patients and to compare various surgical outcomes from different centers around the world. In fact, we propose a software that may lead to performing a standardized grading system and a comparison of 3D human face data.
The detection and tracking techniques may be extended from image data to video data. Since video is more complex, even more efficient retrieval techniques need to be developed using a multi-projection system as in [6], applying the powerful perception-oriented Earth Mover's Distance to video data.

4 Conclusions and Future Works

Detection in large image or other multimedia databases highly depends on the underlying similarity model. In future work, we plan to extend our detection and tracking concept techniques from image data to video data. Since video is more complex, even more efficient retrieval techniques need to be developed using a multi-projection system as in ([6]).
We plan to employ generative face models (i.e., models that can produce synthetic face images) which can be used for visualization of prognosis appearance of the patient's mimic and facial movements. Predictions of facial movements can be based on the statistical analysis of empirical data such as the past progression (e.g., preoperative/postoperative appearance) of facial movements of the subject or the class of subjects sharing similar pathologies. The ability to generate synthetic images of a face can further be exploited for biofeedback training of mimic musculature. Another important aspect in the future work will be the ability of quantifying and assessing mimic function by spontaneous facial movements as well.

Bibliography

[1] A. F. Abate, M. Nappi, D. Riccio, and G. Sabatino, 2d and 3d face recognition: A survey, *Pattern Recognition Letters*, 28(14):1885 - 1906, 2007.

[2] M. Frey, A. Jenny, P. Giovanoli, and E. Stussi, Development of a new documentation system for facial movements as a basis for the international registry for neuromuscular reconstruction in the face, *Plast Reconstr Surg*, 93(7):1334-1349, 1994.

[3] M. Găianu, *Contributions to the research of some problems of image recognition and retrieval (in Romanian)*, Thesis, West University of Timişoara, 2011.

[4] P.L. Hammer, S. Rudeanu, *Boolean methods in operations research and related areas*, Springer-Verlag, 1968.

[5] M. Kass, A. Witkin, and D. Terzopoulos,Snakes, active contour model, *International Journal of Computer Vision*, 321-331, 1988.

[6] D. Onchis and H. Feichtinger. Constructive reconstruction from irregular sampling in multi-window spline-type spaces, *General Proceedings of the 7th ISAAC Congress*, London, 2010.

[7] S. Osher and J. A Sethian. Fronts propagating with curvature-dependent speed: Algorithms based on hamilton-jacobi formulations, *Journal of Computational Physics*, 79(1):12 - 49, 1988.

[8] A. Rosenfeld, Conectivity in Digital Pictures, *J. ACM*, 17(1):146-160, 1970.

[9] Rubner, Y., Guibas, L. and Tomasi, C. The Earth Mover's Distance, Multi-Dimensional Scaling, and color based image retrieval. In *Proc. of the ARPA Image Under- standing Workshop*, 661-668, 1997.

[10] Rubner, Y. and Tomasi, C., *Perceptual Metrics for Image Database Navigation*, Kluwer Academic Publishers, 2001.

[11] J. A. Sethian, A fast marching level set method for monotonically advancing fronts, *Proceedings of the National Academy of Sciences of the United States of America*, 93(4):1591-1595, 1996.

[12] J. A. Sethian. *Level set methods and fast marching methods - evolving inter- faces in computational geometry, fluid mechanics, computer vision, and materials science.* In Interfaces in Computational Geometry, Fluid Mechanics, Computer Vision, and Materials Science. Cambridge University Press, 1998.

[13] J. Sethian, *Level Set Methods and Fast Marching Methods.* Cambridge Monographs on Applied and Computational Mathematics, Cambridge University Press, 2nd ed., 1999.

[14] S.M. Smith, J.M. Brady, SUSAN - a new approach to low level image processin, *Int. Journal of Computer Vision*, 23(1):45-78, 1997.

INT J COMPUT COMMUN, ISSN 1841-9836
8(3):425-431, June, 2013.

A Proactive VHD Algorithm in Heterogeneous Wireless Networks for Critical Services

C. Lozano-Garzon, N. Ortiz-Gonzalez, Y. Donoso

Carlos Lozano-Garzon, Nicolas Ortiz-Gonzalez, Yezid Donoso
Universidad de los Andes, Bogotá, Colombia
E-mail: ca.lozano968@uniandes.edu.co
n.ortiz908@uniandes.edu.co, ydonoso@uniandes.edu.co

Abstract:
Progress in the telecommunications sector has opened new scenarios where users want to access any application or service from any device anywhere at any time, connected to any network. In this environment, the Heterogenerous Wireless Networks (HWN) is the main operating infrastructure, intended to support the technical and quality needs that these users and services demand, along with the versatility and availability that comes with being able to connect to any interface. One of the most important characteristics of HWN is the possibility to connect many kinds of Radio Access Networks (RAN) like WiFi, WiMAX,GSM, UMTS, HSPA, LTE, among others. This brings many challenges in HWN surroundings, one of the most important is ensuring that a user terminal can move from one access network to another without losing connectivity and, of course, the service.
The aim of this paper is to propose a Vertical Handover Decision Algorithm (VHO-DA) that enables a single user terminal to initiate a proactive decision based on user preferences and QoS parameters, while at the same time considering the networks conditions to avoid over burdening an interface. The development of our VHO-DA was addressed like a Multi Criteria Decision Making Problem (MCDM) in order to provide the best possible connection for critical services and maintaining load balancing in networks.
Keywords: Multi criteria decision making problem, Handover decision, Heterogeneous wireless networks, Vertical handover.

1 Introduction

Thanks to advances in the areas of electronics, computers and communications, the way we perceive and interact with the world has been transformed. Nowadays the majority of our daily activities are related in some way with the use of these technologies, from how to educate, to health care processes, and access to government services, to name a few. So it's clear to the academic community and the business world that Information Communications and Technologies (ICT) play an important role in their daily lives and in all business and market processes that surround them.

A study conducted by International Data Corporation (IDC) on the top 10 current trends in the ICT sector for Latin America, found that two of them are directly related to the topic of infrastructure for mobile communications. The first trend shows an environment where the impact of mobility is very high, as consumers of multiple services want to access their information anywhere at any time, while the second shows that the incursion of fourth generation networks will facilitate the first trend, causing an explosion of new services that need to be supported by this new infrastructure [1]. That is, we have a scenario where users (both personal and corporate) can access any application from any device, anywhere, anytime. This new scenario is an infrastructure that operates what is now known as the Heterogeneous Wireless Networks (HWN) or Next Generation Mobile Networks (NGMN) which are intended to support the growing needs, both technical and qualitative, that users demand from their current and new services.

Among the most important characteristics defined for HWN networks are: to support data transmission up to 100 Mbit/s in downlink and 50 Mbit/s in uplink in a channel with a bandwidth of 20 MHz and a low latency from one end to another in less than 30 ms. As a result of proposed developments within the new networks, HWN is looking to provide wireless competitive broadband services with high data rates and an excellent balance between cost and performance. Not only will it help to achieve better technical standards, but it's also expected to achieve great benefits for end users, significantly improving the user's experience with existing services and future data and multimedia services, which will make broadband Internet easily accessible with excellent mobile performance [2].

This new proposed ecosystem is expected to generate multiple challenges for telecommunication service operators, especially in the design and implementation of network infrastructure since it must allow the provision of various services independent of location, time, device or access network. One of the most challenging problems is maintaining service continuity across this ecosystem, the possibility that one user can change their access network without the loss of the service. This transfer between RANs of different technologies is called Vertical Handover and is usually driven by the requirements of the services, and also by the need to improve network performance [3], [4], [5], [6].

2 Related Works

Lots of articles mention the subject of the different phases in handover, in [7] the authors describe the decision, radio link transfer and channel assignment phases of the handoff. In [8] the authors establish the phases of network discovery, handoff decision and handoff execution. From these it's determined that there is a data acquisition phase where the information the algorithm uses is obtained and that afterwards the choice elected by it commences the handover execution without affecting any other part of the process. In other words, since it's isolated, it can't affect the rest of the process beyond its decision, and so the work can be specified to only the decision algorithm. It concentrates mainly on applying the decision function to the values given as input, which are obtained by the candidate interfaces and given to the mobile device. The way the operators give this information or how the handoff works after the decision is made is not considered.

In recent years, many VHO - DA have been proposed, these algorithms use different decision strategies to select the best connection. In [9] Kassar, Kervella, and Pujolle propose a classification of them into five categories: functions, user-centric, Fuzzy Logic and Neural Network-based, multi-criteria, and context-aware strategies; although these are not mutually exclusive.

Several decision algorithms developed use a multi criteria strategy, for example in [10] Zhang presents an algorithm that uses fuzzy logic combined with some classical Multi Attribute Decision Making (MADM) methods, Simple Additive Weighting (SAW) and Technique for ordering preferences by similarity to ideal solution (TOPSIS), for handover decision in order to combine and evaluate multiple criteria simultaneously. Song and Jamalipour in [11] explain an algorithm that combines the analytic hierarchy process (AHP) and the grey relational analysis (GRA) methods to decide the best network for mobile users through finding the tradeoff among service application, network condition, and user's preference.

In [12] by Yang and Wu, their proposal uses fuzzy logic and MADM; the proposed Algorithm is divided into four parts: traffic classification, resource estimation for reservation, admission control and RAT selection. One similar algorithm was presented by lsmail and Roh [13], their proposal was a user adaptive fuzzy MADM handover decision scheme. They applied different fuzzy MADM methods (TOPSIS, SAW, Maximin, ELECTRE and AHP) to find out best alternative for handover and to evaluate the performance of these methods. Lahby, Leghris,

and Adib [14] focuses their work in a hybrid method based on multi attribute decision making methods AHP and TOPSIS to select the best network alternative.

The work presented in [15] by Tamea, Biagi, and Cusani, proposes and analyzed a modified version of TOPSIS to include risk information; this proposal allows the reduction of outage probability at the cost of parameters performance loss. Inside the work of Kim Et al. [16] , they design a vertical handover decision algorithm that is a combination of a policy and a multi-criteria decision making approaches; this algorithm intends to achieve an effective and seamless handover between heterogeneous radio access networks, especially between the LTE and the WLAN systems.

3 Problem Statement

As previously stated this work focuses on proposing a Vertical Handover Decision Algorithm (VHO-DA) that enables a single user terminal to propose a proactive decision based on user preferences and QoS parameters, while at the same time considering the networks conditions to avoid over burdening an interface. Since the proposed problem involves more than one decision parameter, we intend the use of a multi criteria decision making method with the aim to provide always the best possible interface connection available for critical services.

Some MADM Algorithms were addressed like TOPSIS, GRA and SAW. Each of them work in a different way, but they're all decision algorithms, which is to say that they compare many different options based on one or more attributes and choose the alternatives which satisfy the conditions the best. However, according to [17] the results of each are almost the same.

In addition a VHO-DA must consider the limitations associated with the computing power in a mobile user device; this is the reason why we need to select the algorithm with lowest algorithmic complexity in order to lessen the burden placed on the mobile device. Based in [18] we selected a Simple Additive Weighting (SAW) Method as it was the MADM Algorithm with the lowest computational complexity.

3.1 Simple Additive Weighting (SAW) Method

SAW Technique is one of the most used MADM techniques. It is simple and is the basis of most MADM techniques such as AHP and PROMETHEE that benefits from additive property for calculating final score of alternatives.

SAW for all the m alternatives determined a score (V_i) calculated by multiplying the weight assigned to each attribute (w_j) by a comparable rating scale of each attribute (r_{ij}) and then summing these products over all the n attributes.

$$V_i = \sum_{j=1}^{n} w_j \cdot r_{ij}, \forall i = 1, \ldots, m. \tag{1}$$

3.2 Mathematical Model

In order to take this decision, all factors available in a heterogeneous network must be evaluated. In this article, the factors chosen were QoS parameters and charging rates available on 3GPP/LTE, Wi-Fi and WiMAX. The QoS parameters are divided into two main groups: Ascending parameters, those who are deemed better the larger in value they are, and descending parameters, those who are deemed better the smaller in value they are.

The ascending parameters (ap) are: Received Signal Strength Indicator(rss) and Availability(av). The rss determines how strong the interface's signal is. Availability is the rate of the

interface's uptime over its uptime plus its downtime. While the descending parameters (dp) are: Packet Loss(pl), Jitter(j), Delay(d), Cost(c) and Load(l). Packet loss is the rate of how many packets were received over how many were sent. Delay is amount of time it takes for a packet to travel from one point of the network to another. Jitter is the variation of the delay of multiple packets over a network. Also it's important to establish that there is a set of n interfaces I which includes the one we are already connected to, and a set of n-1 interfaces to which we could connect named J.

For our case the alternatives are the RANs available at a given point in time. The decision maker assigns the weight of every attribute based on the needs of each service, so each operator can state which parameters are most important for it and find the most appropriate network.

Given the above statement the mathematical model proposed is a SAW equation, where all the parameters are accounted for and evaluated. Attributes are normalized and if it's a parameter where less is better, it is inverted or subtracted from a total percent.

$$V_i = W_d \cdot \frac{1}{(\frac{d}{d_m})} + W_j \cdot \frac{1}{(\frac{j}{j_m})} + W_{pl} \cdot \frac{1}{(\frac{pl}{pl_m})} + W_{av} \cdot (\frac{av}{av_n}) + W_{rss} \cdot (\frac{rss}{rss_n}) + W_c \cdot (1 - \frac{c}{c_n}) + W_l \cdot (1 - \frac{l}{l_n}) \quad (2)$$

Where the n_{th}value of a parameter is the highest of the available interfaces and the mth value of a parameter is the lowest of the available interfaces.

Some Specific Parameter Functions

Cost. Cost must also be determined. In this paper, the charging models evaluated are: Free, Monthly fee, Bits consumed rates and Time consumed rates. Free are interfaces where the user would not incur in any financial cost if he were to connect to them. Monthly fee are interfaces which use fixed rate charging so no matter how much is consumed, they charge the same. For the purposes of this paper, Monthly fee and Free are essentially the same, as the user doesn't incur in any additional cost by connecting to that interface. Bits consumed rate are interfaces which charge by how many bits are used in the connection. Time consumed rate are interfaces that have a flat-rate charging model that bills according to how much time the user is connected to the Interface. In order to compare the two, time consumed rate interfaces are converted into Bits consumed rate using the following formula:

$$Bit\ consumed\ rate = \frac{\frac{T.\ consumed\ rate(in\ minutes)}{60}}{Throughput} \quad (3)$$

Load. Load is the representation of the load balancing factor into the equation; it's the theoretical capacity of the network according to its technology, which the mobile device already has, minus the current throughput of the interface, given to the mobile device by the network; all of this over the theoretical capacity.

$$Load_i = \frac{Theoretical\ Capacity_i - Throughput_i}{Theoretical\ Capacity_i} \quad (4)$$

It should be noted that this configuration of load is done in order to maintain the idea that lower the Load of a network, the less it is being used and the more available the resources are.

All of these parameters, excluding Load, are either percent's or values given by the interfaces, so no calculation must be done with them. Except in the case that it's a Time consumed rate and must be converted to Bit consumed rate.

3.3 Heuristic Implementation

We chose to solve this problem through a heuristic method do to it being the fastest and most precise way that the answer could be found with the information available and the restrictions placed by the infrastructure.

The chosen VHO-DA is a straightforward process that runs continuously in the background. First, it searches for all the available networks it detects. Then it gathers all the information of those interfaces, including QoS parameters and its condition, in addition to the preferences of the active services (Critical Services). Then it compares the information of each interface in order to determine the highest and lowest values, and then proceeds to normalize all of them and obtain it's SAW weighted value. The first interface that scores the highest value is the chosen interface to switch to; that is, if it is different from the current interface. Figure 1 present the flow diagram of the heuristic described.

For our case the alternatives are the RANs available at a given point in time. The attributes chosen to take part in the decision are: Delay (d), Jitter (j), Packet Loss (pl), Availability (av), Cost (c), Received Signal Strength (rss), and Load (l). The decision maker assigns the weight of every attribute based on the needs of each service, so each operator can state which parameters are most important for it and find the most appropriate network.

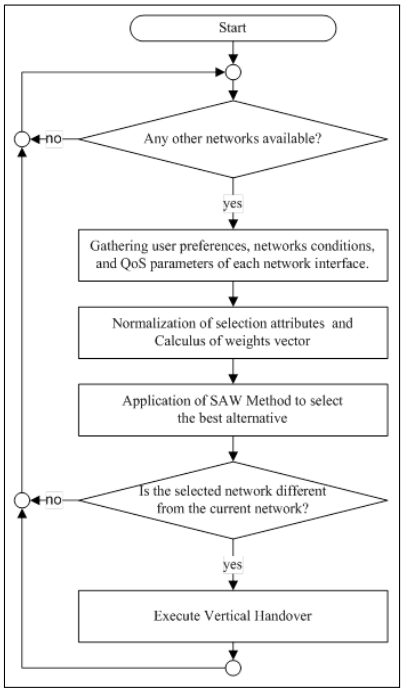

Figure 1: Proposed Heuristic Algorithm

3.4 Experimental Results

In order to verify the correct function of the proposed heuristic, we uses a case study scenario extracted from [19] in which multiple interfaces (UMTS, WiFi, WiMAX, GSM, HSPA+, EDGE, LTE) are given QoS attributes to be compared. The case is modified, to give it RSS values and the theoretical capacity of each interface. This scenario is just an example and is not meant to be a definitive sample of any of these interfaces.

We execute the VHO-DA on the scenario to evaluate its effectiveness using a demonstrative set of weights in which Load was given special consideration. The test results showed a satisfactory

Interface	Delay	Jitter	Packet Loss	Cost	RSS	Throughput	Availability	Th. Capacity	Load	Ranking
UMTS	45	1	0,0001	0	0,4398	384	0,99999	2400	0,984	0,6545
WiFi 1	180	11	0,4	4,35E-8	0,9473	23000	0,999999	54000	0,57407	0,5115
WiMax	70	9	0,0001	0,0001	0,4120	4000	0,99999	100000	0,96	0,47
EDGE 1	150	10	0,01	0,003	0,5904	178	0,9999	384	0,5375	0,4685
HSPA	**55**	**2**	**0,0001**	**0**	**0,8528**	**2000**	**0,999**	**7200**	**0,722**	**0,6767**
WiFi 2	110	9	0,0001	0,006	0,5204	4500	0,99999	65000	0,981	0,4421
GPRS 1	90	9	0,001	0,008	0,9851	80	0,9999999	114	0,298	0,6279
GPRS 2	135	9	0,005	0,003	0,6550	60	0,9999999	114	0,47368	0,5055
EDGE 2	100	7	0,0001	0,0016	0,4379	237	0,9999	384	0,383	0,5787

Table 1: Parameters values in the study case

result and prove that the algorithm first and foremost considers the burden on a channel before selecting it, while at the same time considering QoS values. Considering that this study case is specifically intended for critical services, we distributed the weights of the parameters as follows: Delay (0,15), Jitter(0,1),Packet Loss(0,1), Cost(0,05), Availability(0,15), RSS(0,15) and Load(0,3). It's important to know that result of the SAW vector V_i is represented by the value "Ranking", since we compare the result and from the highest we extract which interface should we connect to.

The VHO-DA was executed with the parameters values that you can see in Table 1. The highlighted interface, HSPA, is the chosen interface to connect to due to its results, being the interface with the highest Ranking. This is partly due to it having the second lowest delay, jitter, and shares the lowest cost and packet loss with a few other interfaces. And what's also noticeable is that the options is very well rounded, as it's only the best in two parameters that aren't the heaviest (Packet Loss and Cost). It definitely considered what we needed for the critical service.

4 Conclusions

The work concludes in three points. The first is that this VHO-DA proves to have a holistic consideration of the values, and forms a multicriterial decision that guarantees the best connection possible to the critical service. The second is that since it's also modifiable (to consider the necessities of the service in question), it's highly flexible and can be applied to any critical service and any network. Finally, the third point is that this VHO-DA considers special limitation for mobile devices and networks, implementing load balancing to assure the most advantageous use of the HWN infrastructure. Considering these three points make this algorithm an improvement in the VHO-DA field.

Bibliography

[1] IDC Latin America Predictions Team., *IDC Predictions 2011. Welcome to the New Mainstream.*, IDC Corporate, Framingham, MA, 2011.

[2] NGMN Alliance,*Next Generation Mobile Networks* Beyond HSPA & EVDO. , NGMN Alliance, 2006.

[3] I. F. Akyildiz, J. Xie, and Mohanty. S.,A survey of mobility management in next-generation all-IP-based wireless systems, *IEEE Wireless Communications*, 11(4):16-28, 2004.

[4] X. Yan,*Optimization of Vertical Handover Decision Processes for Fourth Generation Heterogeneous Wireless Networks*, Monash University, Dept. of Electrical and Computer Systems Engineering, Melbourne, Australia, PhD Thesis, 2010.

[5] J Márquez-Barja, C. T. Calafate, J.C, Cano, P. Manzoni, An overview of vertical handover techniques: Algorithms, protocols and tools, *Computer Commun*, 34(8):985 - 997, 2011.

[6] X Yan, Y. A. Sekercioglu, S. Narayanan, A survey of vertical handover decision algorithms in Fourth Generation, *Computer Networks*, 54(11):1848 - 1863, 2010.

[7] Nasser, N.; Hasswa, A.; Hassanein, H., Handoffs in fourth generation heterogeneous networks, *IEEE Commun Magazine*, 44(10):96-103, 2006.

[8] J.D. Martínez-Morales, U. Pineda-Rico, E. Stevens-Navarro, Performance comparison between MADM algorithms for vertical handoff in 4G networks, in *7th Int. Conf. on EE Computing Science and Automatic Control (CCE)*, Tuxtla Gutierrez, Mexico, 309 - 314, 2010.

[9] M Kassar, B Kervella, G. Pujolle, An overview of vertical handover decision strategies in heterogeneous wireless networks, *Computer Commun*, 31(10):2607-2620, 2008.

[10] W. Zhang, Handover decision using fuzzy MADM in heterogeneous networks, *IEEE Wireless Commun and Networking Conference*, WCNC., Atlanta, USA, 2:653- 658, 2010.

[11] Q. Song, A. Jamalipour,A network selection mechanism for next generation networks, *IEEE International Conference on Communications*, Seoul, Korea, 2:1418- 1422, 2005.

[12] S. Yang, J. Wu, Fuzzy based joint radio resource management in heterogeneous wireless networks, *13th Asia-Pacific Network Operations and Management Symposium*, Taipei, Taiwan, 1 - 4, 2011.

[13] A. Ismail, B. Roh, Adaptive Handovers in heterogeneous networks using fuzzy MAD, *Int Conf on Mobile IT Convergence*, Gumi, Korea, 99-104, 2011.

[14] M. Lahby, C. Leghris, and A. Adib, A Hybrid Approach for Network Selection in Heterogeneous Multi-Access Environments, *4th IFIP Int Conf on New Technologies, Mobility and Security*, Paris, France, 1 - 5, 2011.

[15] G. Tamea, M. Biagi, R. Cusani, Soft Multi-Criteria Decision Algorithm for Vertical Handover in Heterogeneous Networks, *IEEE Communications Letters*, 15(11):1215 - 1217, 2011.

[16] T Kim et al., Cell selection and trigger point decision for next generation heterogeneous wireless networking environment: Algorithm & evaluation, in *5th Int. Conf. on New Trends in Information Science and Service Science*, Macao, Korea, 247-254, 2011.

[17] Yoon K. P., C. L. Hwang, *Multiple Attribute Decision Making. An Introduction*, Susan McElroy, Ed. Thousand Oaks, C.A, United States of America: Sage Publications, 1995.

[18] I. Chantaksinopas, P. Oothongsap, A. Prayote, Network selection delay comparison of network selection techniques for safety applications on VANET, *13th Asia-Pacific Network Operations and Management Symposium*, Taipei, Taiwan, 1 - 7, 2011.

[19] C. Fortuna, M. Mohorcic, B. Filipic,*Multiobjective optimization of service delivery over a heterogeneous wireless access system*, ISWCS 2008, Reykjavik, Iceland, 2008.

INT J COMPUT COMMUN, ISSN 1841-9836
8(3):432-443, June, 2013.

SkyDe: a Skype-based Steganographic Method

W. Mazurczyk, M. Karaś, K. Szczypiorski

Wojciech Mazurczyk, Maciej Karaś,
Krzysztof Szczypiorski
Warsaw University of Technology
Poland, 00-661 Warsaw, Plac Politechniki 1
wmazurczyk@tele.pw.edu.pl, karas.maciek@gmail.com,
ksz@tele.pw.edu.pl

Abstract: This paper introduces SkyDe (Skype Hide), a new steganographic method that utilizes Skype encrypted packets with silence to provide the means for clandestine communication. It is possible to reuse packets that do not carry voice signals for steganographic purposes because Skype does not use any silence suppression mechanism. The method's proof-of-concept implementation and first experimental results are presented. They prove that the method is feasible and offers steganographic bandwidth as high as 2.8 kbps.
Keywords: Information hiding, network steganography, Skype.

1 Introduction

Voice over IP (VoIP) or IP telephony is one of the services of the IP world that is changing the entire telecommunications landscape. It is a real-time service, which enables users to make phone calls through data networks that use an IP protocol. Currently, one of the most popular of the IP telephony systems that have shaken the global telephony market in the last decade is Skype (www. skype.com). It is a proprietary P2P telephony service originally introduced in 2003 by creators of the famous P2P file sharing system Kazaa - Niklas Zennström and Janus Friis. Skype is owned by Microsoft and it has been reported that it has about 663 million registered users (September 2011). In March 2012, it was reported to have had 35 million users online simultaneously [5]. It has also been estimated that in 2011, Skype had acquired about 33% of the world's international telephone market [18].

Steganography encompasses various information hiding techniques, the aim of which is to embed a secret message into a carrier. Network steganography, to perform hidden communication, utilizes network protocols and/or their relationships as the carrier for secret data. Because of its popularity, IP telephony is becoming a natural target for network steganography [6]. Steganographic methods are intended to hide the very existence of the communication and therefore, any third-party observers should remain unaware of the presence of the steganographic exchange.

Generally, every network steganographic method can be described by the following set of characteristics: its steganographic bandwidth, its undetectability, and robustness [1]. The term "steganographic bandwidth" refers to the amount of secret data that can be sent per unit time when using a particular method. Undetectability is defined as the inability to detect a steganogram within a certain carrier. The most popular method by which to detect a steganogram is to analyze the statistical properties of the captured data and compare them with values typical for that carrier. The final characteristic is robustness, which is defined as the amount of alteration that a steganogram can withstand without its secret data being destroyed. A good steganographic method should be as robust and as difficult to detect as possible whilst offering the highest bandwidth. However, it must be noted that there is always a fundamental trade-off necessary among these three measures.

Additionally, it is also useful to measure the steganographic cost. This is a characteristic that belongs to the sphere of carrier fidelity and has a direct impact on undetectability. It describes

the degradation or distortion of the carrier caused by the application of the steganographic method. For example, in the case of VoIP steganography methods, this cost can be expressed as a measure of the conversation quality degradation induced by applying a particular technique for hiding information.

One of the most important aspects for every steganographic method is the selection of the most suitable carrier for the secret data. The most favorable carrier for secret messages must have two features:

- It should be popular, i.e., usage of such a carrier should not be considered as an anomaly in itself. The more such carriers are present and utilized on the network the better, because they mask the existence of hidden communication.
- Modification of the carrier related to the embedding of the steganogram should not be "visible" to the third party, who is unaware of the steganographic procedure.

Thus, because of its popularity and traffic volume, Skype traffic is an ideal candidate for a secret data carrier. It should also be emphasized that the purpose of establishing any information hiding exchange varies - possible uses can fall into the category of legal actions (e.g., circumvention of web censorship and surveillance, computer forensics or copyright protection) or illicit activity (e.g., criminal communication, confidential data exfiltration or industrial espionage). This trade-off is typical in steganography and requires consideration in a broader steganography context, which is beyond the scope of this paper.

One can always question why use steganography for Skype, which as is commonly known, uses cryptographic means to provide confidentiality for every type of users' message that is exchanged (text messages, voice signal, files). First of all, hidden communication need not necessarily be conducted in an end-to-end manner, i.e., covert data can be sent using third party VoIP calls. Secondly, discussion has recently arisen on whether Skype, whose calls were commonly believed very hard to wiretap, is providing lawful interception services to law enforcement agencies [7]. Additionally, Skype is proprietary and closed software and thus, ultimately cannot be trusted.

This is why in this paper we discuss how Skype can be utilized to provide means for clandestine communication. Experiments performed on real Skype traffic prove that the proposed method - SkyDe (Skype Hide) - is feasible and offers high steganographic bandwidth and reasonable steganographic cost in terms of undetectability.

The rest of this paper is structured as follows. Section 2 presents the current state of research efforts on VoIP steganography and on Skype in particular. In Section 3, Skype basics are presented, as well as an analysis of its traffic and a detailed description of the proposed method and the prototype implementation. Next, in Section 4, experimental results for the method are presented. Finally, the last section concludes our work and indicates directions for further research.

2 Related Work

A number of steganographic approaches for VoIP have been proposed, which have been recently exhaustively surveyed by Mazurczyk [1]. Because of space limitations only steganographic methods related to Skype and silence suppression mechanisms will be mentioned here.

The only Skype-dedicated method was introduced by Wang et al. [4]. The authors proposed embedding a 24-bit watermark into the encrypted stream (e.g., Skype call) to track its propagation through the network and thus, providing its de-anonymization. The watermark is inserted by modifying the inter-packet delay for selected packets in the VoIP stream. The authors demonstrated that depending on the watermark parameters chosen, they were able to achieve a 99%

true positive and a 0% false positive rate, while maintaining good robustness and undetectability. However, they achieved steganographic bandwidth of only about 0.3 bit/s, which is enough for the described application, but rather low for performing clandestine communication.

The deployment of speech codecs' Silence Insertion Description (SID) frames that are sent when voice is not present in the input signal, was proposed as a secret data carrier by Mazurczyk and Szczypiorski [2]. However, the authors noted that the steganographic bandwidth for this method is rather low, but that it is possible to influence the rate at which SID frames are issued.

Recently, a high-capacity steganography technique based on the utilization of the inactive frames of the G.723.1 speech codec was introduced by Huang et al. [3]. The authors proved that the inactive frames of VoIP streams are more suitable for data embedding than the active ones and thus, a greater amount of hidden data can be embedded within them with the same imperceptibility. They then proposed a steganographic algorithm in different speech parameters of the inactive frames for the G.723.1 codec with a 6.3 kbits bitrate. Experimental results show the solution is imperceptible and that a quite high steganographic bandwidth of up to 101 bits/frame is achieved.

Proposed in this paper, the SkyDe method operates by reusing encrypted packets with silence, by substituting this information with secret data. When compared with existing solutions, it is characterized by significantly higher steganographic bandwidth and good undetectability.

3 Skype Traffic Analysis and Proposed Method Description

3.1 Skype basics

Skype is a hierarchical P2P network with a single centralized element (login server) that is formed by two types of nodes [11]:

- Ordinary Nodes (ONs) that can start and receive a call, send instantaneous messages, and transfer files, and
- Specialized nodes called Super Nodes (SNs) that are responsible for helping ONs find and connect to each other within the Skype network

The login server is responsible for the authentication of ONs and SNs before they access the Skype network.

Skype offers two communication modes, namely:, End-to-End (E2E) and End-to-Out (E2O). The first is possible between two Skype clients within the IP network. The second occurs if one of the endpoints is a Skype client within the IP network and the other is a PSTN phone (SkypeIn/SkypeOut services). In this paper, we focus solely on the Skype E2E mode.

Skype is based on proprietary protocols and makes extensive use of cryptography, obfuscation, and anti-reverse-engineering procedures, and all information about its traffic characteristics, protocols, and behaviors comes from numerous measurement studies, e.g., [8] [9].

All traffic in Skype is encrypted; neither signaling messages, nor the packets that carry voice data can be uncovered. Typically, the preferred, first-choice transport protocol of Skype is User Datagram Protocol (UDP), which as the traffic analysis in [9] showed, is being used in about 70% of all calls. However, if Skype is unable to connect using UDP it falls back to TCP. In this paper, we focus solely on UDP-based Skype calls.

For TCP-based transport, the entire Skype message is encrypted. In cases of unreliable UDP, at the beginning of each datagram's payload, an unencrypted header is present that is called the Start of Message (SoM). It is unencrypted in order to be able to restore the sequence of packets that was originally transmitted, to detect a loss, and to quickly distinguish the type of data that is carried inside the message. SoM consists of the following two fields [8] (Fig. 1):

- *ID* (2 bytes) that is used to uniquely identify the message; it is randomly selected by the sender query, and copied in the receiver reply.

- *Fun* (1 byte) that describes the payload type. For example, values: 0x02, 0x03, 0x07, and 0x0f are typically used to indicate signaling messages (used during the login phase or for connection management). 0x0d indicates a DATA message that can contain: encoded voice or video blocks, chat messages or fragments of files.

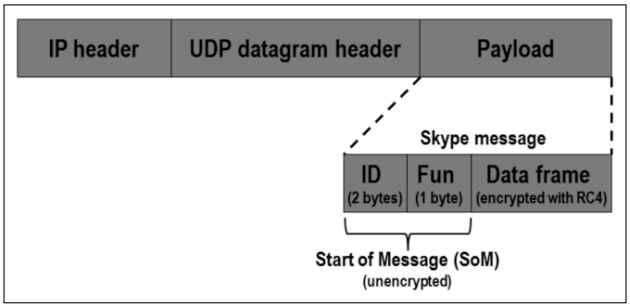

Figure 1: UDP-based Skype message format.

Skype estimates the available bandwidth and the packet loss probability, and it dynamically adapts to the detected network conditions by adjusting the codec's bitrate or by introducing higher redundancy in packets [9]. Typically, the resulting packet rate is about 16, 33, or 50 packet/s [11].

From the perspective of the steganographic method proposed in this paper, it is also important to emphasize that Skype does not utilize any silence suppression mechanism, i.e., even if there is no voice activity during the conversation, the packets that carry the silence are still generated and sent. The lack of support for silence suppression is intentional - it helps to obtain better voice quality and maintain UDP bindings at the NAT (Network Address Translation) [10].

3.2 Skype traffic analysis

For the purpose of the proposed steganographic method, outlined in detail in Section 3.3, an analysis of Skype traffic was carried out to prove that the method is feasible.

An experimental test-bed was set up (Fig. 2) that included two Skype clients (Skype for Linux v. 2.2.0.35 and for Windows v. 6.0.60.126) and a Linux-based application designed and developed by authors that could intercept Skype packets before they reached (for the transmitting side) and after they entered the (for the receiving side) network interface. Two instances of this application were synchronized using NTP (Network Time Protocol) and were responsible for the generation of reports regarding the Skype packets' statistics.

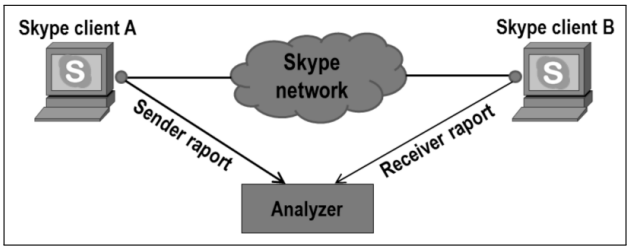

Figure 2: Experimental Skype test-bed.

Then, reports from both sides: transmitting and receiving, were analyzed and joined in an analyzer. This helps to observe the same Skype encrypted stream in two network localizations.

Using this test-bed, a number of measurements were carried out on Skype traffic. In each experiment, the number of analyzed Skype packets was larger than 100 000 and was repeated four times. Here, only the averaged results are presented.

Skype packets' size distribution

In 2008, Chang et al. [10] observed that in Skype traffic, speech activity is highly correlated to packet size, as more information is encoded into a voice packet while a user is speaking. Experimental results revealed that the packet size and speech volume are highly correlated because they fluctuate in tandem.

This feature of Skype traffic is utilized in SkyDe to identify the packets that carry silence. That is why we wanted to verify whether the same behavior as in [10] can be observed for current Skype software. Fig. 3 presents the obtained experimental results.

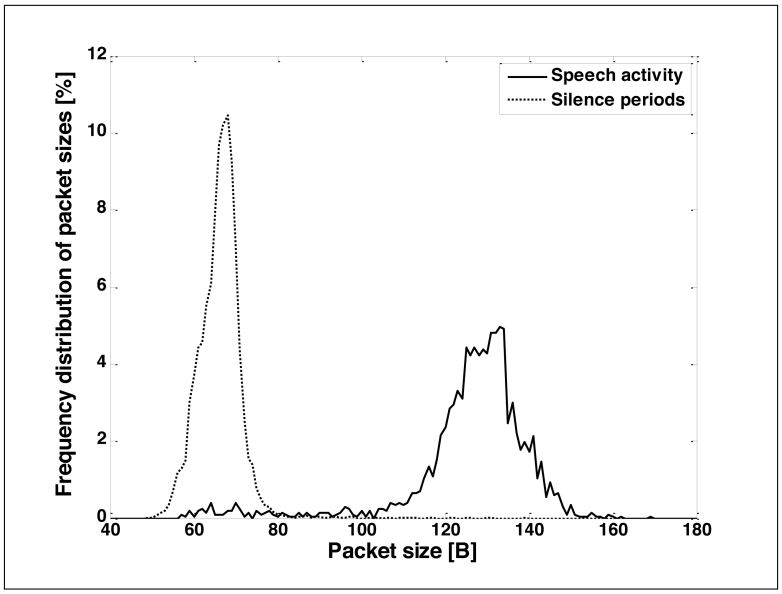

Figure 3: The distribution of packets' size during conversation and periods of silence.

As can be observed, the previously reported high correlation between speech activity and packet size is still evident. This means that based on the size of each Skype packet we can assess with high probability whether it carries voice or silence. As mentioned before, this effect will be also utilized by SkyDe.

Skype bytes distribution in packets' payload

To later prove SkyDe undetectability, the following characteristic of Skype bytes distribution for typical Skype calls was carried out (Fig. 4).

It can be observed that there are certain bytes values (in hex), i.e., 0x0d, 0x1d, 0x2d, 0x3d, 0x4d, 0x5d, 0x6d, and 0x7d that are more frequent than others, whereas the rest are almost equally distributed. The popular eight bytes are the typical values from the Fun field for each UDP-based Skype packet (see Sec. 3.1). The distribution of the rest of the byte values is almost equal because they represent the encrypted payload of Skype packets.

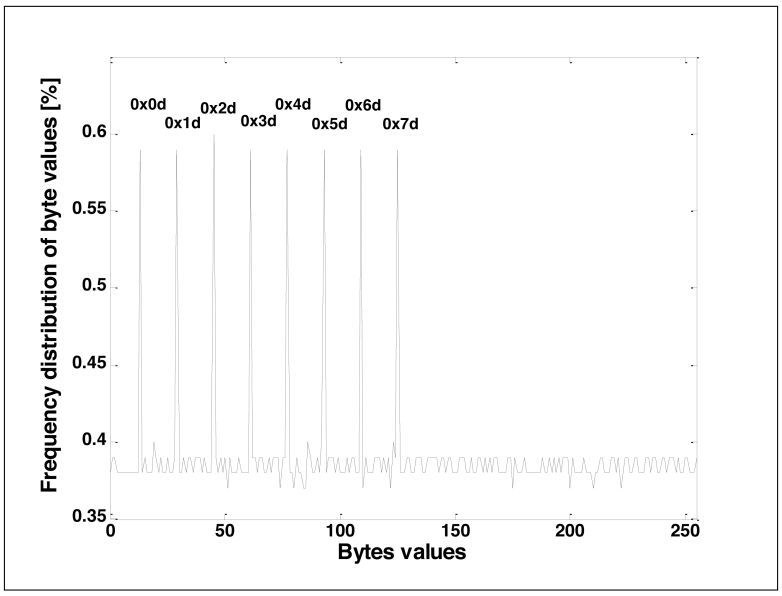

Figure 4: The bytes distribution in packets' payload for typical Skype calls.

Skype resistance to packet losses

We also investigated Skype's maximum threshold of packet losses that could be sustained by a UDP-based connection without falling back to TCP. It transpired that this value is about 70%. Of course, when this level of losses is reached, the voice quality is degenerated to the point where no further conversation is possible.

3.3 Proposed method and its implementation

SkyDe is designed to utilize Skype encrypted voice streams to enable clandestine communication. This secret data exchange can be realized between: (a) two Skype users, i.e., they use their own call for steganographic purposes, or (b) a steganogram transmitter and receiver that utilize an existing, third party Skype call (in this case the original caller and callee are not aware of the information hiding procedure).

SkyDe utilizes encrypted Skype voice packets as a hidden data carrier. By taking advantage of the high correlation between speech activity and packet size (described and verified in Sec. 3.2.1), packets without voice signal can be identified and used to carry secret data (by replacing the encrypted silence with secret data bits). As is commonly known, typical VoIP calls contain 35% to 70% silent periods in each direction [12], [13]. Skype does not utilize any silence suppression algorithm; thus, generally, all packets with silence can be utilized for steganographic purposes. However, SkyDe should have potentially low impact on voice quality because it does not affect packets with voice signals, which are more significant from the point of view of conversation.

SkyDe transmitting side

First, to create the secret data to be sent, as with the replaced (encrypted) data, they are encrypted prior sending. The cryptographic key utilized for encryption is a shared secret between SkyDe communication sides. Then a CRC-16 checksum is calculated on the payload and is inserted into the ID field (16 bits) of SoM (see Section 3.1). Such an approach provides steganogram integrity verification and facilitates the identification of packets that carry secret data at the receiving end.

Then, those packets that contain silence must be identified. Their size can change while the connection lasts (due to network conditions), so we propose a "sliding time window" algorithm that calculates the reference size of the packet with silence. It is also responsible for keeping the total packet losses at a safe level, because as mentioned earlier, steganographic utilization of each packet with silence will increase the overall packet loss for the call. Thus, it is important not to exceed the measured threshold of about 70% total packet losses (see subsection 3.2.3) because then the connection will fall back to TCP.

The proposed algorithm works as follows. First, the size of the "sliding time window" w (in seconds) is selected, in which the reference value r of Skype packets with silence is continuously updated during the call. Every second, the packet with the lowest size is determined and stored. When all of the values in the window are measured, then the average reference value is calculated based on the three packets with the lowest size. Additionally, a certain deviation in packet size (Δ) r $\pm$ Δ is acceptable for consideration as a packet for SkyDe purposes. In the same time window w, it is also verified whether the total packet loss level reached 70% and if it does; the steganographic method ceases to utilize packets with silence until the losses are again at a safe level.

After the packets with silence are identified, their payloads are replaced with encrypted secret data and they are sent to the receiving side.

To provide reliability for the proposed method, an additional protocol in a hidden channel might be required. One solution is to use an approach proposed by Hamdaqa and Tahvildari [17] because it can be easily incorporated into SkyDe. It provides a reliability and fault-tolerance mechanism based on a modified (k, n) threshold of a Lagrange Interpolation and the results demonstrated in that paper prove that the complexity of steganalysis is increased. Of course, the "cost" for the extra reliability would always be a loss of some fraction of the steganographic bandwidth.

SkyDe receiving side

At the receiver side, each packet with silence is recognized by the same means (packet size) as at the transmitter side. These packets are then copied to the buffer and for each of them, a CRC-16 checksum is verified and the secret data is extracted. It is not important to erase or replace secret data embedded into packets because the Skype client will treat these packets as losses. However, only the receiving end will be aware of the loss; thus, these modified SkyDe packets will not be discarded while traveling through the network.

SkyDe was implemented in the same network environment as depicted in Fig. 2, by enhancing the functionality of the application that was used to gather statistics about Skype traffic (see Section 3.2). Based on the experimental results, it transpired that SkyDe performs best when w = 10 seconds and Δ = 20 bytes. The selection of the most optimal values of w and Δ will be not covered in this paper due to space limitations.

4 Experimental Results

4.1 Experiments methodology

For SkyDe evaluation, we prepared a .wav file that consists of male and female voices speaking English. The .wav file contains five minutes of imitated telephone conversation, i.e., sentences interleaved with periods of silence (similar to that designed in [13]) with a ratio of 55:45 (55% speech activity and 45% silence). In our experiments, we compiled the .wav file using audio recordings from the TIMIT [14] continuous speech corpus - one of the most widely used corpora

in the speech recognition community. In our analysis, we use the subjective measure MOS (Mean Opinion Score) [16] calculated with the Perceptual Evaluation of Speech Quality (PESQ) method [15].

The .wav file was used as the source of the voice signal during the Skype call and was saved at the receiving end. Then, the original and degraded file were compared through the use of PESQ and the resultant MOS-LQO (MOS-Listening Quality, Objective) was returned to assess the SkyDe impact on voice quality (steganographic cost). During the same experiments, the steganographic bandwidth and bytes distribution in the packets' payload (as in Fig. 4) were measured. Each experiment was repeated three times and averaged values are presented. It is worth noting that during the experiments none of the calls was disconnected or reverted to TCP, which proves the correct design of the proposed method.

4.2 Steganographic bandwidth and cost

Using the methodology presented in the previous subsection, the results of steganographic bandwidth and cost were obtained. Steganographic bandwidth was calculated by analyzing and extracting the secret data from the Skype packets with silence that were utilized by SkyDe. Also, for these connections, the corresponding voice quality MOS-LLQ scores were determined.

First, the reference MOS-LLQ value without SkyDe applied was obtained. It transpired that the resulting quality is about 3.94, which is considered to be a good quality. The steganographic cost is then determined as a difference between the reference MOS-LLQ without steganography and that with SkyDe applied. The steganographic utilization of packets with silence was increased in a range from 0% to 100% and the obtained results regarding voice quality are presented in Fig. 5.

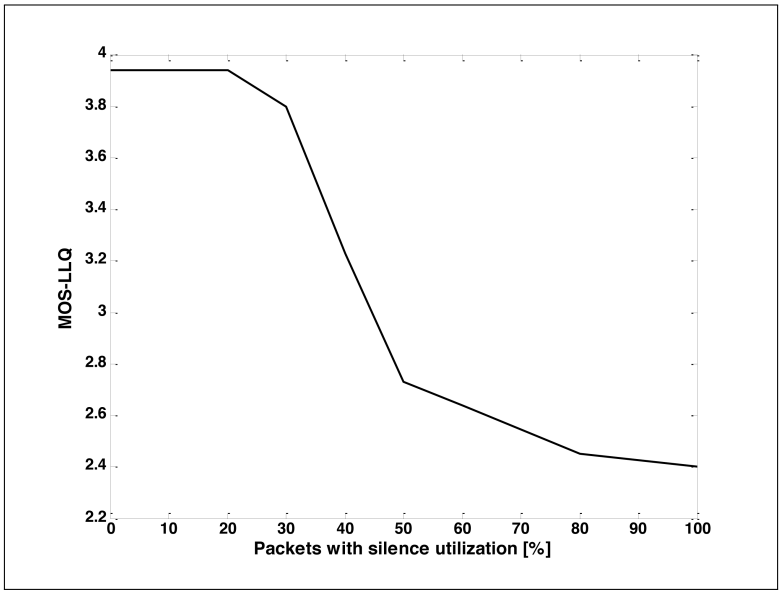

Figure 5: Voice quality experimental results.

When up to 20% of the packets with silence are utilized for steganographic purposes, the resulting voice quality is not degraded at all. For 30%, the disruption in voice quality is negligible. For higher utilization rates, the quality begins to deteriorate more quickly and after exceeding 50% it is considered as poor; however, conversation is still possible.

The results of SkyDe steganographic bandwidth and cost are presented in Table 1. With up to 30% utilization of SkyDe, the steganographic bandwidth continues to increase to finally

reach about 1.8 kbps. This must be considered as a high steganographic bandwidth. For higher utilization rates, the steganographic bandwidth drops because of the decrease in packet rate - this is Skype's reaction to the elevated level of overall packet losses. For 40% utilization rate, it drops almost a half (from about 46 to 24 packet/s) and continues to decrease until it reaches levels of 17 packet/s. Simultaneously, the size of the packets increases even by 36% (for 50% to 60% silence utilization rate). This explains the drop in resulting steganographic bandwidth to the level of 1.5 kbps and then the subsequent rise to the point of about 2.8 kbits for 100% utilization rate.

Packets with silence utilization [%]	0	20	30	40	50	60	80	100
Steganographic bandwidth [kbps]	N/A	1.37	1.83	1.52	1.5	1.81	2.47	2.78
Steganographic cost	N/A	0	0.14	0.71	1.21	1.3	1.49	1.54
Packets with silence reference size [B]	37.86	35.95	33.98	35.23	48.98	48.42	46.10	43.82
Packet rate [packet/s]	50.17	49.14	45.61	23.68	17.08	16.97	17.17	17.84

Table 1: Experimental results

Thus, the proper selection of the level of utilization of packets with silence is necessary and typically, it will be a trade-off between Skype call quality, desired steganographic bandwidth, and undetectability.

4.3 Undetectability

User perspective

Detection of SkyDe, as well as steganographic bandwidth, depends on the hidden communication scenario in which it is utilized. SkyDe can be used between two Skype clients that are aware of the steganographic procedure (secret data is sent in an end-to-end manner), or some intermediary nodes can rely on third party Skype calls to exchange steganograms. In the first case, users can select the desired steganographic bandwidth because they do not necessarily expect high voice quality. Additionally, they do not care about the elevated overall packet loss level; thus, they are able to transmit about 3 kbps. However, in the latter case, the degradation of voice quality or introduced losses cannot be excessive because it could make overt users suspicious. Thus, this could potentially limit the maximum steganographic bandwidth that could be achieved. Therefore, from the point of view of voice quality and packet losses, SkyDe would be most undetectable for 30% utilization of packets with silence rate (1.8 kbps of steganographic bandwidth).

Network perspective

To prove that the proposed method is difficult to detect, we performed similar experiments with bytes distribution in packets' payload (Fig. 4). It was conducted for SkyDe utilizing 100% of packets with silence. The obtained results are presented in Fig. 6. To determine to what extent the results are similar to those of Fig. 4, we used correlation coefficients to quantity the strength of their relationship. It transpired that the correlation coefficient between the bytes distribution in packets' payload for typical Skype and SkyDe calls is 0.96, which indicates a very strong relationship. This makes the proposed steganographic method very difficult to detect.

However, if someone is monitoring Skype traffic, e.g., the packets rate and their sizes, then for SkyDe, higher utilization rates could be more easily visible (of course, if the monitoring entity were able to distinguish between worsening network conditions and hidden communication). Therefore, for this case also, utilization rates that mimic typical Skype call parameters should be used, i.e., up to 30% utilization of packets with silence (almost no difference in packets rate and sizes from typical Skype calls).

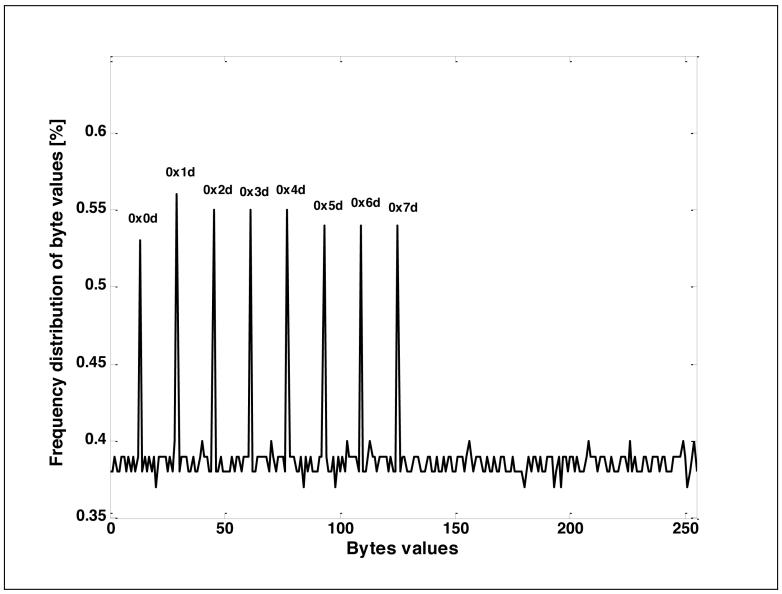

Figure 6: The bytes distribution in packets' payload for SkyDe.

It should be also noted that for poorer network conditions, the more non-steganographic losses would be introduced and the less steganographic information could be transferred due to the 70% total packet losses limit.

It is also important to add that we also observed that the results could be different and fluctuate depending on the day of the week (working days or weekend), or even depending on the time of the day (office or non-office hours). These changes in Skype traffic were also discovered in other studies, e.g., in [9]. This fact also works in the favor of SkyDe because it would be difficult to establish some baseline values needed for steganalysis purposes. Therefore, this makes SkyDe more difficult to detect.

5 Conclusions and Future Work

In this paper we introduced SkyDe, a steganographic method that utilizes encrypted Skype packets as a hidden data carrier. By taking advantage of the high correlation between speech activity and packet size in Skype, we identify those without voice and use them to carry secret data. Experimental results show that such an approach offers a high steganographic bandwidth of up to 1.8 kbps (for 30% utilization of packets with silence), whilst introducing almost no distortion to the Skype call. Moreover, we prove that in these circumstances, the method operates under terms of undetectability.

It should be also noted that SkyDe can be also used for other IP telephony systems that encrypt their traffic and follows the same relationship between speech activity and packet size. Chang et al. [10] point that this is also a case for UGS (Unsolicited Grant Service) [19].

Future work will include developing an improved SkyDe algorithm for the selection of packets

with silence that can increase the steganographic bandwidth whilst keeping the voice distortion at a safe level. We will also conduct more in-depth studies by taking into account different parts of the week or day. We are also going to experiment with SkyDe resistance to network packet losses and their influence on the performance of the proposed steganographic method.

Moreover, we will pursue the effective steganalysis method for SkyDe. One promising research direction worth pursuing is the adoption of the method proposed by Wright et al. in [20], which can be utilized for encrypted voice payload. The authors of this work discovered that the lengths of encrypted voice packets can be used to identify phrases spoken within a call. Therefore, if extended, this approach can be applied to deduce the characteristics of the carried speech and silence periods to be able to detect packets with 'fake silence'.

6 Acknowledgments

This research was partially supported by the Polish Ministry of Science and Higher Education and Polish National Science Centre under grants: 0349/IP2/2011/71 and 2011/01/D/ST7/05054.

Bibliography

[1] Mazurczyk, W. (2013); VoIP Steganography and Its Detection - A Survey, *ACM Computing Surveys* (accepted for publication), ISSN 0360-0300.

[2] Mazurczyk, W.; Szczypiorski, K. (2008); Steganography of VoIP Streams, In Proc. of *3rd Int Symp Information Security (IS'08)*, Monterrey, Mexico, 1001-1018.

[3] Huang, Y.; Tang, S.; Yuan, J. (2011); Steganography in Inactive Frames of VoIP Streams Encoded by Source Codec, *IEEE Transactions on information forensics and security*, ISSN 1556-6013, 6(2):296-306.

[4] Wang, X., Chen, S., Jajodia, S. (2005); Tracking anonymous peer-to-peer VoIP calls on the internet, In Proc. of *12th ACM CCS '05*, 81-91.

[5] Caukin, J. (2012); 35 Million People Concurrently Online on Skype, Skype Big Blog, URL: `http://blogs.skype.com/en/2012/03/35_million_people_concurrently.html`.

[6] Lubacz, J.; Mazurczyk, W.; Szczypiorski, K. (2010); Vice over IP, *IEEE Spectrum*, ISSN 0018-9235, 40-45

[7] Timberg, C.; Nakashima, E. (2012); Skype makes chats and user data more available to police, URL: `http://www.washingtonpost.com/business/economy/skype-makes-chats-and-user-data-more-available-to-police/2012/07/25/gJQAobI39W_story.html`

[8] Bonfiglio, D.; Mellia, M.; Meo, M.; Rossi, D.; Tofanelli, P. (2007);Revealing Skype traffic: when randomness plays with you, In Proc. of *SIGCOMM '07*, NY, USA, 37-48.

[9] Bonfiglio, D.; Mellia, M.; Meo, M.; Ritacca, N.; Rossi, D. (2008); Tracking Down Skype Traffic, In Proc. of *IEEE INFOCOM '08*, Phoenix, USA.

[10] Chang, Y.C.; Chen, K.T.; Wu, C.C.; Lei, C.-L. (2008); Inferring speech activity from encrypted Skype traffic, In Proc. of *IEEE Globecom '08*, Los Alamitos, USA, 1-5.

[11] Molnar, S.; Perenyi, M. (2011); On the identification and analysis of Skype traffic, *International Journal of Communication Systems*, ISSN 1074-5351, 24(1):94-117.

[12] Iwano, Y., Sugita, Y., Kasahara, Y., Nakazato, S., Shirai, K. (1997); Difference in visual information between face to face and telephone dialogues, In Proc. of *IEEE ICASSP '97*, 1499-1502.

[13] Berger, J.; Hellenbart, A.; Weiss, B.; Moller, S.; Gustafsson, J.; Heikkila, G. (2008); Estimation of quality per call in modelled telephone conversations, In Proc. of *IEEE ICASSP '08*, 4809-4812.

[14] Garofolo, J.S. et al. (1993); TIMIT Acoustic-Phonetic Continuous Speech Corpus Linguistic Data Consortium, Philadelphia, USA.

[15] ITU-T (2001); Recommendation. P.862. Perceptual evaluation of speech quality (PESQ): An objective method for end-to-end speech quality assessment of narrow-band telephone networks and speech codecs.

[16] ITU-T (1996); Recommendation. P.800. Methods for subjective determination of transmission quality.

[17] Hamdaqa, M.; Tahvildari, L. (2011); ReLACK: A Reliable VoIP Steganography Approach, In Proc. of *5th International Conference on Secure Software Integration and Reliability Improvement (SSIRI '11)*, Korea, 189-197.

[18] TeleGeography Report (2012); International Call Traffic Growth Slows as Skype's Volumes Soar, URL: `http://www.telegeography.com/press/press-releases/2012/01/09/international-call-traffic-growth-slows-as-skypes-volumes-soar/index.html`

[19] IEEE (2004); I. S. 802.16-2004, IEEE standard for local and metropolitan area networks part 16: Air interface for fixed broadband wireless access systems.

[20] Wright, C.; Ballard, L.; Coulls, S.; Monrose, F.; Masson, G. (2008); Spot me if you can: recovering spoken phrases in encrypted VoIP conversations. In Proc. of *IEEE Symposium on Security and Privacy*, May, 2008

INT J COMPUT COMMUN, ISSN 1841-9836
8(3):444-459, June, 2013.

Comparative Study of Methods for Estimating Technical Losses in Distribution Systems with Distributed Generation

J.E. Mendoza, M. Lopez, S. Fingerhuth, F. Carvajal, G. Zuñiga

Jorge E. Mendoza, Miguel López, Sebastián Fingerhuth
Felipe Carvajal, Gonzalo Zuñga
Pontificia Universidad Católica de Valparaíso
Escuela de Ingeniería Eléctrica, Valparaíso, Chile.
Brasil 2147, Valparaíso, 4059, Chile.
E-mail: jorge.mendoza@ucv.cl, miguel.lopez@ucv.cl,
sebastian.fingerhuth@ucv.cl, fcarvajal@volta.cl,
gzuniga@esinel.cl

Abstract: In this work four methods for estimating annual technical power losses in distribution networks due to the distributed generation (DG) connection are studied. The methods are obtained of professional sources, and are evaluated in a test system. A new method is proposed in this work to be contrasted to previous methods. To find the best method, the power losses of a base case are estimated with simulations every 15 minutes, considering variability of load demand and power generation. Results indicate the effectiveness of the proposed method respect of other analyzed methods. The proposed method can be a useful tool within a Decision Support System for optimizing control, operation and planning of the distribution network.
Keywords: Distribution Network, Distributed Generation, Active Power Losses.

1 Introduction

Nowadays there is a growing concern in using, in the most efficient possible way, the different types of energy available on our country. From this point of view, proposals which foster efficient use of this energy will significantly contribute to solve the possible future problems related to its supply. This can be seen in the continue development and construction of new and more efficient electrical equipment both from the energy consumption point of view as for the benefits they are able to render to an electrical network.

This concern is also shared with the areas involved in the generation, transmission and distribution process where the studies and analysis from the perspective of planning and operation of the network are basic from a technical/economical point of view for an optimum functioning. In this way, electrical distribution systems are of primary importance for the development of research efforts on finding methods and techniques aiming to optimize their design and operation. This is due to the fact that this is the level were a great quantity of customers concentrates entailing the use of lower voltage levels generating greater current flows and finally a less efficient use of energy (increase of energy losses).

1.1 Distributed Generation

Today there exist a global tendency to allow electric energy injection from clients, electrical industries or from third parties on distribution networks which is called Distributed Generation (DG) [1].

These presents two advantages. Firstly, allows an efficient energy use by way of using energy surplus from industries connected to the network fostering also non-conventional energy generation. Secondly, energy injection close to the load allows an improvement on customers quality service due to an efficient energy transport. The above facts are also supported worldwide [2],

by facilitating some regulatory aspects associated to the integration of DG to electric networks. In Chile, this can be seen on modifications that laws NÂş 19.940 y 20.018 introduce to D.F.L. 1/82 [3] [4], pointing out incentives and procedures for energy injections on electrical networks. Traditionally, utilities design their networks to receive energy from the transmission system and then deliver it to consumers in the distribution system [8]. For this reason, many radial distribution feeders have a conical configuration, i.e., lines start with larger gauge conductors which are reduced along the feeder. This type of configuration can have drawbacks for DG projects. However, a DG can be favorable to the distribution company, reducing losses in the conductors and energy demand of the substation; therefore, this must be assessed by feasibility studies.

1.2 Losses Estimation

The main difficulty in power loss evaluation is the nonlinear relationship with power injections in the network buses. For this reason, the use of tools such as load flow is required for proper evaluation. This implies necessarily having a lot of information about lines, transformers and equipment, which can be hard to obtain. Furthermore, load variations are a very important factor to evaluate these losses. However, in practice, this variability is not properly registered due primarily to economic factors. This results in application of factors, approximate curves and simplifications, which surely entail a relatively large degree of uncertainty.

Knowing or estimating system losses in real time or in a time window can help operators make better decisions regarding the dispatch of other generation units in real time energy markets [10], or as a way to effectively assess the benefits of DG in distribution networks [11]. For example, the proposed power losses estimation technique can be used as an online, real-time diagnostic device that helps a better and more efficient control of distribution power networks.

1.3 Decision Support System (DSS)

Today technical and social systems are becoming increasingly complex. Their models have a large number of state and control variables, delays and different time constants. Also they show limitations in their information infrastructure and risk sensitivity aspects. Such systems are called large-scale complex systems. Hierarchical approach has been for decades one of the most used methods for controlling these large-scale systems. When human intervention is necessary, Decision Support Systems (DSS) can provide a solution. A DSS is an adaptive and evolving information system intended to implement some of the functions of a human support team that otherwise would be required to assist the decision-maker to overcome the limits and constraints when approaching decision problems [12] [13].

This work allows the development of a useful tool that can be included to a DSS for power distribution networks, as it will provide fast information for decision making. This way, the method will allow optimizing the power distribution system control and operation, especially in presence of DG.

This paper addresses the problem of technical power losses estimation in radial distribution network when incorporating DG, to estimate energy and power losses in an effective manner, considering all the technical limitations inherent to the lack of data on real systems for developing a quick, precise and reliable tool that can be included to a DSS.

2 Description of methods and loss calculation proposal

This section describes three models used by consulting firms mainly. These methods will be analyzed and compared with a new proposal, explained in the final part of this section.

2.1 Viera-Bonessi Method

Viera-Bonessi method is used for distribution network planning [5]. It is developed for three types of primary sources: wind, biomass and hydropower. In this work, only wind type method is considered.

With the latest available annual active power demand curve, a power duration curve is built. From this curve three scenarios are calculated: maximum (peak) demand, average demand and minimum demand to be used for each simulation. The scenarios are shown in Figure 1. From these scenarios, the time duration of each stage is obtained. In this example, $T1 = 1460$ hours for peak demand, $T2 = 4745$ hours for average demand and $T3 = 2555$ hours for minimum demand.

Then, each demand scenario P_i is defined. These are calculated by (1), where Ai is the area under the power duration curve and T_i is the duration of stage i demand in hours.

Factors to be applied to the peak power load in all nodes are then calculated. This way, the loads to be used for power flows for each demand scenario are obtained. These factors are calculated by (2), where P_i is the demand under the i^{th} scenario and $\widehat{P}$ is the maximum load associated with the zone of influence of the generator. After obtaining the demands and the factors for each scenario, the whole network to be affected by the DG is modeled. Maximum loads must be corrected by the obtained factor f_i, thereby determining loads for different types of scenarios.

$$P_i = \frac{A_i}{T_i} \tag{1}$$

$$f_i = \frac{P_i}{\widehat{P}} \tag{2}$$

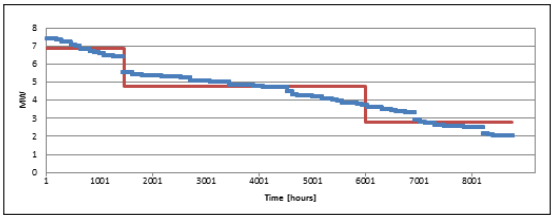

Figure 1: Power duration curve and demand scenarios

Losses without Distributed Generator

Having conducted the above, a power flow is performed and the network losses are calculated for each demand scenario. Then, to get the annual energy losses (3) is used. EPSG are annual energy losses without the generator, in MWh and P_{PSGi} are power losses in the system obtained with the power flow for each demand scenario, without the DG. T_{DI} is the duration of the demand scenario i, in hours.

$$E_{PSG} = \sum_{i=1}^{3} P_{PSGi} \cdot T_{Di} \tag{3}$$

$$E_{PCG} = f_p \sum_{i=1}^{3} P_{PCGi} \cdot T_i + (1 - f_c) \cdot E_{PSG} \tag{4}$$

Losses with Distributed Generator

To calculate the annual energy loss with wind based generators (4) is used. The f_p is the annual loss factor, P_{PCGi} are losses in the system connected with the DG at full load obtained from simulations, E_{PSG} is the annual energy loss in MWh without the DG, E_{PCG} is the annual energy loss of the generator in MWh and f_c is the factor of the generator plant. The annual loss factor f_p is calculated with (5), where f_c is the capacity factor, x is a variable whose value depends on the shape of the generating curve, with a typical value of 0.3 [5]. This method does not indicate how to forecast demand feeder for analysis in future years.

$$f_p = x \cdot f_c + (1 - x) \cdot f_c^2 \tag{5}$$

2.2 3G-3D Method

In this method, the maximum, medium and minimum demand scenarios, P_i, f_i values and losses without DG are calculated in the same way as Viera-Bonessi method. This method was developed and is used by a consulting engineering firm in Chile, for hydraulic projects evaluation mainly. The principal difference to the Viera-Bonessi method, is the way of estimating the generation stages, as indicated below.

Energy Losses with Distributed Generator

At this stage, the method proposes performing the analysis with 3 generation scenarios. For this, the maximum, medium and minimum generation scenarios are obtained: Maximum generation (TG1): 1825 hours/year, mean (TG2): 4380 hours/year and minimum (TG3): 2555 hours/year. The following defines the power generation P_{GJ}, corresponding to each generation stage. These are is calculated by (6), where A_{Gj} is the area under the curve generation duration during the active power generation stage j, for T_{GJ} time, which is the duration of the stage of generation j, in hours. A_{Gj} is obtained from the annual expected generation curve of available active power, in hourly basis. The sum of the first 1825 values is AG1, the sum of next 4380 values is AG2 and the sum of the other 2555 values is AG3. This yields the 3 stages of generation for the simulations.

$$P_{Gj} = \frac{A_{Gj}}{T_{Gj}} \tag{6}$$

$$E_{PCG} = \frac{1}{9760} \cdot \sum_{\substack{i=1:3 \\ j=1:3}} P_{CGD} \cdot T_{Di} \cdot T_{Gj} \tag{7}$$

Generation scenarios are shown in Figure 2, where the blue curve is the expected annual generation duration curve of the generation group and in red the generation scenarios indicated by the method. With each generation stage, a power flow is performed for the three demand scenarios (high, medium and low). This way, power losses are obtained for the 9 cases. Then, with the times of occurrence of each scenario, the energy losses of the feeder are obtained using (7), where P_{PCGij} are the system losses with i^{th}-demand scenario and the jth-generator stage, in MW. T_{Di} is the duration of the demand scenario i, in hours, T_{Gj} are the duration of the generation stage j in hours. E_{PCG} is the annual energy loss with the generator, in MWh.

Regarding to feeder demand forecasting, this method proposes to use the country's GDP as growth rate.

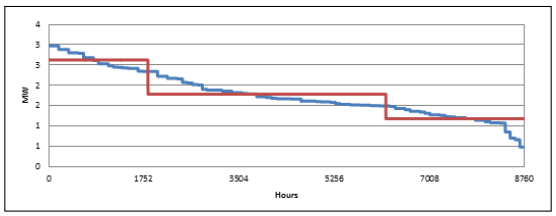

Figure 2: Generation Duration Curve and Generation Scenarios

2.3 Monthly Blocks Method

This method take into account relevant aspects of the above two methods. With the active and reactive power hourly demand curve at the feeder head, a monthly demand curve is created, which is sorted in decreasing active power, maintaining the respective reactive power. With each monthly demand curve, two blocks, B1 and B2 Block are calculated. B1: High power block and B2: Low power block. This totalizes 24 blocks; these blocks will be defined in the same way as does the Chilean National Energy Commission [6]. Table 1 shows the distribution of records (hours) per month of each block used for example.

To calculate demand for each block P_B and Q_B, the procedure is: for January block B1, active power is defined by the average of the first 240 records of the data, assorted from highest to lowest value for the month; i.e., P_B of B1 is determined by the average of the 240 highest active power records in January. The reactive power of B1 (Q_B), is determined by the arithmetic mean of reactive power of the same 240 records considered in the PB calculation of B1 block.

For the January block B2, the procedure is the same, but taking the remaining records of that month (504 records). B1 and B2 blocks for other months are determined in the same way, but considering the distribution of Table 1.

Table 1: Monthly blocks header demands

Month	B1 (Records)	B2 (Records)	NÂ° Records
January	240	504	744
February	86	586	672
Mars	69	675	744
April	288	432	720
May	298	446	744
June	312	408	720
July	340	404	744
August	296	448	744
September	258	462	720
October	42	702	744
November	44	676	720
December	46	698	744
		Total	8760

The demands of each block should be apportioned in proportion to the capacity of distribution transformers (DT) plus lines losses; that is, when making the load flow, power demand in the header must match the demand of the block, considering a degree of tolerance. This assessment can be made proportionally distributing the capacity of transformers. Similarly, the reactive power is calculated.

With the demand for DT obtained through apportionments described above, the functions

"$P_{Total\ TDs}$ Estimate" and "Estimating $Q_{Total\ TDs}$" are defined. These functions relate block demand (demand in the header) with the demand of the DT (8). The coefficients A, B, C, D, E, F, G, H, I and J are constants that can be estimated by a regression.

$$\begin{bmatrix} P_{Total\,DTS} \\ Q_{Total\,DTS} \end{bmatrix} = \begin{bmatrix} A & B \\ F & G \end{bmatrix} \cdot \begin{bmatrix} P_B \\ Q_B \end{bmatrix} \cdot \begin{bmatrix} C & D \\ H & I \end{bmatrix} \cdot \begin{bmatrix} P_B^2 \\ Q_B^2 \end{bmatrix} + \begin{bmatrix} E \\ J \end{bmatrix} \tag{8}$$

Functions "$P_{Total\ TDs}$ Estimate" and "$Q_{Total\ TDs}$ Estimate" are evaluated with data from more recent feeder hourly demand, which gives the DT demand curve; this curve is called "TD demand curve".

Losses without Distributed Generator

The $P_{Total\ TDS}$ and $Q_{Total\ TDS}$ previously calculated for each block (blocks calculated with the demand curve latest feeder, which demand curve will name as year 0) are projected to the year 1, year 3 and year 5, thereby get DTs demand for each block of the mentioned years. The method intends to make the projection considering a growth rate provided by the distributing company or any reliable study.

Power flows are performed for each block (72 blocks, 24 per year) and losses are recorded. The feeder characteristic loss function without DG, (9), where PL is the losses obtained in the simulations, the coefficients K, L, M, N and O are constant and can be determined analogously to the procedure performed to determine the coefficients in (8).

$$P_L = \begin{bmatrix} K & L \end{bmatrix} \cdot \begin{bmatrix} P_{Total\,DTS} \\ Q_{Total\,DTS} \end{bmatrix} + \begin{bmatrix} M & N \end{bmatrix} \cdot \begin{bmatrix} P_B^2 \\ Q_B^2 \end{bmatrix} + O \tag{9}$$

The demand curve DTs projected year 0 to year 1 and the feeder characteristic loss function is calculated, this way hourly losses feeder in year 1 are obtained; these are multiplied by an hour (demand time duration) and then energy losses in an hour are obtained. Then adding up all the energy losses of the year, the total energy losses of the year 1 are obtained. The DT demand curve is projected to years 3 and 5, and the procedure is repeated to determine the energy losses of 3 and 5 years. With total energy losses for years 1, 3 and 5, a quadratic trend curve is adjusted, which allows the estimation of total energy losses for the intermediate years.

Losses with Distributed Generator

This model proposes to conduct analyzes with a single generation scenario. The generator is modeled with the power available, whereas it has this power available (or not) throughout the year. To get the power output of the generator, it is necessary to know its rated power and capacity factor. This is obtained according to the available power (10), where P_{nom} is the rated output power and P_{disp} is the available generator power.

$$P_{disp} = P_{nom} \cdot f_c \tag{10}$$

With the 72 DT demand blocks previously calculated, power flows are executed for each block, considering the available power injection of the generator. Then, generator losses estimation is analogous to the case without generator.

2.4 Proposed Method

The proposed approach arises from the combination of 3G-3D and monthly blocks method. From the latest active and reactive power hourly demand curve of the feeder header, a demand duration curve based on the active power is built. From this curve, maximum, medium and minimum demand scenarios to be used for each simulation are calculated. TDi time duration of each stage are the same as regards the Viera-Bonessi method.

Then, each demand scenario P_i and Q_i are defined. The calculation of P_i and Q_i is done with (11), where A_i is the area under the curve of the active power demand duration during the demand scenario i, for the time T_{Di}; B_i is the area under the reactive power demand curve during stage i, for the time T_{Di}, T_{Di} is the duration of stage i demand in hours. To calculate A_i the curve using active power duration (Figure 1) is used.

$$\begin{bmatrix} P_i \\ Q_i \end{bmatrix} = \frac{1}{T_{Di}} \begin{bmatrix} A_i \\ B_i \end{bmatrix} \tag{11}$$

Losses without Distributed Generator

With the demand values of each scenario, the apportionment proposed in monthly blocks method is done. Then, the energy losses without generator are calculated using (3).

Losses with Distributed Generator

The same generation scenarios of 3G-3D method are used, which is calculated from the expected generation curve: Generation maximum T_{G1}: 1,825 hours/year, mean T_{G2}: 4,380 hours/year minimum T_{G3}: 2,555 hours/year. Then, the calculation of the P_{GJ} values is the same as in 3G-3D method (see 2.2.1). To demand forecast of the feeder, a growth rate provided by the utility or by any reliable study can be used; which will be applied to the DT demands.

3 Estimation of real losses

To know which method obtains the best results, the simulation of a system with different kinds of loads and known daily power variations, as well as the behavior of the DG. This will get different levels of demand and losses for different hours. This system is called the "Base Case" and will be the benchmark to compare the methods.

3.1 Distributed Generator

This study uses a wind park with a nominal power of 2 MW [7]. The daily generation curve of the park, for the winter, summer and fall are shown in Figure 3, discretized every 15 minutes. The analysis considers that spring and autumn curves are the same. According to the same study, the capacity factor of the park is 0.445 and considers that each turbine has a capacitor bank that allows only active power injected to the grid. The DG wind park is simulated as a PQ bar where only the active power injected into the network.

3.2 Test Network

The analysis is done on a test system consisting of 17 bars and 16 lines, with loads connected in all buses. Figure 4 shows the network topology.

Grid parameters can be found in [8]. These values are in per unit, with base values of 23 [kV] and 100 [MVA]. The total active power is 13.88 MW and reactive power is 5.96 MVAr.

Selection of connection points of the DG for evaluating the methods was made considering the power injection at nodes located at the end of feeder, i.e. the node 11 and 17, where a greater impact on loss is expected. Also two other feeder midpoints were considered in nodes 6 and 12.

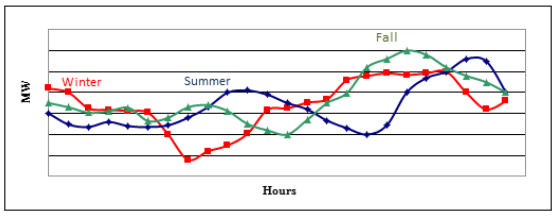

Figure 3: Supply of power to the grid by the wind farm

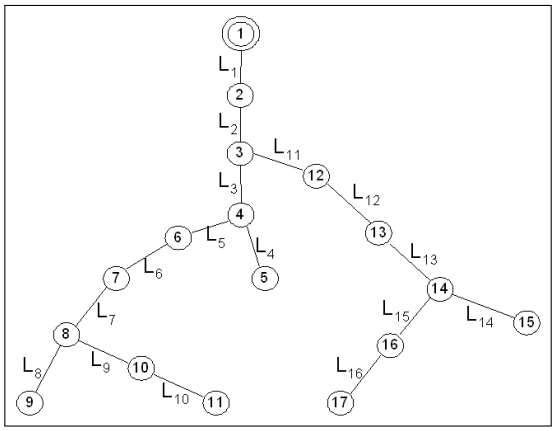

Figure 4: Test System

3.3 Base Case Details

The base case is intended to represent the behavior of a real system. For this reason, hourly variations are considered for the various loads connected to the network distributed along the feeder and with different power levels.

Hourly behavior curves of the considered loads are shown in Figures 5 and 6 [8]. Besides differentiate types of loads, the seasonal variability of demand is taken into account. Demand curves for seasons were obtained from [9] and are shown in Figure 7. Autumn and spring demands are considered equal. The duration of each station are 94 days Summer, Fall 93, Winter 89 and Spring 89. The data from these load curves are discretized every 15 minutes.

4 Results and Comparison of Methods

To apply the methods presented in the test system, the hourly demand curve at the top of the feeder in year cero, without DG, obtained from the base case analysis is used. Each method is evaluated considering a five years horizon, where the DG is connected in year 1. Losses estimated by each method will be compared to the base case. The rate of growth in demand to be used is 4.5% per year, the same as used in the base case.

From the hourly demand curve at the head of the feeder in year 0 without GD, maximum demand is 7.156 MW; minimum demand is 1,966 MW. Power factor varies between 0.90 and 0.92, whereby, in evaluating the methods, this range is considered.

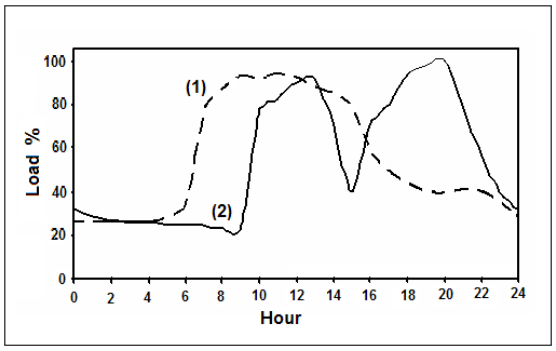

Figure 5: Commercial (1) and industrial (2) type load curve

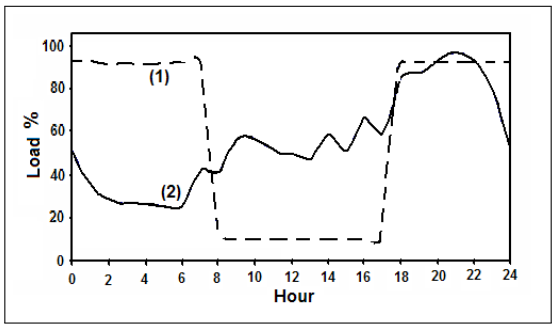

Figure 6: Commercial (1) and industrial (2) type load curve

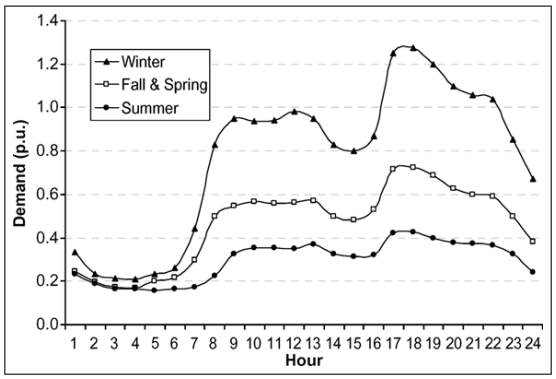

Figure 7: Commercial (1) and industrial (2) type load curve

4.1 Viera-Bonessi Method

The generator power injection is 4 MW, the capacity factor, annual loss factor and the variable x values are: fc = 0.445, fp = 0.272 and x = 0.3 respectively. Demand scenarios are shown in Table 2. According to the results in Table 3, the method has low error in estimating losses without DG. However, the result shown in tables 4 and 5 shows an abnormal operation of Viera-Bonessi method, in the estimation of losses with DG and savings in energy losses.

4.2 3G-3D method

Demand scenarios are the same as in Viera-Bonessi method (Table 2). The power losses estimation without GD is also equal, thus the results are the same (Table 3). This method proposes to perform the analysis with three stages of generation these are shown in Table 6.

Nine power flows resulting from considering each generation scenario with three demand scenarios are carried out. Results are shown in Table 7. These results show that the method estimated correctly the losses with DG. The energy savings achieved by the method over 5 years in the analysis and comparison with the calculated base case are shown in Table 8.

Table 2: Demand scenarios. Viera-Bonessi method

Demand	A_i	T_i [h]	P_i [MW]	f_i
Maximal	10065	1460	6,894	0,497
Average	22542	4745	4,75	0,342
Minimal	7081	2555	2,77	0,199

Table 3: Comparison of total losses without DG. Viera-Bonessi method

Losses M1 [GWh]	Losses CB [GWh]	% Error
3,99	3,77	5,77

Table 4: Losses with DG comparison. Viera-Bonessi method

Bus	Losses [GWh]	Base case losses [GWh]	% Error
6	2,74	2,2	24,54
11	3,61	2,4	50,18
12	2,94	2,81	4,77
17	3,26	3	8,51

4.3 Monthly Blocks Method

The active and reactive power hourly demand curve at the head of the feeder in year 0 without DG is brought to a demand curve for each month, which are sorted in descending order of active power demand. This result in demand blocks B1 and B2 of each month taking into account the distribution records of Table 1. Table 9 shows the demand blocks.

Then the apportionment of the extraction points is carried so that the feeder head power is equal to the sum of DT demands plus lines losses. With this apportionment, DT demand for

Table 5: Savings in energy losses. Viera-Bonessi method

Bus	Savings [GWh]	Base case savings [GWh]	% Error
6	1,25	1,57	-20,58
11	0,38	1,37	-71,97
12	1,05	0,97	8,65
17	0,73	0,77	-4,92

Table 6: Generation scenarios. 3G-3D method

Generation	A_i	T_i	P_i
Maximal	4786	1825	2,623
Average	7802	4380	1,781
Minimal	3005	2555	1,176

Table 7: Losses with DG comparison. 3G-3D method

Bus	Losses [GWh]	Base case losses [GWh]	% Error
6	2,37	2,2	7,54
11	2,26	2,4	-5,67
12	2,95	2,81	5,19
17	3,07	3	2,25

Table 8: Savings in energy losses. 3G-3D method

Bus	Savings [GWh]	Base case savings [GWh]	% Error
6	1,62	1,57	3,28
11	1,73	1,37	25,77
12	1,04	0,97	7,44
17	0,92	0,77	19,42

Table 9: Demand blocks, year 0

Month	Blocks	P_B [MW]	Q_B [MVAr]
January	B1/B2	4,12 / 3.00	1,89 / 1.39
February	B1/B2	3,32 / 3,37	1,53 / 1,55
Mars	B1/B2	3,36 / 3,37	1,55 / 1,55
April	B1/B2	3,92 / 4,20	1,80 / 1,92
May	B1/B2	4,17 /4,22	1,91 / 1,93
June	B1/B2	4,20 / 4,20	1,92 / 1,92
July	B1/B2	5,00 / 5,65	2,28 / 2,56
August	B1/B2	5,58 / 5,66	2,53 / 2,57
September	B1/B2	5,61 / 5,64	2,55 / 2,56
October	B1/B2	5,52 / 4,27	2,53 / 1,95
November	B1/B2	4,17 / 4,21	1,92 / 1,93
December	B1/B2	4,21 / 4,20	1,93 / 1,92

each block is obtained, which is necessary to calculate the functions "$P_{TotalTDs}$ Estimate" and "Estimating $Q_{TotalTDs}$" (8) that relate the block demands to the DT demands.

DT Demand curves are projected years 1, 3 and 5, and then evaluated in the "characteristic feeder losses without DG function", so power losses in every hour for the same years are obtained. Table 10 shows the losses without GD and Figure 8 shows the graph of each year losses and the quadratic trend curve used to calculate losses in years 2 and 4.

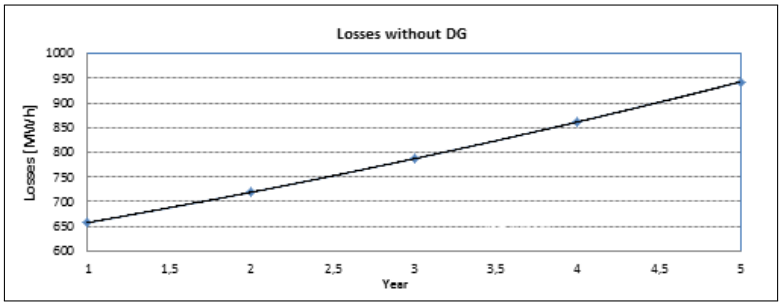

Figure 8: Commercial (1) and industrial (2) type load curve

It is noted that the method estimates with good precision losses in the feeder without DG. For analysis with DG, the method proposes making simulations with the generator injecting its available power, which is calculated by the product of the nominal power factor for the plant, which in this case would $P_{DISP} = 1.78$ MW.

With the blocks 72 previously calculated, power flows are carried with the DG injecting its available power. The procedure is analogous to the case without DG. Losses with and without DG along the 5 years in analysis for each injection point and the comparison with the base case are shown in Tables 11 and 12 respectively. Energy savings achieved over the five years are shown in Table 12.

Table 10: Comparison of total losses without DG. Monthly blocks method

Losses method [GWh]	Base case losses [GWh]	% Error
3,97	3,77	5,18

Table 11: Losses with DG Comparison. Monthly blocks method

Year	Losses method [GWh]	Base case losses [GWh]	% Error
Bus 6	2,33	2,2	5,88
Bus 11	2,15	2,4	-10,55
Bus 12	2,92	2,81	4,09
Bus 17	3,01	3	0,44

4.4 Proposed Method

The active and reactive power hourly demand curves at the head of the feeder in year 0 without DG, are sorted in descending order of active power. Thus demand scenarios are calculated (Table 13). For analysis with DG the same generation scenarios of 3G-3D method are considered (Table 6). The 9 power flows resulting from each stage of generation and the three demand scenarios are then made. The method results for loss estimation without DG are shown

Table 12: Savings in energy losses. Monthly blocks method

Bus	Savings [GWh]	Base case savings [GWh]	% Error
6	1,64	1,57	4,2
11	1,82	1,37	32,7
12	1,05	0,97	8,33
17	0,95	0,77	23,57

in Table 14, which shows that the method is very accurate in the estimation. The results along the 5 years of analysis of the method for estimating losses with DG are shown in Table 15.

The method results in estimating loss savings over 5 years of analysis for each injection point are shown in Table 16.

Table 13: Demand scenarios proposed method

Demand	A_i	B_i	T_i	P_i	Q_i
Maximal	9631	4348	1460	6,597	2,978
Average	21571	9840	4745	4,546	2,074
Minimal	6776	3173	2555	2,652	1,242

Table 14: Comparison of total losses without DG. Proposed method

Losses M1 [GWh]	Losses CB [GWh]	% Error
3,92	3,77	3.98

4.5 Discussion

Regarding Viera-Bonessi method, it considers that the DG always inject its rated power, so the scenarios proposed for power flows are not representative of what actually take place. Moreover, it shows the condition of flow reversal in the substation; but this condition never happens in the base case, so the results are far from the expected values. Therefore it is considered that the Viera-Bonessi method is not reliable, especially when the rated value of the DG is much higher than its usual power injection. Therefore, for comparison Viera-Bonessi method is discarded and we will proceed to an analysis of the results of the three remaining methods, to determine which is the best.

To determine which method is better, errors in estimating losses without DG, losses with DG and feeder energy losses savings due to DG operation are compared. Table 17 shows errors of each method in estimating losses without DG. It is noted that in estimating losses without DG, the proposed method is winner. The errors in estimating losses with DG are shown in Table 18 for each evaluated method. The proposed method has a clear advantage over the rest in the average values (absolute) and their standard deviations also. Table 19 shows the victorious method for each connection point for the DG, considering the estimated savings in losses. It can be seen that the proposed method obtains fewer errors compared to other evaluated methods, so it can be considered the winner.

Table 15: Losses with DG comparison. Proposed method

Bus	Losses [GWh]	Base case losses [GWh]	% Error
6	2,38	2,2	8,2
11	2,29	2,4	-4,45
12	2,94	2,81	4,67
17	3,05	3	1,74

Table 16: Savings in energy losses. Proposed method

Barra	Savings [GWh]	Base case savings [GWh]	% Error
6	1,53	1,57	-2,37
11	1,62	1,37	18,24
12	0,98	0,97	1,27
17	0,86	0,77	11,8

Table 17: Error of Methods in estimation of losses without GD

Method	Error [%]
3G-3D	5,77
Monthly blocks	5,18
Proposed	3,8

Table 18: Porcentual error of methods in estimation of losses with DG

Method	Bus 6	Bus 11	Bus 12	Bus 17	Average/ Deviation
3G-3D	7,54	-5,67	5,19	2,25	5.16 / 4.79
Monthly blocks	5,88	-10,55	4,09	0,44	5.24 / 4.20
Proposed	8,2	-4,45	4,67	1,74	4.76 / 2.64

Table 19: Error of methods in energy losses savings for each DG connection point

Method	Bus 6	Bus 11	Bus 12	Bus 17
3G-3D	3,28	25,77	7,44	19,42
Monthly blocks	4,2	32,7	8,33	23,57
Proposed	-2,37	18,24	1,27	11,8

5 Conclusion

This study addressed the problem of estimating technical losses of a radial feeder when incorporating a DG. For this a test system was chosen in which 4 connection points were tested, to evaluate different methods of loss assessment.

As for the method validation, is can be concluded that the Viera-Bonessi method is unreliable for plants where rated power is far from the power that usually provide. For the other methods, it is demonstrated first that their error varies according to the point of injection; second, an hypothesis arises: the error in saving energy loss increases as the GD injection point is further away from the feeder head; this due to error values obtained when the generator is connected to the feeder center points (specifically on the buses 6 and 12), are lower than when the DG is connected to the endpoints (buses 11 and 17). The analysis determines that the proposed method provides the best results by combining the best aspects of 3G-3D and monthly blocks method, although it involves more computational effort than the previous methods.

The proposed method is a valuable technique that can be easily programmed for its implementation in a Decision Support System that will assist the decision maker for a fast, accurate and reliable control, operation and planning of the distribution network.

Acknowledgement

The authors wish to thank the National Scientific and Technological Research Commission of the Chilean Government (CONICYT) for the financial support given through FONDECYT Regular Project No. 1120178.

Bibliography

[1] A. Bayod-Rjula (2009); Future Development of the Electricity Systems with Distributed Generation, *Energy*, 34: 377-383.

[2] Frias, P.; Gołmez, T.; Cossent, R.; Rivier, J. (2009); Improvements in Current European Network Regulation to Facilitate the Integration of Distributed Generation, *Int. J. of Electric Power and Energy Systems*, 31(9):445-451.

[3] Ley General de Servicios Eltricos (2007), Decreto Fuerza de Ley No4 20.018, 05 de Febrero de 2007, Chile

[4] Ley General de Servicios Eltricos (2007), Decreto Supremo No244. Reglamento para Medios de Generacion no Convencionales y Pequeaąos Medios de Generacion, Santiago, 02 de septiembre de 2005, Chile.

[5] Viera, J.; Bnessi, G. (2008), Calculo de Pardidas Tacnicas en Redes de Distribucion con Generacion Distribuida, *7th IEEE Meeting on Energy, Power, Instrumentation and Measurements,*, Montevideo Uruguay.

[6] Preliminary Technical Rapport (2008), Fijacion De Precios De Nudo Abril 2008 Sistema Interconectado Central.

[7] Final rapport, Energy Area from the Departamento de IngenierĂa Electrica de la Universidad de Chile (2003), Simulacin preliminar de desempeo operacional y comercial de centrales de generacion electrica geotermicas y elicas.

[8] Mendoza, J.E.; Pena, H.E. (2011), Automatic voltaje regulator siting in distribution systems considering hourly demand, *Electric Power System Research*, Vol. 81, 1124-1131.

[9] Ochoa, L.F.; Pafilha-Ferrin, A.; Harrison, G.P. (2008) Evaluating Distributed Time. Varing Generation Througth a Multiobjective Index, *IEEE Transaction on Power Delivery*, 23:1132-1138.

[10] Zhu, Jizhong; Hwang, Davis; Sadjadpour, Ali;(2005) Real time loss sensitivity calculation in power systems operation, *Electric Power System Research* 73:53-60.

[11] Pecas Lopes, J.A; Hatziargyriou, N; Mutale, J; Djapic, P.; Jenkins, N; (2007) Integrating distributed generation into electric power systems: A review of drivers, challenges and opportunities, *Electric Power System Research*, 77:1189-1203.

[12] Filip, F.G.; (2008) Decision support and control for large-scale complex systems, *Annual Reviews in Control*, 32:61-70.

[13] Filip, F.G.; (2012) A Decision-Making Perspective for Designing and Building Information Systems, *INT J COMPUT COMMUN*, ISSN 1841-9836, 7(2):264-272.

INT J COMPUT COMMUN, ISSN 1841-9836
8(3):460-468, June, 2013.

A Tight Coupling Cooperation Scheme in WiFi/WiMAX Heterogeneous Mesh Networks

W. Sun, P. Zhang, Y. Chen, Z. Qin, D. Teng

Weifeng Sun, Peng Zhang, Zhenquan Qin
School of Software
Dalian University of Technology, Dalian 116620, China
wfsun@dlut.edu.cn, terence_zhang@126.com, qzq@dlut.edu.cn

Yuanfang Chen
Institut Mines-Telecom
Pierre-and-Marie-Curie University (UPMC, Paris VI), France
yuanfang_chen@ieee.org

Da Teng
Tencent Technology (Beijing) Co.Ltd
Beijing 100080, China
tengda.ustc@gmail.com

Abstract: A tight coupling cooperation scheme for WiFi/WiMAX networks with QoS provisioning has been proposed in this paper. A new WFW (WiMAX for WiFi) module which enables WiMAX fulfill the procedure of bandwidth request-confirm-grant for WiFi was described with a modified MAC layer of which MSH-DSCH (Mesh Distributed control message) renewed, and thus overhead of interacting of WiFi control message was eliminated. The schedule is then evaluated through simulations in two typical transmission scenarios. Numerical results show that more effective WiFi/WiMAX heterogonous networks which offer QoS guarantees are obtained with the utilization of the scheme. The efficiency of WiFi Mesh networks increase sharply without obvious decrease of WiMAX performance.
Keywords: tight cooperation, WiMAX for WiFi, heterogeneous mesh networks.

1 Introduction

Broadband wireless communication has been a promising area compares to the conventional wireless networks over the last decade [1]. Also the technique has diversified different Radio Access Technologies (RATs) such as WiMAX, WiFi etc. [2]. Heterogeneous networks make an expecting tendency that nodes within which could be embedded with multiple RATS. The nodes mentioned above could also work simultaneously in different networks so as to acquire a better QoS. In [3], the author explores the resource allocation of nodes in heterogeneous network which could solve some traditional wireless networks'resource allocation problem. Author in [4] introduces a Call-Level quality of Service vertical handoff algorithm which could be applied to heterogeneous wireless networks. A further progress could achieved by the use of different RATS in a single heterogeneous wireless network.

Generally speaking, when concerning RAT cooperation, two possible classifications are available. A loosely cooperation is often designed by a coordinate MAC layer which could effectively allow fast switching be- tween different RATs which is transparent to the upper layer [4]. For example, in [6], the author proposes a loose cooperation scheme between WiMAX and WiFi in the Airtime-based module which can make the cooperation strategy and control the RATs through the collection of each RAT's information. And in [5] a simple integration of WiFi/WiMAX network model was studied, the performance of the heterogeneous network was improved to some degree. Tight cooperation, however, could relate RATs and MAC straightly, so as to make

more effective ways to take the proper strategies without decreasing the networks performance obviously. In [8], the author introduces a cooperation scheme between WiFi and WiMAX. The scheme could make WiFi offload some WiMAX traffic which is limited and intelligible. Further solutions should be given in order to get a better use of the tight cooperation schemes advantages. Specifically, a new module and more particularly schemes could be given in order to improve the performance of the networks ulterior.

In this paper, we propose a tight coupling cooperation scheme for the WiFi/WiMAX heterogeneous networks. A new WiMAX for WiFi (WFW) module was developed to share the WiMAX time slot for WiFi. In addition, a modified MSH-DSCH (M-DSCH) was designed to consult for both WiFi and WiMAX about bandwidth request information. By making use of different RATs, WiMAX RATs could take up the request-confirm-grant procedure for the WiFi RATs; WiFi control message was eliminated. The QoS and higher throughput for the whole heterogeneous network could also be guaranteed because of the tightly coupled cooperation.

2 M-DSCH Message Scheduling

2.1 Structure of M-DSCH

The tight coupling cooperation scheme could be fulfilled by the WiMAX's replacing for WiFi in the bandwidth request-confirm-grant procedure.

Table 1 illustrates the M-DSCH message structure to realize the tightly coupled cooperation scheme.

The item marked by a "*" was the original item which also included in the original MSH-DSCH. When we use distributed coordination function (DCF) in the traditional WiMAX networks. Grant/Request Flag was permanently fixed by a zero. Signifying signal contains MSH-DSCH_Request_IE(), MSH-DSCH_Grant_IE() simultaneously. The parameters we need to know are the No.Request, No.Availabilities, and No.Grants represents the numbers of the Request_IE, Avaliable IE, and Grant IE respectively. The data structure and the other parameters' connotation could refer to the IEEE Std 802.16-2004 [3]. Additional items in the M-DSCH message are WiFi Grant/Request Flag, No.WiFi Request, No.WiFi Availabilities, and No.WiFi Grants. Similarly when we use DCF, the WiFi Grant/Request Flag was fixed a zero permanently, represents that the signifying signal could also request, confirm and grant for the WiFi RATs, WiFi Grant/Request Flag, No.WiFi Request, No.WiFi Availabilities, and No.WiFi Grants represents the numbers of the Request_IE, Avaliable_IE, and Grant_IE which has the identical data structure of the WiMAX RATs.

2.2 Performance Analysis of M-DSCH

Analysis of Signaling Size

M-DSCH control signal message should transmit trough 7 OFDM symbols without split into segments. The size of the No.Grants was 6bits in the original DSCH, while it is changed into to 5 bits in the M-DSCH. The size of No.WiFi Grants is fixed in a 5 bits size. In order to meet the demands with the requirement of the signaling transmission delay, the maximum figure of MSH-DSCH_Grant_IE() was decrease from the original 63 to 31.

Analysis of Transmission Delay

Suppose the maximum length of the M-DSCH is S_MAX. When compute with the existing parameters, the result of S_{MAX} is 1263 Bytes. Suppose the original DSCH message length is

Table 1: Structure of WIMAX Mesh MDSCH Message

Syntax	Size	Syntax	Size
MSH-DSCH_Message format()			
{		* *if(CoordinationFlag == 0)*	
* Management Message Type = 41	8 bits	* MSH-DSCH_Scheduling_IE()	varialbe
* Coordination Flag	1 bit	* *for(i=0;i < $No_{Requests}$;++i)*	
* Grant/Request Flag	1 bit	* MSH-DSCH_Request_IE()	16 bits
* Sequence counter	6 bits	* *for(i=0;i < $No_{Availabilities}$;++i)*	
* No. Requests	4 bits	* MSH-DSCH_Availability_IE()	32 bits
* No. Availabilities	4 bits	* *for(i=0;i < No_{Grants};++i)*	
* No. Grants	5 bits	* MSH-DSCH_Grant_IE()	40 bits
WiFi Grant/Request Flag	1 bit	* *for(i=0;i < $No_{WiFi_{Requests}}$;++i)*	
* reserved	2 bits	* MSH-DSCH_Request_IE()	16 bits
No. WiFi Requests	4 bits	* *for(i=0;i < $No_{WiFi_{Availabilitiess}}$;++i)*	
No. WiFi Availabilities	4 bits	* MSH-DSCH_Availability_IE()	32 bits
No. WiFi Grants	5 bits	* *for(i=0;i < $No_{WiFi_{Grants}}$;++i)*	
reserved	3 bits	* MSH-DSCH_Grant_IE()	40 bits
}			

$\prime_{MAX}$. Compute with existing parameters, the size of $S\prime_{MAX}$ is 1176 Bytes. So far a conclusion could be inferred that M-DSCH was 87 Bytes more than the DSCH. Through the equation, the requirement that MDSCH should transmit trough 7 OFDM symbols without split into segments could be assured. M-DSCH frame design is reasonable.

Analysis of the WiFi and WiMAX Mesh Network Performance Using M-DSCH Message

Time slots are divided into frames in the WiFi MAC layer. In our scheme, the n^{th} frame of WiFi starts from the n^{th} data sub-frame of WiMAX, and finishes at the end of $(n+1)^{th}$ control sub-frame.

Suppose the length of the WiMAX frame is $l(s)$, the percentage of the control sub-frame is $r(0 < r < 1)$, the length of the WiFi frame is the same l as WiMAX. When $r = r_1(0 < r_1 < 1)$, the length that could be scheduled in each WiFi frame l_s is described in Equation 1:

$$l_s = r_1 l + (1 - r_1)l = l \tag{1}$$

Then the performance efficiency of the WiFi mesh is δ theoretically, then $\delta = l_s/l = 100\%$. Namely WiFi mesh network could reach the maximum throughput in theory.

The increasing number of the signaling message of M-DSCH could affect the performance of WiMAX mesh network, here is the analysis of the effect. Imagine a network with K nodes, N_i represents the node $i(i \in \{1, .., K\})$. M-DSCH runs only for WiMAX. In a sequential ξ scheduler control frames, node N_i occupies n_i control frames, which means a total n_i transmits chances, here comes the Equation 2.

$\Phi(rl)$ is transmits chances of control frames which is rl in length. Equation 2 based on an assumption that the control frames was saturated, the transmit chances could be utilized completely.

$$\sum_{t=1}^{K} n_i = \xi\Phi(rl) \tag{2}$$

Suppose ξ series scheduler control frames make the bandwidth request simultaneously, and then the M-DSCH messages transmit through node N_i could be divided into α M-DSCH messages which merely contain the three-way handshake procedure information for WiMAX, β M-DSCH messages which contains the grant, confirm messages for WiFi and WiMAX simultaneously, γ M-DSCH messages which merely contain the three-way handshakes procedure information for WiFi. Because the WiMAX and the WiFi bandwidth arrangement are off interference, then $\alpha + \beta = n_i$ was inferred. If P is the ratio that M-DSCH messages which merely contain the three-way handshake procedure information for WiFi of the total M-DSCH messages in the same nodes, then Equation 3 is conducted.

$$P = \gamma/(\alpha + \beta + \gamma) = \gamma/(n_i + \gamma) \tag{3}$$

When the scheme uses for WiMAX only, node N_i has n_i transmit chances. When using for both WiMAX and WiFi in order to fulfill the same requirement, suppose the node N_i has $n\prime_i$ transmit chances, $n\prime_i$ could be conducted as Equation 4.

$$n\prime_i = n_i/(1 - P) \tag{4}$$

Then the total transmission chances of all nodes in the network environment are as the following Equation 5:

$$\sum_{i=1}^{K} n\prime_i = \sum_{i=1}^{K} n_i/(i - P) = 1/(1 - P)\sum_{i=1}^{K} n_i = 1/(1 - P)\xi\Phi(rl) = \xi\Phi(rl/(1 - P)) \tag{5}$$

In order to meet the total requirement of all the nodes in our scheme, the percentage of the control sub-frame should increase from r to $1/(1 - P)$. Compared with the total WiMAX environment, the total decreasing throughput is τ:

$$\tau = ((1 - r) - (1 - r/(1 - P)))/(1 - r) = r/(1 - r)(1/(1 - P) - 1) \tag{6}$$

Since r is a constant, P and τ are of the positive pertinence, a conclusion could be concluded that when P becomes smaller, the loss of the WiMAX performance becomes fewer. When P was 0, then r is zero, and WiMAX performance is lossless. Hence, reducing the percentage of the M-DSCH messages which service for WiFi only was the key point designing the scheme.

3 Designing of the Tight Coulping Cooperation System

3.1 DSCH Handshaking Procedure in WiMAX

WiMAX MAC layer is composed by the core disposal WiMAX MAC Module (WMM), Bandwidth Request Queue (RQ), the Availability Queue, and the Grant/Confirm Queue. WiMAX MAC layer use a feigned random algorithm to provide the transmission chance for the DSCH message, the detail of the algorithm could refer to [3]. The DCF process as the following description:

- When receives a bandwidth request from the other nodes, WMN compute the bandwidth grant information (Grant) bases on the Available information in AQ, then insert Grant into GCQ (Grant Confirm Queue).
- When receives a Grant in which destination address is the same as the node itself, update AQ (Availability Queue) and generate the Confirm information and insert into the GCQ. Simultaneously inform the Node combined with Grant information to transmit data in the allocated minislot. If the received destination address if different from the nodes itself, update the AQ only.

- When a node receives Confirm information, update the AQ.

- When the nodes get the transmission chances of the DSCH, generate the DSCH information firstly, WMN fills the parameters's domain and MSH-DSCH_Schedulin_IE(), RQ, AQ, GCQ fills the MSH-DSCH_Request_IE(), MSH-DSCH_Availability_IE(), MSH-DSCH_Grant_IE() respectively. DSCH will transmit during the beginning of the transmission chance.

The available time slots and the time slot duration information is recorded in the data structure of AQ, but the specific design is not given in [3]. In the supposed system, linked list is chosen to achieve the storage function. Using the procedures above, WiMAX MAC could fulfill the 3-shook hands procedure of DSCH and assure the data sub-frame transmits successfully without any collision.

3.2 Implementation of WiFi and WiMAX Tight Coupling Cooperation System

Design of the System

A WFW module is set up between the MAC layer of WiFi and WiMAX which is utilized to fulfill the requirement of the system. The module was composed as follows.

- Information Sharing Module: WiFi and WiMAX synchronized through the acquired timing information. WiFi shares the Links ID, Neighbor MAC address, Minislot Number and other related information with WiMAX. And WiMAX shares Current frame number, Fram start time, Fram duration, Data subframe start time and Minislot length. Hence, WiMAX could take the WiFi request-grant-confirm procedure. The Data sub-frame of WiMAX is divided into 256 minislots. Supposing each WiFi frame has minislots, σ could be computed as the Equation 7.

$$\sigma = floor(l/((1-r)l/256)) = floor(256/(1-r)) \tag{7}$$

- WFW processing module: this module is used to receive the mutual require-grant-confirm information between the WiMAX and WiFi MAC layer, and then delivers the related information to the other side. When generating the M-DSCH, the module is used to fill the related data structure.

- WiFi Request Queue (WRQ), WiFi Available Queue (WAQ), and WiFi Grant/Confirm Queue (WGCQ): WRQ is used to store query information generated by WiFi MAC layer; WAQ is used to record the location information of the available time slots; WGCQ is used to store the grant and confirm information in responding to the neighbors.

Working Procedure of the System

The proposed system works as the following procedures:

- When a bandwidth request is generated from the WiFi MAC layer, the message is submitted to the WFW processing module. The WFW module then inserts it into the WRQ.

- When the WiMAX MAC layer receives WiFi Grant information, it generates bandwidth grant information named Grant based upon the Information Sharing module and then inserts it into the WGCQ.

- When WiMAX MAC layer receives the WiFi Grant information, the layer will submit it to the WFW module. if the information's destination address is exactly the address of the WiFi MAC layer. Then submits the Grant to the WiFi MAC, WiFi MAC layer will inform the related connection to transmit data in the stipulated minislots. WFW updates the WAQ and generates the confirm information which is inserted into the WGCQ. If the destination address is not the address of the WiFi MAC layer, update the WAQ.
- When WiMAX receives the WiFi Confirm information, it will submit the information to the WFW processing module, then updating the WAQ through the confirm information.
- When WiMAX gets the transmission change of the M-DSCH and generates the M-DSCH messages, WiMAX MAC will fill the related domains of the WiMAX. WFW update the domains of WiFi, the MSH-DSCH_Request_IE(), MSH-DSCH_Availability_IE(), MSH-DSCH_Grant_IE() was filled by the WRQ, WAQ, WGCQ respectively. M-DSCH starts transmission from the beginning of the transmission chances.

Performance Analysis of the System

The performance analysis of the system is as the Theorem 1.

Theorem 1. *The tightly coupling cooperation scheme of the WiMAX and WiFi draws lossless impacts to the original WiMAX scheme.*

Proof: When WiFi MAC layer generates the bandwidth Request, WFW module will put it into the WRQ. Imagine the WRQ's length is infinity, then WiMAX will obtain the M-DSCH transmission chances using the feigned random algorithm based on the request, grant, confirm requirements. When generating M-DSCH messages, MSH-DSCH_Request_IE() and MSH-DSCH_Grant_IE() in the M-DSCH contains one or more effective information thus $\alpha+\beta+\gamma = \alpha = \beta$, then $\gamma = 0$ and $P = 0$. Theorem 1 is proved. □

4 Performance Evaluation Through Numerical Simulations

In this section, we evaluated the performance of the proposed scheme through simulations over NS-2. Based on the platform, two typical scenarios are carried out.

4.1 Network Topology and Parameter Settings

Network Topology

In order to analysis the performance of the proposed scheme, two scenarios are introduced in this paper:

- Fixed topology of double data flows in a single hop. The network contains 2 fixed nodes; each node is embedded with WiFi RATs and WiMAX RATs. When we take the noncooperation mode: WiFi and WiMAX works independently, WiFi occupancy rate of the channel is larger, the throughput and the network efficiency work nearly the maximum value in theory. While the WiMAX performance will suffer a sharply decrease compared to the network using the cooperation mode.
- Random topology of multi-hop and multi flows. Several nodes are randomly distributed in the scenario; each node is embedded with WiFi RATs and WiMAX RATs. In this scenario, the average throughput and the efficiency comparisons between WiFi and WiMAX will help in analyzing the performance gain in our proposed system.

Parameter Settings

In order to measure the performance of WiFi and WiMAX respectively, each node is configured with two constant CBR flows of witch the packet length is 1000 Bytes and packet generation interval is 0.005s, each RAT serves one CBR flow. The parameters of WiFi are set as follows: the signal range of RTS/CTS and data is 550m, 250m respectively. A 50 length of queue is used with physical layer, of which the highest transmit rate is 1Mbps. Modified WiFi layer does not contain the RTS/CTS and ACK procedure, the other parameters is set upon the [3]. The parameters of WiMAX are set as follows: the queue length of WiMAX MAC layer is set with a 50, the percentage of the control sub-layer is 30%, the Scheduling frames is with a 1 set which means 4 scheduling frames emerges during every two control frames. The protocol of the physical layer is using the OFDM and with a 5MHz bandwidth. The band is set to 3.5GHz; Modulation mode of the control sub-frame is set with the OFMD_QPSK_1_2 according to [3], data transmission modulation mode is set with the OFDM_16QAM_1_2.

4.2 Simulation Results

Performance Evaluation in Single Hop Scenario

The scenario contains two nodes within each other's signal coverage. Figure 1(a)(b) depicts the average throughput in the single hop scenario, of which the data flow starts at 30s and end at 130s. Solid points in the Figure 1(a)(b) represent the average throughput in the following 10s from time point it correlates. Fig 1(a) shows the WiFi performance comparison between cooperation and noncooperation scheme. When using the DCF mode, the average throughput is 0.77Mbps. The efficient of the scenario is 0.77Mbps/1Mbps*100%=77%, which is conform to the analysis in the preceding section. When using the cooperation scheme, the average throughput is 0.96Mbps, the network efficient is 0.96Mbps/1Mbps*100%=96%, the network efficient is approximate to 100%. The 4% loss is due to the inefficient use of the mini-slot during the simulation which could be solved by constraining the length of the data flow.

Figure 1(b) shows the WiMAX performance comparison between cooperation and noncooperation scheme. When using the noncooperation scheme, the average throughput of the network is 1.5248Mbps; while using the cooperation scheme, the average throughput of the network is 1.5244Mbps with a deviation of 0.0026%. Hence, the proposed scheme maximizes the throughput and the network efficiency of the WiFi Mesh, assured a nearly lossless WiMAX Mesh network.

Performance Evaluation in the Random Topology

The scenario contains 10 nodes, distributed randomly in a 1000m*1000m area, with 4 CBR flows transmitting simultaneously. Simulation results are showed in the Figure 1(c)(d), the data flow similarly starts at 30s and end at 130s. The solid points in the figure are the same as the points defined in the preceding parts. Figure 1(c) is the shows the comparison between cooperation and noncooperation scheme. When using the DCF mode the average throughput is 1.91Mbps in the noncooperation mode and 2.82Mbps in the cooperation mode. The performance of the network increased by (2.82Mbps-1.91Mbps)/1.91Mbs*100%=47.6%.

Figure 5(d) is the WiMAX performance comparison between cooperation and noncooperation scheme. When using the noncooperation scheme, the average throughput is 5.184Mbps; while using the cooperation scheme, the average throughput is 5.181Mbps. The performance of it decreases by a 0.057%. WiMAX suffer a subtle decrease nearly lossless as well.

The result of the simulations indicates that the proposed tight coupling cooperation scheme works in accordance with our anticipation that the scheme could guarantee the WiMAX RATs

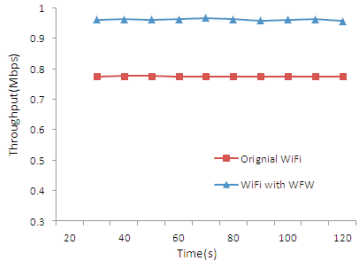

(a) Throughput of WiFi mesh in single hop scenario

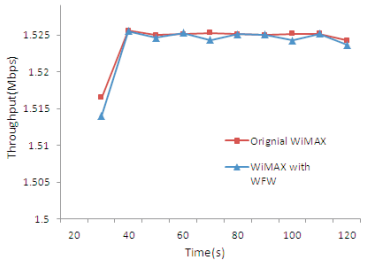

(b) Throughput of WiMAX mesh in single hop scenario

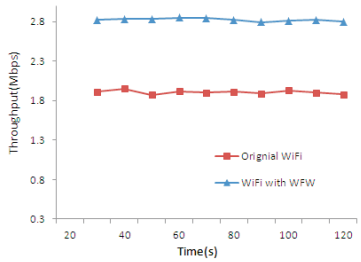

(c) Throughput of WiFi mesh in random distributed scenario

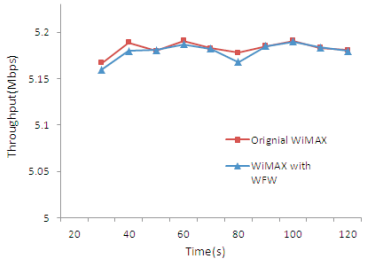

(d) Throughput of WiMAX mesh in random distributed scenario

Figure 1: Average throughput in random distributed scenario

with a lossless performance and the WiFi RATs performance with an evident promotion. In our network environment, the throughput and network efficient could reach the max value in theory.

5 Conclusion

The paper is concerned with a tight coupling operation scheme which could support the effective transmission among the WiMAX RATs and WiFi RATs. A WFW module is employed to do the bandwidth negotiation for WiFi. A novel M-DSCH was proposed to support the WiMAX to fulfill the bandwidth request-grant-confirm procedure. Numerical results have confirmed that the proposed scheme improve the performance of WiFi, and also draws subtle inference to the original WiMAX performance. Increasing performance of the network assures the QoS of the heterogeneous network.

In the future, we intends to examine the performance of the hybrid network in which the users are equipped with single WiFi RATs or WiMAX RATs or equipped with the two RATs simultaneously. Compatibility of the proposed scheme is another direction we will work on.

Acknowledgement

This work is supported by Natural Science Foundation of China under grant No. 61103233, 61202442, 61202443, the Fundamental Research Funds for Central Universities (DUT12JR08).

Bibliography

[1] Weifeng, S. et al. (2012); An Optimal ODAM-Based Broadcast Algorithm for Vehicular Ad-Hoc Networks, *TIIS*, ISSN 2160-6455, 6(12): 3257-3274.

[2] Hanaoka, S.; Yano, M.; Hirata, T. (2008); Testbed System of Inter-Radio System Switching for Cognitive Radio, *IEICE Transaction on Communications*, ISSN 1745-1345, 5(4): 432-446.

[3] Pignaton de Freitas, E.; Heimfarth, T.; Allgayer, R.S.; Wagner, F.R.; Larsson, T.; Pereira, C.E.; Ferreira, A.M. (2010); Coordinating Aerial Robots and Unattended Ground Sensors for Intelligent Surveillance Systems, *International Journal of Computers Communications & Control*, ISSN 1841-9836, 5(1): 52-70.

[4] Arun, E.; Moni, R.S. (2012); Optimization of Vertical Handoff Decision Algorithm for Wireless Networks, *International Journal of Computers Communications & Control* ,ISSN 1841-9836, 7(2): 218-230.

[5] Lior, O.; Yigal, B.; Itay, S. (2004); Wi-Fi (IEEE 802.11) and Bluetooth Coexistence: Issues and Solutions, *IEEE PIMRC*, ISSN 0-7803-8523-3, 2: 847 - 852.

[6] Jong-Ok, K.; Shigeno, H.; Yamaguchi, A.; Obana, S. (2007); Airtime-based Link Aggregation at the Co-Existence of WiMAX and WiFi, *IEEE PIMRC*, ISSN 978-1-4244-1144-3, 1-5.

[7] Ghazisaidi, N.; Kassaei, H.; Bohlooli, S. (2009); Integration of WiFi and WiMAX-Mesh Networks, Advances in Mesh Networks, *Second International Conference on Advances in Mesh Networks*, ISSN 1978-0-7695-3667-5, 1-6.

[8] Hae Jung, K.; Chan Jung, P.; Ronny Yongho, K. (2011); Cooperative Heterogeneous Network Interworking between WiMAX and WiFi, *Communication in Computer and Information Science*, ISSN 1865-0929, 206(1): 62-69.

[9] IEEE Std 802.16-2004. (2004); IEEE Standard for Local and Metropolitan Area Networks Part 16: Air Interface for Fixed Broadband Wireless Access Systems. *The Institude of Electrical and Electronic Engineers, Inc.*

INT J COMPUT COMMUN, ISSN 1841-9836
8(3):469-476, June, 2013.

On the Characteristic Functions of Fuzzy Systems

H.N.L. Teodorescu

Horia-Nicolai L. Teodorescu
1. Institute of Computer Science, Romanian Academy - Iasi Branch
Romania, Iasi, Carol I, 8
2. Gheorghe Asachi Technical University of Iasi
Romania, Iasi, Str. D. Mangeron, 67
hteodor@etti.tuiasi.ro

Abstract: We provide several properties of the input-output function of the SISO / MISO Sugeno fuzzy systems with center of gravity defuzzification. The properties analyzed are related to continuity under various conditions for the input membership functions, including the case when the input space is a topological space.
Keywords: Sugeno fuzzy system , characteristic function, continuity, domain.

1 Introduction

The progress of knowledge on fuzzy systems historically followed a bifurcated path. On one way, the engineering applications drove the development [8] (Tong), with the underlying foundations following. On the second way, logic and mathematics produced advances with limited reference to the applications. That left several area in-between the two paths partly unclarified, especially regarding fuzzy logic systems (FLS) foundations.

We address several properties of the characteristic function of the SISO / MISO (Single Input Single Output / Multiple Input Single Output) fuzzy systems with defuzzification, for Sugeno fuzzy systems. As far as we know, these properties have been explicitly addressed until now only sporadically. The main issues concern the continuity of the characteristic functions of the fuzzy systems with center of gravity (c.o.g.) defuzzification, as continuity is essential in understanding the applicability and constraints when using fuzzy systems in control, system modeling (approximation), predictors and other current applications.

The approximation properties of fuzzy logic systems with defuzzification have been extensively studied starting in the 1990s [6] (Teodorescu 1990), [1] [2], [3], [7]. However, while somewhat elementary, the properties that guarantee that these systems have derivable or continuous input-output functions have not been investigated in detail, except cases discussed in [4], [9]. The continuity of FLSs is essential in many applications, and is effectively assumed in most control applications, as in [13] (even when not stated, e.g., as in many robotic system papers [10], [15]), and in interpolations and approximation with FLSs, as in [11], [12]. The topic was intensively studied, see e.g. [14], [9], [4] etc.

The organization of the paper is as follows. In the next section we recall a few definition and results and state several working hypotheses that are used in the paper. The third section addresses the continuity of Sugeno-type fuzzy systems. The last section is conclusive.

2 Definitions and hypotheses

Consider two spaces, $S \subseteq X$ named input space and $S\prime \subseteq Y$ named output space, and applications $\mu : S \to [0,1] \subset \mathbf{R}$ named input membership functions and respectively $\eta \dot{:} S\prime \to [0,1] \subset \mathbf{R}$ named output membership functions. The definition domain of all input membership functions is S; the subset of S where the membership functions have values larger than 0 is named the support of the function.

We work under a set of very general hypotheses that simplify the presentation of the main results; most results remain valid without these hypotheses, with slightly more elaborate conditions, but their proofs become tedious and lengthy. The hypotheses are as follows.

All input and output membership functions (H1) are normalized, that is, there is at least one point where the membership functions have value 1.

(H2) have a finite set of α-intervals for every α. (We will not use H2 when building an example in Section 3.)

(H3) have compact supports, that is, compact sets where they are larger than zero.

(H4) have bounded supports.

(H5) The union of all the supports of the input membership functions is compact. This hypothesis has no significant impact on the results, but simplifies the discussion.

Hypothesis H3 is typically accepted for fuzzy sets, yet the hypothesis can be removed by defining two (or several) fuzzy sets with compact support, with their union equal to the given non-compact support set. We will still require that the number of disjoint sets of the support is finite.

Hypothesis H4 (boundedness of the support) is only used to avoid studying one more trivial case for membership functions. It can be removed with no influence on the results. Hypothesis H5 (compactness of the union of the supports) plays no role except of avoiding splitting the problem into sub-problems.

Notice that in many respects, the type of input space is not essential, as far as it is a topological space where continuity of the mappings can be defined. In general, we assume that an input membership function is an application from a compact set in a Hausdorff topological space to the unit interval of the real line, $\mu : S \subseteq X \to [0,1] \subseteq \mathbf{R}$. We assume that the input membership functions are not singletons on X.

Consider a finite set of real numbers, named singletons, $\{\beta_i\}_{i=1,..,Q}$. We recall a few definitions.

Definition 1. A SISO zero-order Sugeno fuzzy system is a construction comprising (i) a set of input membership functions $\mu_k : S \to [0,1], k = 1, \cdots, m$, (ii) a set of output singletons, $\{\beta_h\}$; (iii) an application $i(.) : \{1, a, m\} \to \{1, \cdots, Q\}$, that associates to any $k \in 1, \cdots, m$ a value $i(k) \in \{1, \cdots, Q\}$; each such individual association, that is a value i(k) for a specified k, is named rule; (iv) an application $S \to \mathbf{R}$ defined by $x \to y = \frac{\sum_k \beta_{i(k)} \mu_k(x)}{\sum_k \mu_k(x)}, \beta_{i(k)} \in R$.

The part (iii) in the construction is equivalent to saying that there is a set of m rules, $R(k)$: If input is μ_k, then output is $\beta_{i(k)}$, that is, one singleton is assigned to each input membership function.

A definition a little more general allows for several singletons assigned to one input membership function,

(iii*) An application $i(.) : \{1, \cdots, m\} \to \wp\{1, \cdots, Q\}$, where $\wp$ denotes the set of parts (power set); $i(k)$ for a specified k is named *rule*; (iv) an application $S \to \mathbf{R}$ defined by

$x \to y = \frac{\sum_k \beta_h \max_{js.t.i(j)=h} \mu_j(x)}{\sum_k \max_{js.t.i(j)=h} \mu_j(x)}$.

The part (iii*) in the construction is equivalent to saying that there is a set of rules as

$R(k)$: If input is μ_k, then output is $\beta_{i1(k)}, \beta_{i2(k)}, \cdots, \beta_{ir(k)}$,

that is, several singletons may be assigned simultaneously to a single input (non-univalent, multivalued / multivocal association). Equivalently, one can allow for several rules with the same antecedent and different consequents connected by OR, as

$R(k)$: If input is μ_k, then output is $\beta_{i1(k)}$, OR

$R(k)$: If input is μ_k, then output is $\beta_{ir(k)}$.

The application $x \in S \subseteq X \to y \in Y \subseteq \mathbf{R}$ is named characteristic or input-output function of the FLS. This function is defined in all points where at least one input membership function is not null, for Sugeno-type FLSs. This condition is required by the c.o.g. defuzzification method, specifically by the condition that the denominator in the c.o.g. is not null. For ease, we will say that a fuzzy system is continuous if its characteristic function is continuous.

3 Properties of continuity SISO Sugeno systems

The simplest way to analyze the continuity of Sugeno-type system is to use the formula of the output according to the definition in the previous Section and to consider that all input membership functions are defined on the whole domain, X. When an input membership function is defined on a subset of the input space, $\mu : S \subseteq X \to [0,1]$, the last condition is enforced by extending the definition of the input membership functions to the whole X by $\mu(x \in X \setminus S) = 0$. We will study the cases when all input membership functions are continuous on X. Because we assume that all membership functions are continuous everywhere, moreover because the maximum, minimum and rational functions of continuous functions are continuous (wherever they are defined), we directly have the basic result:

Proposition 1. Sugeno SISO fuzzy systems with continuous membership functions over the whole input space are continuous input-output applications in the subset of the input space where the system is defined.

The input space can be whatever topological space X that allows us building continuous applications from it to $[0,1]$. Beyond this very general condition, all the other conditions regard the interval $[0,1]$ and functions defined on it; hence, the generality of the result in Proposition 1.

While the above result is very general, easy to obtain, in addition easily extendable to all Sugeno systems (of whatever order), it sheds little light on the internal mechanisms of these systems and on what happens outside the subset of the input space where the system is defined. Therefore, we will provide another proof for the continuity, studying along the proof the properties of the frontier of the definition space of the system. The analysis will be developed first for the simplest case of FLSs, namely when the input membership functions are defined on $\mathbf{R}$. Then, we deal with X as a general topological space.

We first introduce a few concepts that simplify the explanations. Consider single-input single-output (SISO) fuzzy systems with input membership functions defined on the real axis (mono-dimensional input functions). We assume that any input membership function is not null on an opened interval and null outside it. Denote by $I_k = (\underline{x}_k, \overline{x}_k)$ the opened interval corresponding to the membership function μ_k, with $\mu_k(x) > 0$ for all $x \in I_k$ and $\mu_k(x) = 0$ for all $x \in \mathbf{R} \setminus I_k$. The case $\underline{x}_k = \overline{x}_k$ is not allowed, as the membership function would be void everywhere except a point, reducing it to an input singleton. While not essential, for ease of exposition consider that the union of all closures $\overline{I}_k$ of the intervals I_k is an interval,$\overline{I} = \cup_k \overline{I}_k$. Consider that the intersection of the closures of two specified intervals, $\overline{I}_k$ and $\overline{I}_j$, is not void. The following cases will play a role in the discussion.

The intersection of two intervals is a single point. Assume that $\overline{I}_k \cap \overline{I}_j = \overline{x}_k = \underline{x}_j$ or $\overline{I}_k \cap \overline{I}_j = \overline{x}_j = \underline{x}_k$. The two intervals are adjacent, non-overlapping. (See Fig. 1 a). Then, in the respective point $\underline{x}_k = \overline{x}_j$ or $\underline{x}_j = \overline{x}_k$, both functions have zero value, therefore another membership function must have non-zero value in that point, for the fuzzy system is defined in that point. In the respective point (x_3 in Fig. 1 (a)), the system is not defined. If the two membership functions are

associated with different singletons, the system will have different values at left and at right of x_3, making it impossible to achieve continuity of the system simply by extending the characteristic function of the system to one of the two values.

The cases $\overline{I}_k \cap \overline{I}_j = \underline{x}_k = \underline{x}_j$ and $\overline{I}_k \cap \overline{I}_j = \overline{x}_k = \overline{x}_j$ are not possible, because we required that $\underline{x}_k \neq \overline{x}_k$ and that the intersection reduces to a single point. Therefore, this case is not allowed under normal circumstances (Sugeno systems are not using input singletons).

The intersection is an interval. When $\overline{I}_k \cap \overline{I}_j = \overline{I}_k$ or $\overline{I}_k \cap \overline{I}_j = \overline{I}_j$, the membership functions may look as in Fig. 1 b. We will take into account this case. The typical case in applications is an intersection that is an interval but not equal to one of the two, I_k, I_j.

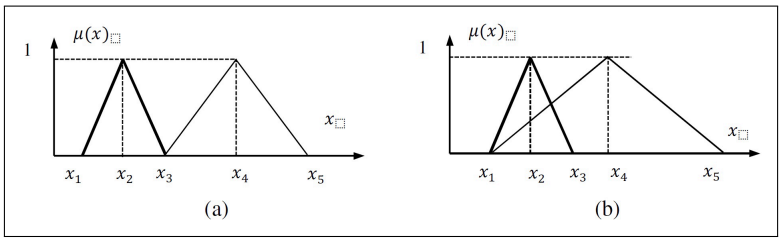

Figure 1: (a) not allowed case, if no other function is non-zero in x_3; (b) allowed case.

Lemma 1. In the case (ii) above, when $I_k \neq I_j$, there is at least one point inside $\overline{I}_k \cap \overline{I}_j$ such that the two membership functions have equal values.

Proof. Indeed, as the membership functions are assumed continuous, so is their difference, $\mu_k - \mu_j$. Denote $\overline{I}_k \cap \overline{I}_j = [a, b]$. Then, either $(\mu_k - \mu_j)(a) < 0$ and $(\mu_k - \mu_j)(b) > 0$, or $(\mu_k - \mu_j)(a) > 0$ and $(\mu_k - \mu_j)(b) < 0$. Therefore, there is a point $x \in [a, b]$ such that $(\mu_k - \mu_j)(x) = 0$.

Consider all points where two membership functions have equal values. Denote these points by e_k and create the ordered set comprising all distinct $e_k, \underline{x}_k, \overline{x}_k$ points. Denote this set of ordered points by $P_C = a_h$. The set of intervals $[a_o, a_1), \cdots, [a_h, a_{h+1}), \cdots, [a_N, a_{N+1}]$ will be named canonical partition of the interval I. The points e_k play a role in considerations only regarding the derivability of Sugeno systems and regarding Mamdani systems; for sake of generality we use them here too. One could define the canonical partition without the points e_k and introduce them only when needed.

Lemma 2. For any interval in the canonical partition, a single rule (iii) or a single subset of rules (iii*) simultaneously apply (are active) in a single-input fuzzy logic system.

Proof. Consider x changing inside some interval of the canonic partition. Because such an interval is included or at most equal to any support (basis interval) for a membership function, moreover no point inside such an interval, $x \in (a_h, a_{h+1})$, represents an edge of the support of an input membership function, the activated rules will remain the same for all inside points.

We recall that the minimum and maximum of two continuous functions are continuous functions, that is, if f and g are continuous functions in some interval, $\min(f(x), g(x))$ and $\max(f(x), g(x))$ are continuous functions on that interval. Consequently, the truncation operation applied to a continuous membership function μ, $\min(\mu(x), \gamma)$, as used for Mamdani systems, is continuous for any $\gamma \in \mathbf{R}$, in the given interval of continuity of μ. We introduce the notion of support of a fuzzy systems defined by the union of the supports of all the input membership functions, $I = \cup_k I_k$. We now can prove

Proposition 2. Any SISO zero-order Sugeno system with continuous input membership functions defined on $\mathbf{R}$ is continuous inside the support of the system.

Proof. According to Lemma 2, a single subsystem of rules always apply inside an interval of the canonical partition, thus the set of integers k for which $\mu_k(x) \neq 0$ in $x \to y = \frac{\sum_k \beta_{i(k)} \mu_k(x)}{\sum_k \mu_k(x)}$

is uniquely defined. As the functions $\mu_k(x)$ are continuous and none null, the denominator is nowhere null inside the interval and both the nominator and denominator are continuous, thus the function $x \in I \to y \in \mathbf{R}$ is continuous.

In the points ending the interval for x, $x \in (a_h, a_{h+1})$, the subset of active rules changes because one or several membership functions become zero. Consider the point a_h, which is not on the frontier of the support of the fuzzy system, $a_h \in \overline{I} \setminus I$. At the limit, we have

$$\lim_{x \to a_h, x > a_h} \frac{\sum_k \beta_{i(k)} \mu_k(x)}{\sum_k \mu_k(x)}.$$

Some of the membership functions tend to zero, while others tend to some non-zero values. Those membership functions not tending to zero remain non-null for $x < a_h$ in some vicinity of a_h, because of continuity. At the same time, other membership functions are non-zero for $x < a_h$ and tend to zero in a_h. Therefore, the limit at right and at left of a_h are equal,

$$\lim_{x \to a_h, x > a_h} \frac{\sum_k \beta_{i(k)} \mu_k(x)}{\sum_k \mu_k(x)} = \lim_{x \to a_h, x < a_h} \frac{\sum_k \beta_{i(k)} \mu_k(x)}{\sum_k \mu_k(x)}$$

and the application is continuous in a_h. Because in the whole closed interval $[a_h, a_{h+1}]$ the system is continuous, it is continuous in the whole definition domain.

The only case we still need to analyze is on the frontier of the union of the supports. Because all the subsequent considerations do not make use of the specific fact that the input membership functions are defined on R, we will continue the discussion in a more general setting. Denote $U = \cup_k S_k$, where S_k is the support of the membership function μ_k. The frontier is $\Gamma = \overline{U} \setminus U$. Because on the frontier all membership functions are null, the FLS is not defined on Γ , yet it can be extended on Γ if the system function has a limit on every point on Γ.

$$\lim_{x \to x_0 \in \Gamma, x \in U} \frac{\sum_k \beta_(i(k)) \mu_k(x)}{\sum_k \mu_k(x)} = \lim_{x \to x_0 \in \Gamma, x \in U} \frac{\frac{\sum_k \beta_{i(k)} \mu_k(x)}{\min_k \mu_k(x)}}{\frac{\sum_k \mu_k(x)}{\min_k \mu_k(x)}}$$

.

In the second limit, the denominator is larger than 1, because all quantities are positive and for $h = \arg\min_k \mu_k(x)$, $(\mu_h(x))/\min_k \mu_k(x) = 1$. When a single membership function has values larger than zero in a vicinity of x_0, that is, when $x \in V_{x_0} \cap U\{x_0\}$ implies that there is some unique h such that $\mu_h(x) > 0$ and $\mu_{k \neq h}(x) = 0$, then the limit is $\beta_{i(h)}$. This is probably the most frequent case in applications.

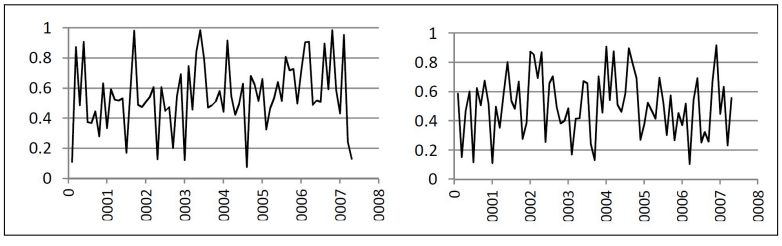

Figure 2: Evolution near zero of the system described in Example 1

However, in general the limit does not exist.

Example 1. Consider $\mu_1(x) = \max(1, x|sin(1/x)|)$, $\mu_2(x) = \max(1, x|sin(1/(2x))|)$, $\beta_(i(1)) = 1, \beta_i(2) = 3$. Notice that these functions do not obey the requirement in the hypothesis (H2). The limit

$$\lim_{x\to 0, x>0} \frac{(\max(1, x|sin(1/x)|) + \sqrt{3}\max(1, x|sin(1/\sqrt{2}x)|)}{\max(1, x|sin(1/x)|) + \max(1, x|sin(1/\sqrt{2}x)|)}$$

does not exist. However, this is not a case of practical interest when choosing membership functions for typical control problems. Figure 3 shows the variation of the above function around zero, at two scales. On the other hand,if for any point x on the frontier of the support of the fuzzy system with continuous input membership functions on X, there is a membership function μ_h such that for all the other membership functions $\mu_{i\neq h}$ there is a finite limit

$$\lim_{u\to x} \frac{\mu_i(u)}{\mu_h(u)} = L_{i,h(x)}(x),$$

then the characteristic function of the Sugeno system can be extended on the frontier as

$$x \to y = \frac{\sum_k \beta_{i(k)}\mu_k(x)}{\sum_k \mu_k(x)}$$

for x inside S^*

$$x \to y = \frac{\beta_(i(h(x))) + \sum_(k \neq h(x))L_(i, h(x))(x))}{1 + \sum_(k \neq h(x))L_(i, h(x))(x)}, x \in \Gamma(S^*)).$$

The extension is obtained as $\lim_{u\to x} \frac{\sum_k \beta_(i(k))\mu_k(x)}{\sum_k \mu_k(x)} = \beta_{i(h(x))} + \sum_{k=h(x)} \beta_{i(k)}\mu_k(x))/(1 + \sum_{k=h(x)} L_{i,h(x)}(x)$. The limit is obtained by factoring in the nominator and in the denominator by $\mu_h(u)$. The possibility to choose several membership functions for μ_h does not modifies the result, as it is easy to check. Example 1. Consider a Sugeno system with only two membership functions, both defined on $[0, 0.1], \mu_1(x) = x, \mu_2(x) = x^2, \beta_1 = 1, \beta_1 = 3$. In this case, $h = 1$. Then, inside $[0, 0.1], x \to y = (x+3x^2)/(x+x^2)$, thus $\lim_{x\to 0}(y) = \lim_{x\to 0}(x+3x^2)/(x+x^2) = 1$.

Remark 1. The characteristic function of the system so defined is continuous in the closure of the support, S^* if the input membership functions are continuous in X. This property results from the above discussion.

Remark 2. Consider the more general case when X is a multidimensional space, for example $x \in X$ and $X = \mathbf{R}^2$ and $\Gamma(S^*)$ is a curve in the plane. It is easy to see that the function $x \to y = (\beta_{i(h(x))} + \sum_{k\neq(x)} L_{i,h(x)}(x)/(1 + \sum_{k\neq h(x)} L_{i,h(x)}(x)$ defined on $\Gamma(S^*)$ may be discontinuous if there are membership functions that are discontinuous even in only one of the variables of the plane.

Because the standard definition of the fuzzy logic systems forces us to exclude the definition of the characteristic function on the support of the system, that is, forces the support to be an open set, we suggest the next extension of the definition for SISO Sugeno systems by replacing condition (iii) in the definition:

(iii**) The output of the system is

$$x \to y = \lim_{u\to x} \sum_k \beta_{i(k)}\mu_k(u) / \sum_k \mu_k(u),$$

whenever the limit exists. This definition generalizes (iii) covering it as a specific case. In addition, it allows us to use membership functions as in Fig. 1 (b) and still have the system defined in the closed interval corresponding to the bases of the triangles. Moreover, the definition completes the domain of definition of the system to a closed set, and makes it continuous (when the input membership functions are continuous and satisfy the other conditions regarding the limit) on its whole (closed) domain. Of course, outside the reunion of the input membership functions support, the system is undefined.

The case of multi-input single-output MISO case, with membership functions defined on R for each input (mono-dimensional input functions) is dealt similarly. We do not study it here because of space limits.

4 Conclusions

We provided several properties of the input-output (characteristic) function of the SISO and MISO Sugeno fuzzy systems with defuzzified output by the center of gravity method. These properties regard the continuity of the characteristic functions of the fuzzy systems and are essential in understanding the applicability and constraints when using fuzzy systems in control, system modeling (approximation), predictors and other current applications. We made a clear difference between the domain of definition of the input membership functions and the domain of the characteristic (input-output) function of the fuzzy system, stressing that they are not identical. The continuity inside the system domain was proved for input topological spaces that allow the definition of the membership functions. Next, we showed cases when it is possible to and explained how to extend the definition of Sugeno fuzzy systems to a closed domain, preserving the continuity of the system. While we provided a proof of continuity for the opened domain of the systems, proof that is valid for general topologic spaces, we worked out a second proof, which is longer but has the advantage of detailing the internal mechanics of Sugeno systems. The second way of dealing with the continuity problem has the additional advantage of showing a path toward the extending of the domain of the systems to a closed domain, for a case that may be of interest in applications.

Bibliography

[1] Buckley, J.J., Hayashi, Y. (1993), Fuzzy Input-Output Controllers are Universal Approximators, *Fuzzy Sets and Systems*, 58(3):273-278

[2] Buckley, J.J., Hayashi, Y., Numerical Relationships between Neural Networks, Continuous Functions, and Fuzzy Systems. *Fuzzy Sets and Systems*, 60(1):1-8, 1993.

[3] Buckley, J.J., Hayashi, Y., Can Fuzzy Neural Nets Approximate Continuous Fuzzy Functions? *Fuzzy Sets and Systems*, 61(1):43-51, 1994.

[4] Dongrui W., Mendel, J.M., On the Continuity of Type-1 and Interval Type-2 Fuzzy Logic Systems. *Fuzzy Systems, IEEE Trans.*, 19(1):179-192, 2011.

[5] Mendel, J.M., John, R.I., and Liu, F., Interval Type-2 Fuzzy Logic Systems Made Simple. *IEEE Transactions on Fuzzy Systems*, 14(6):808-821, 2006.

[6] Teodorescu, H.N., Relations between Fuzzy and Crisp Systems. In: Teodorescu H.N. (Editor), *Fuzzy Signals and Systems*. AMSE Press, Lyon, France, 1990

[7] Teodorescu, H.N., Taylor and Bi-local Piecewise Approximations with Neuro-Fuzzy Systems, *Studies in Informatics and Control*, 21(4):367-376, 2012.

[8] Tong, R.M., A Control Engineering Review of Fuzzy Systems, *Automatica*, 13(6):559-569, 1977.

[9] Yu-Ru S., Sugianto, L.F., Lee, E.S., A Note on Continuity and Semicontinuity of Fuzzy Mappings. *Fuzzy Information Processing Society*, 2007. NAFIPS '07. Annual Meeting of the North American , 24-27 June 2007, 106 - 111.

[10] A. Bazoula, M.S. Djouadi, H. Maaref, Formation Control of Multi-Robots via Fuzzy Logic Technique, *INT J COMPUT COMMUN*, ISSN 1841-9836, Suppl. issue, 3(S):179-184, 2008.

[11] D.Dubois, H. Prade, On Fuzzy Interpolation, *Int J of General Systems*, 28(2-3):103-114, 1999.

[12] E.P. Klement, L.T. Koczy, B. Moser, Are Fuzzy Systems Universal Approximators?, *Int J of General Systems*, 28(2-3): 259-282, 1999.

[13] Pierre Borne, Mohamed Benrejeb, On the Representation and the Stability Study of Large Scale Systems, *INT J COMPUT COMMUN*, ISSN 1841-9836, Suppl. issue, pp. 3(S):55-66, 2008.

[14] P.J.S.G. Ferreira, M.J.C.S. Reis, Fuzzy Information on Discrete and Continuous Domains: Approximation Results, *Int J of General Systems*, 33(5):583-591, 2004.

[15] S.B. Cononovici, A. Curaj, An Approach to Walking Robots Planning and Control, *Proceedings of the Romanian Academy*, Series A, 11(1):75-82, 2010.

INT J COMPUT COMMUN, ISSN 1841-9836
8(3):477-485, June, 2013.

Improved ACO Algorithm with Pheromone Correction Strategy for the Traveling Salesman Problem

M. Tuba, R. Jovanovic

Milan Tuba
Faculty of Computer Science
Megatrend University, Belgrade, Serbia
Bulevar umetnosti 29
11070 N. Belgrade, Serbia
E-mail: tuba@ieee.org

Raka Jovanovic
Texas AM University at Qatar
PO Box 23874, Doha, Qatar
E-mail: rakabog@yahoo.com

Abstract:
A new, improved ant colony optimization algorithm with novel pheromone correction strategy is introduced. It is implemented and tested on the traveling salesman problem. Algorithm modification is based on undesirability of some elements of the current best found solution. The pheromone values for highly undesirable links are significantly lowered by this a posteriori heuristic. This new hybridized algorithm with the strategy for avoiding stagnation by leaving local optima was tested on standard benchmark problems from the TSPLIB library and superiority of our method to the basic ant colony optimization and also to the particle swarm optimization is shown. The best found solutions are improved, as well as the mean values for multiple runs. The computation cost increase for our modification is negligible.
Keywords: ant colony optimization (ACO), traveling salesman problem (TSP), nature inspired algorithms, metaheuristics, swarm intelligence.

1 Introduction

Most real-life problems can be represented as some kind of optimization. Nowadays only hard optimization problems are of research interest. Many discrete (combinatorial) as well as continuous optimization problems are of great practical interest but intractable i.e. cannot be solved within reasonable time by standard, mathematical, deterministic methods. Traveling salesman problem (TSP) is a classic combinatorial example that was researched for the longest period of time and because of that is often used as a benchmark. There are also a number of engineering design problems with mixed continuous and discrete variable and nonlinear objective function and nonlinear constraints that are used as benchmarks for optimization algorithms. For such intractable problems acceptable suboptimal solutions can usually be found by some metaheuristics, recently very successfully by nature inspired algorithms and as a subclass, swarm intelligence algorithms which include artificial bee colony [1], [2], particle swarm optimization [3], [4], cuckoo search algorithm [5], [6], seeker optimization algorithm [7], [8] etc.

A large number of different algorithms have been developed to find suboptimal solutions for the traveling salesman problem (TSP) in polynomial time. Examples are nearest neighbor, greedy, insertion heuristics, christofides, 2-opt and 3-opt. The non-deterministic metaheuristics like simulated annealing (SA) [9], [10], tabu search [11], genetic algorithms (GA) [12] and particle swarm optimization (PSO) [13] have also been used, giving better results than previously mentioned deterministic algorithms. There are efficient algorithms for the TSP [14]

This research was supported by Ministry of Science of Republic of Serbia, Grant III-44006.

(http://www.tsp.gatech.edu/concorde.html) but the research continues on different metaheuristic algorithms [15].

Ant colony optimization (ACO) is another metaheuristic that was successfully used for the TSP [16]. The effectiveness of the ACO has been improved by use of different types of hybridization, like addition of local searchers [17] or combining ACO with GA [18], [19], [20], differential evolution (DE) [21] or kangaroo algorithm [22]. These types of hybridization methods usually have a drawback of complexity of implementation and computation time penalty. It has also been shown that, although adding a local searcher is a good approach in the majority of cases, it may prevent ACO from finding the optimal solution [23]. A very interesting hybridization of ACO is given in article [24] were scout ants, which search the solution space in a more systematic way, are added to the algorithm. Multi-colony systems [25] have been developed, as well as variations of the basic ACO like elitist ant colony, rank based ant colony system and min-max ant system (MMAS) to improve the performance on the TSP [26] in a more natural way, with different pheromone strategies. All these variations have the problem of becoming trapped in local optima due to the fact that they increase the efficiency by making their search more greedy by intensifying the search near the best found solution. Min-max ant system (MMAS) [27] tries to solve this problem by bounding the pheromone values and resetting the pheromone trail if better solutions have not been found in a large number of iterations. Minimum pheromone threshold strategy (MPTS) is another approach to avoid early stagnation applied to the quadratic assignment problems [28]. MPTS adds an additional minimum threshold value and if a pheromone value falls below, it is set to the maximal allowed value of the pheromone trail. Thus the MPTS avoids reinitialization of the pheromone trail like in the MMAS and explores the solution search space more systematically. Another interesting approach is in introducing variable pheromone sensitivity within population of ants [29].

In this paper we propose a new type of hybridization for the ACO and implement it for the TSP. We improve the ACO algorithm with a strategy for avoiding stagnation i.e. leaving local optima if trapped in search for optimal solution. This method is based on the pheromone trail correction. The correction calculation is based on the properties of the best-found solution so far. We have previously used a similar type of improvement on the minimum weight vertex cover problem with great success [30]. We have adopted this approach to TSP and further improved it. The basic idea of this correction is to lower the possibility of edges with high level of undesirability to belong to the optimal solution. We show that our strategy is simple to implement, computationally inexpensive and improves results compared to the pure ACO or PSO [13]. Other relevant research includes [31], [32], [33], [34], [35].

In Section 2 we give an outline of the ACO algorithm. In Section 3 our hybridization used for escaping search stagnation is explained. In Section 4 we analyze and compare experimental results of our algorithm against pure ACO and PSO algorithms for TSP tested on benchmark problems from the TSPLIB [36].

2 Ant Colony Optimization

The ACO algorithm is based on mimicking the behavior of ants colony while gathering food. Each ant starts from the nest and walks towards food until it reaches an intersection, where it has to decide which path to select. In the beginning this choice is random, but after some time the majority of ants will be moving along the optimal path. This happens because of the colony's collective intelligence. Each ant, as he moves, deposits chemical called pheromone thus marking the route taken. Pheromone trail evaporates as time passes. Accordingly, a shorter path will have more pheromone because it will have less time to evaporate before it is deposited again. Each ant chooses paths that have more pheromone so shorter routes will be selected with higher

and higher probabilities until practically all ants go along shortest path. But, it case of dynamic change, some new obstacle or new passage, ants will quickly adopt to new situation.

The described behavior can be converted into a computational system as presented by Marco Dorigo and Luca Maria Gambardella [16], with small modifications:

$$s = \begin{cases} \arg\max\limits_{u \notin M_k} \left\{ {\tau_{rs}}^{\alpha} {\eta_{rs}}^{\beta} \right\} & , q \leq q_0 \\ S & , q > q_0 \end{cases} \tag{1}$$

$$p_{rs}^k = \begin{cases} \dfrac{{\tau_{rs}}^{\alpha} {\eta_{rs}}^{\beta}}{\sum\limits_{u \notin M_k} {\tau_{ru}}^{\alpha} {\eta_{ru}}^{\beta}} & , s \notin M_k \\ 0 & , s \in M_k \end{cases} \tag{2}$$

Equations (1) and (2) define the probabilistic decision method that is used by ants during the iterative construction of the path. An artificial ant at step k, currently at node r, after visiting nodes in M_k, uses these probabilities for choosing the next node s. In these expressions q is a random variable chosen uniformly from [0,1] and q_0 is a predefined parameter that gives a balance between exploitation (use of known good paths, $q \leq q_0$) and exploration (search for new paths, $q > q_0$).

In the case of exploitation, the next node is selected by the highest value of S, which gives the value of desirability of an edge depending on the amount of pheromone and its length. In Equations (1) and (2), τ_{rs} is the value corresponding to the amount of pheromone deposited on edge connecting r and s, and η_{rs} is the length of rs which is used as a heuristic. α and β are predefined parameters that specify the influence of the pheromone and the heuristic, respectively.

In the case of exploration the next node is chosen at random with a probability distribution given by Equation (2), where p_{rs} is the probability of choosing edge rs.

The pheromone trail is created using two types of updates. Global update is used to reward good paths by depositing more pheromone on better paths. This is achieved by using the following formula:

$$\tau_{ij} = (1 - \gamma)\tau_{ij} + \gamma \Delta\tau^k \,, \quad \forall (ij) \in B^k \tag{3}$$

where B^k is the set of all edges in the path ant k used, $\Delta\tau^k$ is the quality of that solution, and γ is a predefined constant from the interval $[0, 1]$.

In practical application of ACO, not all the ants deposit pheromone but only the one with the best path. In some cases, only the best path found so far is used to deposit pheromone, to make the search more greedy.

The local updating is used to avoid creation of a very strong edge used by all ants, and it emulates pheromone evaporation. Every time an edge is chosen by an ant it loses some pheromone according to the following formula:

$$\tau_{ij} = (1 - \delta)\tau_{ij} + \delta\tau_0 \tag{4}$$

where δ is a predefined constant from the interval $[0, 1]$, and τ_0 is the quality of the solution created by the greedy algorithm for solving TSP when the heuristic function is the length of an edge.

3 Suspicious elements exclusion pheromone correction strategy (SEE)

The analysis of the ACO algorithm for the TSP when it gets trapped in local optima indicates which corrections should be made, or more precisely what should not appear in the shortest path. There are two simple criteria that can be used on the edges belonging to the best found tour: very long edges and intersecting edges are very unlikely to be a part of the optimal path. The next step was to find a way to, without major corrections to the ACO algorithm, remove suspicious elements from the ants search path. The solution was to significantly lower the amount of pheromone on randomly selected highly suspicious edges belonging to the best path and letting the colony resume its search.

We have divided the correction into two parts: one considering the edge lengths, and the other one that is related to intersecting edges. All intersecting edges are considered highly suspicious and the pheromone trail is corrected on them. Edges for which pheromone trail correction will be applied due to their length are defined in the following way. First we define a heuristic for suspicion $Sus(rs) = length(rs)$. Using this heuristic, we define the probability of edge rs being selected for pheromone correction

$$p_{selected}(rs) = \frac{RK - RankSusp(rs)}{2 * RK} \tag{5}$$

In Equation (5) instead of using the value of Sus for edges, we used $RankSusp$ which represents their rank by suspicion. RK is the maximal number of edges that are considered for correction. The final step is to lower the pheromone trail for the selected edges:

$$(\forall (rs) \in Selected)(\tau_{rs} = \delta \tau_{rs}) \tag{6}$$

where τ_{rs} is the amount of pheromone deposited on edge rs and δ is a fixed small constant that is used to significantly reduce the value of pheromone on edge rs.

The use of suspicion defined as length is not fully effective because the same group of edges would be repetitively selected until a better tour was found. Because of this we introduce an improved suspicion criteria:

$$CorSusp(rs) = Susp(rs) * ExSusep(rs) \tag{7}$$

The improvement consists of tracking which edges have already been selected and preferring the selection of new edges. To do this, a new array $ExSusp$ is introduced with elements initially set to 1. If edge rs is selected, the following correction is done

$$ExSusp(rs) = ExSusp(rs) * \lambda * \frac{len(rs)}{len(MaxEdge)} \tag{8}$$

In Equation (8) $\lambda \in (0, 1)$ is a fixed parameter and $MaxEdge$ is the longest edge in the best solution. The fraction in Equation (8) makes the probability that the edge will be removed proportional to the length of the inspected edge, which makes longer edges selected more often that short ones, even after a large number of corrections. This is an improvement to our previous implementation of SEE to the minimum weight vertex cover problem were the suspicion was always equally reduced [30]. If a new best set is found, the values of $ExSusp$ are reset to 1. A more complex suspicion criteria could have been used that would better analyze the properties of the best found solution, but we wished to show that even with a relatively simple heuristic, improvements can be archived.

For stagnation criterion we used the fact that there was no change to the global best solution for at least n iterations. If this criterion is satisfied, we apply previously defined correction algorithm to the pheromone trail. The pseudo-code for an iteration step for the improved ACO is:

```
Reset Solution for AllAnts
while(! AllAntsFinished) do
   for AllAnts do if(AntNotFinished) do begin
      Add new edge rs to the solution based on probability
      Local update rule for rs
   end for; end while;
Compute Global Update
If (Stagnation) and (UsingSuspisionImprovement)
   Use SuspisionCorrectionMethod
```

The computation cost for this modification is negligible: fraction of one percent of the total computation time. It can be estimated as follows:

The time required to generate one ant solution is of the order n^2 since it includes n steps to create a solution (adding nodes) and for each of these steps on average $n/2$ steps to recalculate probabilities and pheromone corrections.

Computation time for one correction is also of the order n^2. It consists of three steps where the first one is dominant. The first step is to check all pairs of nodes for intersections and it requires $(n-1)n/2 \sim n^2$ operations. This step is not even performed if the solution has not been improved since last correction. The second step is to sort links, which requires order of $n * log(n)$ operations and finally, to select suspicious elements in n operations. The total time is $(n-1) * n/2 + n * log(n) + n \sim n^2$, or even less when the first term is missing.

One corrections is computationally equivalent (or less) to one ant solution generation and since the correction is done rarely, for our tests we used 30 iterations as a criterion, and each iteration includes 10 ants, the total correction time is 1/300 of the total time or 0.33%.

The most important difference between our proposed algorithm and all other algorithms used so far is in the way how trapping in local minima is avoided. All other algorithms include fresh elements in the search by rather nondiscriminatory increasing pheromone level for large number of elements currently not in the best solution. Out method, however, lowers the pheromone levels for few undesirable elements in the current best solution letting the ant colony replace them with the most appropriate elements. This proved to be a significant new approach applicable to many situations [30], [37].

4 Tests and Results

In this section we present the results of applying our improved version of the ACO on 11 standard benchmark problems from TSPLIB [36], [38] (acceptable by Concorde software). All of the test have been done on the symmetric version of the TSP. We compared our hybridized ACO algorithm with the PSO algorithm [13] and simple ACO in MMAS variation. For each of these three methods we compared the best found solution and the average error over all runs. The results for ACO are calculated using our software system [39]. Results are presented in Table 1.

Columns 3, 5 and 7 (Best) show best results of all runs, columns 4, 6 and 8 (AvgErr) show quality of average solution of all runs: $AvgErr = (Avg - Opt)/Opt * 100\%$.

For the first five problems we used 100 runs to make it comparable to [13]. We also included 6 larger cases and for these cases we used 10 runs since there was no significant difference. For

Table 1: Comparison of PSO, simple ACO and ACO combined with SEE

Problem	OPT	PSO		ACO		SEE	
		Best	AvgErr%	Best	AvgErr%	Best	AvgErr%
eil51	426	427	2.58	427	0.52	427	0.23
berlin52	7542	7542	3.85	7542	0.28	7542	0.13
st70	675	675	3.34	676	1.50	675	1.36
eil76	538	546	4.17	538	1.21	538	1.19
pr76	108159	108280	3.82	108359	2.94	108358	2.62
kroa100	21282	-	-	21282	0.77	21282	0.72
lin105	14379	-	-	14379	0.38	14379	0.38
pr124	59030	-	-	59385	0.84	59030	0.72
pr136	96772	-	-	96785	1.09	96781	0.70
u159	42080	-	-	42080	1.27	42080	0.45
kroa200	29368	-	-	29532	1.21	29490	0.93

each of the runs we created 200,000 tours. All the colonies had the following parameters: $\alpha = 4$ and $\beta = 1$ which control the influence of pheromone and edge length in the transition rule, $q_0 = 0.9$ specifies the exploitation/exploration rate, $\gamma = 0.1$ and $\delta = 0.1$ specify the global and local update rules, the initial value of the pheromone is given by $\tau_0 = 1/n * L_{nn}$ where L_{nn} is the length of the path calculated by the nearest neighbor heuristic.

For SEE we used the following parameters $RK = ProblemSize/10$, $\lambda = 0.9$, $\delta = 0.1$ and $n = 30$. In our test we used 10 colonies for both, ACO and the improved SEE version. In both cases we used random seeds with values from 0 to 9. This make possible comparison of the effect of SEE. SEE used a separate random number generator for the corrections which provides ants having the same behavior.

The first five problems are the same as used in [13] and the results of our method are better compared to the PSO algorithm. Best solutions were equal in three cases, better in one and worse in one case, but average solutions were significantly better in all five cases. We also compared our hybridized algorithm to simple ACO in MMAS variation. Here we have best solutions equal 6 times and improved 5 times by our algorithm, but again average solutions are improved in 10 cases and equal in one.

5 Conclusion

We have introduced a new type of hybridization for the ACO applied to the TSP. It adds a pheromone trail correction method to ACO metaheuristic which is activated in the situations when the search algorithm has started to stagnate. It is based on the analysis of properties of the best-found tour. SEE adds a new heuristic for determining the undesirability of edges belonging to the tour and significantly decreases their pheromone values. The calculation time for this heuristic is negligible compared to the other parts of the algorithm. We compared our hybridization to the use of the simple ACO and PSO and the positive effect of this hybridization was evident on standard benchmark problems.

This type of improvement has the potential of application to different problems previously solved using ACO with appropriate heuristics defined for measuring the desirability or suspicion on parts of the solution. In most cases these heuristic functions are easy to calculate and implement. A great advantage of SEE is that it can easily be added to the existing ACO algorithms,

with minimal change to the original source code.

Bibliography

[1] Brajevic, I. and Tuba, M., An upgraded artificial bee colony algorithm (ABC) for constrained optimization problems. *Journal of Intelligent Manufacturing*, **published Online First**, DOI:10.1007/s10845–011–0621–6, 2012.

[2] Bacanin, N. and Tuba, M., Artificial bee colony (ABC) algorithm for constrained optimization improved with genetic operators. *Studies in Informatics and Control*, 21(2):137–146, 2012.

[3] Secui, D. C., Felea, I., Dzitac, S., and Popper, L., A swarm intelligence approach to the power dispatch problem. *INT J COMPUT COMMUN*,ISSN 1841-9836, 5(3): 375–384, 2010.

[4] Zamfirescu, C.-B. and Filip, F. G.,Swarming models for facilitating collaborative decisions, *INT J COMPUT COMMUN*,ISSN 1841-9836, 5(1):125–137, 2010.

[5] Yang, X. S. and Deb, S. Engineering optimisation by cuckoo search, *Int. J. of Mathematical Modelling and Numerical Optimisation*, 1(4):330–343, 2010.

[6] Tuba, M., Subotic, M., and Stanarevic, N., Performance of a modified cuckoo search algorithm for unconstrained optimization problems, *WSEAS Transactions on Systems*, 11(2):62–74, 2012.

[7] Dai, C., Chen, W., Song, Y., and Zhu, Y., Seeker optimization algorithm: a novel stochastic search algorithm for global numerical optimization, *Journal of Systems Engineering and Electronics*, 21(2):300–311, 2010.

[8] Tuba, M., Brajevic, I., and Jovanovic, R., Hybrid seeker optimization algorithm for global optimization, *Applied Mathematics and Information Sciences*, 7(3):867–875, 2013.

[9] Wang, Z., Geng, X., and Shao, Z., An effective simulated annealing algorithm for solving the traveling salesman problem, *Journal of Computational and Theoretical Nanoscience*, 6(7):1680–1686, 2009.

[10] Meer, K., Simulated annealing versus metropolis for a TSP instance, *Information Processing Letters*, 104(6):216–219, 2007.

[11] Gendreau, M., Laporte, G., and Semet, F., A tabu search heuristic for the undirected selective travelling salesman problem, *European Journal of Operational Research*, 106(2-3):539–545, 1998.

[12] Liu, F. and Zeng, G., Study of genetic algorithm with reinforcement learning to solve the TSP, *Expert Systems with Applications*, 36(3):6995–7001, 2009.

[13] Shi, X. H., Liang, Y. C., Lee, H. P., Lu, C., and Wang, Q. X., Particle swarm optimization-based algorithms for TSP and generalized TSP. *Information Processing Letters*, 103(5):169–176, 2007.

[14] Applegate, D., Bixby, R., Chvatal, V., and Cook, W., On the solution of the travelling salesman problems, *Documenta Mathematica*, Extra Volume ICM(III), 645–656, 1998.

[15] Rego, C., Gamboa, D., Glover, F., and Osterman, C., Traveling salesman problem heuristics: Leading methods, implementations and latest advances. *European Journal of Operational Research*, 211(3):427–441, 2011.

[16] Dorigo, M. and Gambardella, L. M., Ant colonies for the travelling salesman problem, *Biosystems*, 43(2):73–81, 1997.

[17] Chengming, Q., An ant colony algorithm with stochastic local search for the VRP, *8rd International Conference on Innovative Computing Information and Control*, Los Alamitos, CA, USA, pp. 464–468, IEEE Computer Society, 2008.

[18] Lee, Z.-J., Su, S.-F., Chuang, C.-C., and Liu, K.-H., Genetic algorithm with ant colony optimization (GA-ACO) for multiple sequence alignment, *Applied Soft Computing*, 8(1):55–78, 2008.

[19] Jun-Qing Li, Q.-K. P. and Xie, S.-X., A hybrid variable neighborhood search algorithm for solving multi-objective flexible job shop problems, *Computer Science and Information Systems*, 7(4):907–930, 2010.

[20] Negulescu, S., Dzitac, I., and Lascu, A., Synthetic genes for artificial ants. Diversity in ant colony optimization algorithms, *INT J COMPUT COMMUN*, ISSN 1841-9836, 5(2):216–223, 2010.

[21] Zhang, X., Duan, H., and Jin, J., DEACO: Hybrid ant colony optimization with differential evolution, *IEEE Congress on Evolutionary Computation*, 921–927, IEEE Computer Society, 2008.

[22] Serbencu, A., Minzu, V., and Serbencu, A., An ant colony system based metaheuristic for solving single machine scheduling problem, *The Annals of Dunarea De Jos University of Galati*, 3:19–24, 2007.

[23] Neumann, F., Sudholt, D., and Witt, C., Rigorous analyses for the combination of ant colony optimization and local search. *Ant Colony Optimization and Swarm Intelligence*, LNCS Berlin, Heidelberg, 5217:132–143, Springer-Verlag, 2008.

[24] Gan, R., Guo, Q., Chang, H., and Yi, Y., Improved ant colony optimization algorithm for the traveling salesman problems, *Journal of Systems Engineering and Electronics*, 21(2):329–333, 2010.

[25] Jovanovic, R., Tuba, M., and Simian, D., Comparison of different topologies for island-based multi-colony ant algorithms for the minimum weight vertex cover problem, *WSEAS Transactions on Computers*, 9(1):83–92, 2010.

[26] Stützle, T. and Dorigo, M., ACO algorithms for the traveling salesman problem, *Evolutionary Algorithms in Engineering and Computer Science: Recent Advances in Genetic Algorithms, Evolution Strategies, Evolutionary Programming, Genetic Programming and Industrial Applications*, K Miettinen, P Niettaanmaki, M M Makela and J Periaux, editors, p. 500, Willey, 1999.

[27] Stützle, T. and Hoos, H. H., MAX-MIN ant system, *Future Generation Computer Systems*, 16(9):889–914, 2000.

[28] Wong, K. Y. and See, P. C., A new minimum pheromone threshold strategy (MPTS) for max-min ant system, *Applied Soft Computing*, 9(3):882–888, 2009.

[29] Pintea, C.-M., Chira, C., Dumitrescu, D., and Pop, P. C., Sensitive ants in solving the generalized vehicle routing problem, *INT J COMPUT COMMUN*, ISSN 1841-9836, 6(4):228–231, 2011.

[30] Jovanovic, R. and Tuba, M., An ant colony optimization algorithm with improved pheromone correction strategy for the minimum weight vertex cover problem. *Applied Soft Computing*, 11(8):5360–5366, 2011.

[31] Gan, R., Guo, Q., Chang, H., and Yi, Y., Improved ant colony optimization algorithm for the traveling salesman problems, *Journal of Systems Engineering and Electronics*, 21(2):329–333, 2010.

[32] Crişan, G. C. and Nechita, E., Solving fuzzy TSP with ant algorithms, *INT J COMPUT COMMUN*, ISSN 1841-9836, Suppl. issue, 3(S):228–231, 2008.

[33] Huang, H., Yang, X., Hao, Z., and Cai, R., A novel ACO algorithm with adaptive parameter, *Computational Intelligence and Bioinformatics, LNCS*, 4115:12–21, Springer-Verlag Berlin Heidelberg, 2006.

[34] White, C. and Yen, G., A hybrid evolutionary algorithm for traveling salesman problem, *IEEE Congress on Evolutionary Computation*, 2:1473–1478, IEEE Computer Society, 2004.

[35] Duan, H. and Yu, X., Hybrid ant colony optimization using memetic algorithm for traveling salesman problem, *Approximate Dynamic Programming and Reinforcement Learning*, 92–95, IEEE Computer Society, 2007.

[36] Reinelt, G., TSPLIB - a traveling salesman problem library, *ORSA Journal on Computing*, 3(4):376–384, 1991.

[37] Jovanovic, R. and Tuba, M., Ant colony optimization algorithm with pheromone correction strategy for the minimum connected dominating set problem, *Computer Science and Information Systems (ComSIS)*, 10(1):133–149, 2013, DOI:10.2298/CSIS110927038J.

[38] http://www.iwr.uni heidelberg.de/groups/comopt/software/TSPLIB95/tsp/ .

[39] Jovanovic, R., Tuba, M., and Simian, D., An object-oriented framework with corresponding graphical user interface for developing ant colony optimization based algorithms, *WSEAS Transactions on Computers*, 7(12):1948–1957, 2008.

INT J COMPUT COMMUN, ISSN 1841-9836
8(3):486-491, June, 2013.

A Rate based Congestion Control Mechanism using Fuzzy Controller in MANETs

H. Zare, F. Adibnia, V. Derhami

Hamideh Zare
Department of Computer Engineering, Yazd Branch,
Islamic Azad University, Yazd, Iran
E-mail: Khezrabad@imo.org.ir

Fazlollah Adibnia, Vali Derhami
Yazd University
E-mail: fadib@yazd.ac.ir, vderhami@yazd.ac.ir

Abstract: The traditional congestion control mechanism TCP, performs very poorly in MANETs Because there are a number of new challenges such as wireless link error, medium contention and frequent route failures in this kind of networks [1]. In this paper, we propose a fuzzy adhoc rate-based congestion control (FARCC) to enhance the efficiency of network in MANETs. In FARCC, we use a rate-based transmission scheme using two fuzzy controller of zero order Takagi Sugeno Kang (TSK) model to congestion detection and congestion control. The FARCC sender adjusts data rate by receiving a feedback packet from FARCC destination. NS2-based simulation results show that FARCC outperforms ITP and ATP to achieve, in terms of throughput and fair resource allocation in AdHoc networks under random topology.
Keywords: Rate control, congestion control, fuzzy controller, channel busyness ratio.

1 Introduction

Congestion control is a critical issue to achieve optimal network resource utilization and fairness among end-to-end flows.In MANET with shared resources, where multiple senders compete for link bandwidth, it is necessary to adjust the data rate used by each sender in order not to overload the network. Packets that arrive into router and cannot be forwarded are dropped, consequently an excessive amount of packets arriving at a network bottleneck leads to many packet drops.These dropped packets might already have travelled a long way in the network.Thus consumed significant resources. In recent years, the whole congestion control mechanism designed in manet, specify the number of packets that are droped lead to congestion.These approaches are divided into three categories: window-based, rate-based and a hybrid between a window-based and a rate-based approach. window-based congestion control is not appropriate for MANET to provide high throughput, short delay and stable performance with few packet collisions.
In this paper, we focus on the problems resulting from the medium contention and propose a novel Fuzzy Adhoc Rate based end-to-end Congestion Control scheme (FARCC).This is unlike TCP, a rate-based congestion control and tuning of rate is operated in destination node. Extensive simulations show that our scheme significantly outperforms ITP [2] and ATP [3] in terms of channel utilization, average delay, and fairness between different flows.

2 Fuzzy Adhoc Rate base Congestion Control (FARCC)

In this section, we will elaborate on the specific mechanisms used by FARCC. FARCC primarily consists of mechanisms at the sender to achieve effective congestion control and reliability. Each time the FARCC sender transmits a packet, it attaches a congestion header to the packet. The rate-stamp field in header is sender's current Rate. Which is filled in by the sender and

never modified in transit. The br-stamp field is channel busyness ratio that all the intermediate nodes along the path are calculated and may modify it to control the packet sending rate of the sources. The delay-stamp field is the average queuing delay that all the intermediate nodes along the path may modify it. The destination node is similar to a TCP receiver except that when it receives acknowledging a packet, it copies the congestion header from the data packet to its ACK. It also acts as a collator of the congestion information provided by the intermediate nodes in the network before the information is sent back to the sender. The destination node provides the reliability, flow control, and collated congestion control information through periodic messages. FARCC sender is responsible for the connection management and the startup rate. Estimation and controls the sending rate of each flow by the explicit feedback carried in the ACKs.

2.1 Intermediate node

Delay(q(t)) is queuing delay experienced by per packet traversing the intermediate node. The intermediate nodes maintain an average queuing delay as avg-delay(q(t)) irrespective of the specific flow. It is performed over all the packets traversing through them. Average queuing delay is impacted by the contention between different flows traversing the node. This value is maintained using exponential averaging according to (1). For every outgoing packet, an intermediate node updates its avg-delay(q(t)) and delay(q(t)) values.

$$ave - delay(q(t)) = \alpha * ave - delay(q(t)) + (1 - \alpha) * delay(q(t)) \quad (1)$$

Every packet consists of delay-stamp field. It refers to the maximum avg-delay(q(t)) value at the upstream nodes that packet has traversed through. When the packet is dequeued for transmission, the intermediate node updates the delay-stamp field in the packet with avg-delay(q(t)) value if delay-stamp field is smaller than avg-delay(q(t)) value. The Intermediate node runs an epoch timer of period E. This period E should be larger than the round trip time of a connection, but at the same time must be small enough to track the dynamics of the path characteristics. E is empirically chosen to be one second in our simulations. In addition, the intermediate node computes channel busyness ratio periodically For the whole channels communicating with it according to [4]. Intermediate nodes in the network maintain maximum channel busyness ratio periodically as br(t) values. Each packet consists of a br-stamp field that refers to br(t) value at the upstream nodes which packet traversed through. When the packet is dequeued for transmission, the intermediate node updates the br-stamp field in the packet with br(t) value, If it is smaller than br(t) value.

2.2 Destination node

The destination node provides periodic feedback to sender for the collates congestion information which are provided by the intermediate nodes (through the br-stamp and delay-stamp fields on the packets). When destination node receives a packet, delay-stamp and br-stamp fields in the packet refer to as maximum average queuing delay and maximum channel busyness ratio which are experienced by the packets traversed through intermediate nodes. For every incoming packet belonging to a flow, the destination node performs an exponential averaging of the Delay-stamp value. In addition it performs periodically an exponential averaging of the br-stamp value which is specified in the packet.

The destination nodes in the network maintain avg(br-stamp) and avg(delay-stamp) values. In order to send the feedback periodically, the destination node runs an epoch timer of period T. Note that the period T should be larger than the round-trip time of a connection, but at

the same time must be small enough to track the dynamics of the path characteristics. T is empirically chosen to be one second in simulations.

Congestion probability Estimation using Fuzzy Logic Controller

The destination node gets packets and passes them through both the fuzzy logic congesion detection system and fuzzy logic congestion control system. Then it calculates appropriate transmission rate and piggybacks new rate on packet to the sender node. The fuzzy logic congestion detection system will calculate the probability of congestion using congestion header of packets. In the following section, we will introduce how use the fuzzy logic controller to estimate congestion probability.The system model of FARCC is shown in Fig.1.

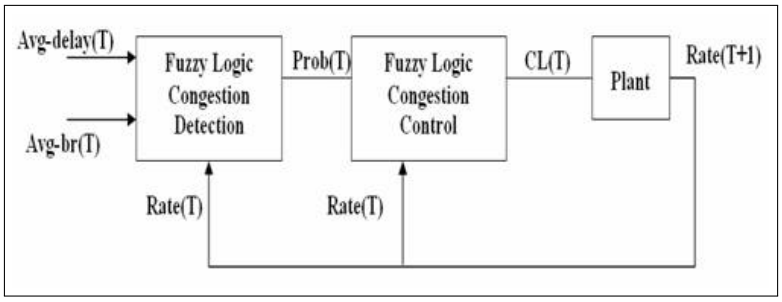

Figure 1: system controller to transmission rate

All inputs to fuzzy logic congestion probability system are considered as T, where T is the sampling period. The fuzzy congestion probability system consist of three inputs. The input avg-delay(T) is avg(delay-stamp) and The input avg-br(T) is avg(br-stamp) that are both calculated by destination node. The input rate(T) to primary system is current data rate in congestion header of packet. The fuzzy system in FARCC is zero order TSK-Fuzzy system. the fuzzy rules are determined based on a full combination of the input variables. Hence, there will be 36 (3*3*4) Fuzzy rules. If rth rule is denoted by R_r then the Fuzzy rule can be described generally as shown in the following equation:
R_r: IF avg-delay(T) is C AND avg-br(T) is D AND rate(T) is P THEN prob(T) is Z_r.
The output of fuzzy model as prob(T) is the probability of congestion, that is a value in the range [0,1] and how input variables are mapped to the probability of congestion detemined by simulation. Parameters Z_r (probability of congestion) are initialized using simulations and gathered experiences. Simulation is performed over 200 simulation runs in section 3. The goal of the proposed fuzzy controller is to determine the probability of congestion using current Network status and parameters except packet loss rate in the network.

Congestion control using fuzzy logic controller

In FARCC approache, There are three congestion levels low, medium and high. The destination node determines network congestion level using secondary fuzzy system at each sampling period according to Fig.1. The transmission rate tuned depends on specified congestion level through one of the three phases; multiplicative increase, additive increase and multiplicative decrease. two inputs of fuzzy logic congestion control system are considered at T, where T is the sampling period. The input prob(T) is congestion probability and output of primary Fuzzy system. The input rate(T) is current data rate in congestion header of packet. The zero order T-S fuzzy model has been selected for this system.

Plant modeling

Plant based on one of the congestion levels(low, medium and high) which is specified in output secondary fuzzy system performs one of three phases of multiplicative increase, additive increase and multiplicative decrease on current transmission rate respectively. If specified congestion level is low then it performs multiplicative increase phase according to (2) inorder the improvement of network throughput. [6]

$$new - rate = old - rate * (\frac{th - br}{avg(br - stamp)}) \tag{2}$$

if congestion level is medium then it performs additive increase phase inorder the increases in transmission rate belong to average queuing delay of path nodes according to (3). [6]

$$new - rate = old - rate + (\frac{1}{avg(delay - stamp)}) \tag{3}$$

If congestion level is high, then probability of congestion event is high. Therefore it performs multiplicative decrease and control send rate using average queuing delay and average channel busyness ratio, according to (4). [6]

$$new - rate = \frac{old - rate * avg(br - stamp)}{avg(delay - stamp) * th - br} \tag{4}$$

The destination node compares the new transmission rate with the current rate. If difference is greater than E then the new transmission rate is stamped on ACK packet and is sent to the sender, since increase in the number of feedbacks lead to an increase in congestion and network load.

2.3 Sender node

In connection initiation phase, the sender node sends a probe packet to receiver. The probe packet is piggybacked on the next data packet in sequence queued for transmission. When a new path is used, the connection is not aware of the available bandwidth on path. The probe packet perform bandwidth estimation once again allows the connection to operate at the true available bandwidth instead of either over utilizing or under utilizing the resources available along the new path.the sender node calculates time interval packets sending using send rate.

3 Simulation results

We used the NS2 simulator [7] to evaluate FARCC under random topology. the default parameter settings are as follows: the two-ray ground reflection model is used as the radio propagation model, IEEE 802.11 DCF as the MAC protocol, and AODV as the routing protocol. The parameters in FARCC are as follows: the initial values of the transmission rates are 110 kbps; The step sizes are appropriately tuned according to the scale of the network and the number of flows in network. In these topologies, each node is 200 meters away from its closest neighbors. The transmission range and the interference range are 250 m and 550 m, respectively. The data transmission rate is 2Mbps. The packets generated are of size 512 bytes in all the simulations. All the simulations are run for 100s and each data point on the figure is averaged over 10 simulation runs.

In this scenario the random topologies are generated for the simulations. The mobility model used for topology generation is the random waypoint model. All the simulations are performed

for a grid consisting of 50 nodes, distributed randomly over the two dimensional grid. The source destination pairs are randomly chosen from the set of 50 nodes in the network. Load on the network is 15 flows and FTP is the application that is used for all the flows in the network.

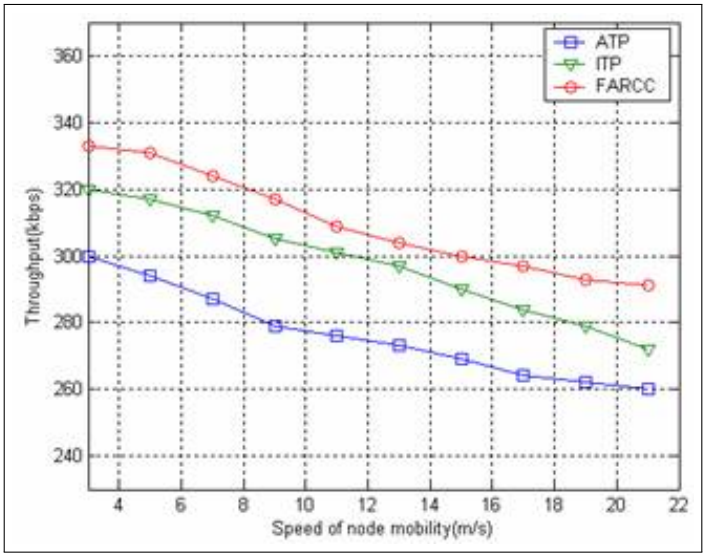

Figure 2: Throughput versus mobility in random topology

The first metric is the overall throughput shown in Fig.2 We observe with The larger speed of the node mobility, the aggregate throughput achieved by FARCC is able to provide an improvement of around 13.8%-48.4% over default ATP, and around 0.7%-23.6% over ITP.

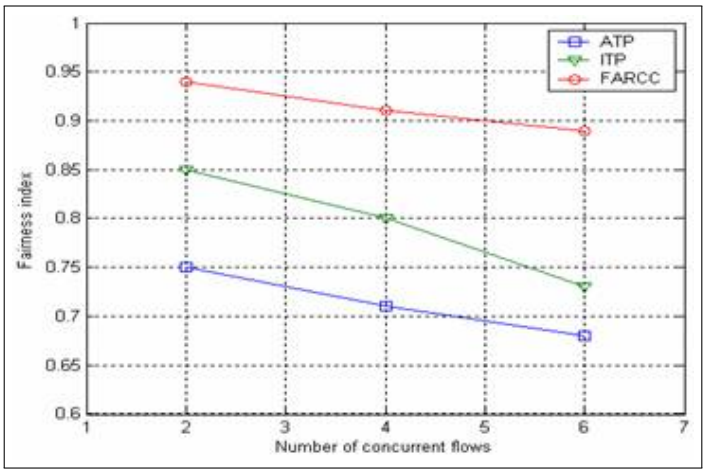

Figure 3: Fairness index in random topology

The result of the fairness index [8] is depicted in Fig.3 which shows a remarkable fairness of FARCC. The more concurrent flows, the better the improvement of FARCC over the congestion control algorithms and the mount of fairness index have an improvement of around 9 percent over ATP,and around 20 percent over ITP.

4 Conclusion

In this paper, we proposed an improved congestion control mechanism called FARCC in MANETs. The proposed scheme uses the fuzzy logic control mechanism to determine an appropriate data rate for sending packets. using the fuzzy logic congestion detection, probability of congestion is estimated. then fuzzy logic congestion control specifies network congestion level based on probability of congestion. The congestion level is used to tune the data Rate in plant. FARCC uses a feedback scheme to adjust data flow rate. Simulation results show that the proposed FARCC performs better than ITP and ATP for aggregate throughput. Consequently, our method supports higher fair resource allocation.

Bibliography

[1] Zhai, H.; Chen, X.; Fang, Y.; Rate-Based Transport Control for Mobile Ad Hoc Networks, *In Proceedings of the IEEE Wireless Communications and Networking Conference*, 4(1): 2264-2269, 2005.

[2] Wang1, N.; Huang2, Y.; Liu2, W.; A Fuzzy-Based Transport Protocol for Mobile Ad Hoc Networks, *In Proceedings of the IEEE International Conference on sensor network*, 2008.

[3] Sundaresan, K.; Anantharaman, V.; Hsieh, H. Y.; Sivakumar, R.; ATP: A Reliable Transport Protocol for Ad-hoc Networks, *In MobiHoc 03: Proc. of the 4th ACM International Symposium on Mobile Ad Hoc Networking & Computing*, 64-75, 2003.

[4] Kumar, S.; Raghavan, V.; Deng, J.; Medium Access Control Protocols for Ad Hoc Wireless Networks: a Survey, *Ad Hoc Networks*, 4(3): 326-358, 2004.

[5] Smitha, K.; Anand, H. U.; Mallapur, J. D., Fuzzy Based Congestion Control In Wireless Network, *International Journal of Computer Science and Communication*, 2(2):469-473, 2011.

[6] Zhai, H.; Chen, X.; Fang, Y.; A Call Admission and Rate Control Scheme for Multimedia Support over IEEE 802.11 Wireless LANs, *In Proc. First International Conference on Quality of Service in Heterogeneous Wired/Wireless Networks (QShine 04)*, 2004.

[7] The network simulator ns-2 website, available at : http://www.isi.edu/nsnam/ns.

[8] Wang, X.; Kar, K.; Cross-layer rate optimization for proportional fairness in multihop wireless networks with random access, *IEEE Journal on Selected Areas in Communications*, 24(8):1548-1559, 2006.

Author index